CATO-2 Deliverable WP 3.03-D06

Site-representative caprock and fault rock samples acquired and characterised (1st Year Progress Report)

Prepared by: Colin J. Peach, J.H.P. de Bresser, R.F.M van der Kroef, A. Mols, B.A. Verbene J. Samuelson

Reviewed by: C.J. Spiers

Approved by: J.Brouwer (CATO-2 Director)

1 Executive Summary (restricted)

WP 3.03 of CATO-2 focuses on caprock and fault integrity, namely on the response of the reservoir-caprock-fault system to injection and storage of CO_2. Experimental studies under WP 3.03 (as well as WP 3.02 on Reservoir Behaviour and WP 3.04 on Wellbore Integrity) accordingly require representative samples of caprocks, reservoir rocks and fault rocks, the last of which often contain components of the other two. In particular, site-specific experimental studies require cm- to dm-sized samples of the underground reservoir rocks and their sealing cap rocks. These studies must address the complex interactions of thermo-mechanical and chemical effects on the reservoir-seal system that may result from injecting CO_2 rich fluids.

Obtaining the necessary information and material from specific sites presents a problem of its own, in that very little actual rock material is available from the earlier drilling operations. However, detailed information on the rock formations is often present in proprietary reports by the well operators. The lack of material to make test samples requires alternative sources of equivalent rocks to be obtained from accessible geological sites such as outcrops on land, or from drilling operation in similar formations where more samples were taken. Once such material is located it must be examined and characterized to assess its suitability and equivalence to the actual in situ material of the target reservoir-seal system. Similarity in mineralogy, grain structure, porosity and permeability are just a few factors which, ideally, need to match the site specific material properties.

Unfortunately the natural environment is heterogeneous and lateral variation in geology is the rule rather than the exception. At UU we have called upon archived material held at NAM (Assen) and TNO (Zeist) to provide site-specific caprock and reservoir samples, as well as similar materials from nearby boreholes for comparative study. Attention to date has focused on reservoir and caprock material from the Bunter sandstone reservoirs and overlying Solling/Röt caprock formations found in the TAQA P18 field and in the nearby Q16 field. The available samples of these units have been characterised by means of microstructual, petrographic and X-ray diffraction analysis and their permeabilities have been measured. Approximately equivalent material from the Triassic Buntersandstein of Germany has been collected and characterised, for comparison with P18 and Q16 material, and as a potential source of larger volumes of sample material. TUD has performed a similar characterisation study of cap rocks from the Carboniferous and Cretaceous for comparison with onshore underground sites, notably the DSM site in Carboniferous strata.

The reports of UU and TUD are combined via Parts I and II of this report to create this deliverable D06 to WorkPackage 3.03 of CATO-2. Characterisation work on Zechstein anhydrite caprock used by the UU team in the experimental programme on Rotliegend reservoir topseal integrity (WP3.03-D-08) has been reported in earlier publications and in D-08.

Distribution List

(this section shows the initial distribution list)

External	copies	Internal	Copies

Document Change Record

(this section shows the historical versions, with a short description of the updates)

Version	Nr of pages	Short description of change	Pages

Table of Content

2 Applicable/Reference documents and Abbreviations

2.1 Applicable Documents

(Applicable Documents, including their version, are documents that are the "legal" basis to the work performed)

	Title	Doc nr	Version date
AD-01	Beschikking (Subsidieverlening CATO-2 programma verplichtingnummer 1-6843	ET/ED/9078040	2009.07.09
AD-02	Consortium Agreement	CATO-2-CA	2009.09.07
AD-03	Program Plan	CATO2-WP0.A-D.03	2009.09.29

2.2 Reference Documents

(Reference Documents are referred to in the document)

	Title	Doc nr	Issue/version	date

2.3 Abbreviations

(this refers to abbreviations used in this document)

3 General Text

Deliverable WP3.03 D06

Progress report on: Site-representative cap rock and fault rock samples acquired and characterised.

Part 1: Contribution from Utrecht University

By Colin J. Peach, J. H. P. de Bresser, R. F. M. van de Kroef, A. Mols, B. A. Verbene, and J. Samuelson

High Pressure and Temperature Laboratory, Utrecht University
31st August 2010.

1. Introduction and aims

1.1. Need for sample material and its characterisation

The experimental work which forms the UU contributions to CATO2 workpackage 3.3 and also packages 3.2 & 3.4 all require site-specific geological material for testing purposes. Particular interest is directed at material relevant to the hydrocarbon reservoirs of the near offshore sector P18 of the North Sea, west of Rotterdam. These fields (see Figure 1) are currently under operation by TAQA (Saudi Aramco) and soon to be depleted, offering an opportunity for future CO_2 storage.

Experimentation, in particular the testing of mechanical behaviour (faulting, compaction etc., with and without CO_2 fluids), requires more material than is directly available from existing cores, recovered during offshore the original drilling operations. Alternative sources of material have therefore been sought. It is important that this material is representative of the *in situ* reservoir and sealing cap rocks. Whilst some material from archived cores in the stores of TNO and NAM has been made available, it has been necessary to search onshore for equivalent geological formations to fulfil our requirements.

The acquisition, characterisation and comparison of material from the offshore P18 field (including nearby wells) with any potential onshore equivalents forms the primary aim of this deliverable.

1.2. Specific site of interest and location of reservoir P18

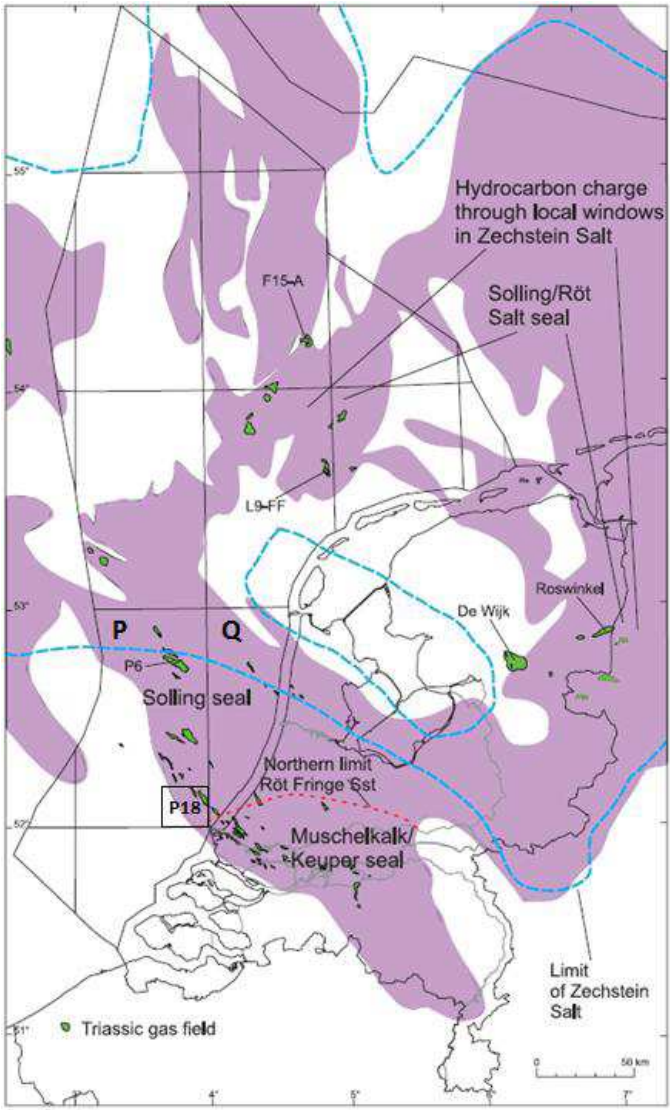

Figure 1: *Near offshore gas fields in Triassic rocks showing location of the P18 quadrant. The cap rock seal for these particular gas fields is the Lower Triassic Solling formation. The extent of the main Buntsandstein Subgroup is shown (purple). The blue dashed line indicates the "zero salt line" (modified from de Jager & Geluk, 2007).*

Reservoir rocks of Lower Triassic age (Main Buntsandstein) form the near offshore P18 gas field in the North Sea – currently operated by TAQA (Saudi Aramco). The P18 field is located at the SE corner of the P quadrant offshore from the Western Netherlands (see Figure 1) and has a potential storage capacity of 10-20 Mt (van Egmond et al., 2009). Wells P18A-05 and P18A-07 have been considered for CO_2 injection. Core material and data, taken in the past from the P18-02 and P18-02-A01 together with nearby material from Q16-04 and Q16-FA101-S wells, forms the basis for our comparisons with equivalent material from other onshore sources. The depths and geological formations hosting these gas fields are indicated in Table 1 which serves to show the close similarity in lithostratigraphy between the near offshore target fields around P18 and the nearby Q16 fields that share the common sealing formation (Solling Fm).

Cap- & Fault rock samples

P18-A-05

Kickoff Depth (m)	Bottom Hole Depth (m)	Stratigraphic Unit
0	974	North Sea Supergroup
974	2280	Ommelanden Formation
2280	2348	Texel Marlstone Member
2348	2440	Texel Greensand Member
2440	2726	Upper Holland Marl Member
2726	2812	Middle Holland Claystone Member
2812	2924	Holland Greensand Member
2924	3064	Lower Holland Marl Member
3064	3431	Vlieland Claystone Formation
3431	3462	Berkel Sandstone Member
3462	3549	Berkel Sand-Claystone Member
3549	3618	Rijswijk Member
3618	3717	Nieuwerkerk Formation
3717	4057	Lower Werkendam Member
4057	4487	Aalburg Formation
4487	4553	Sleen Formation
4553	4562	Upper Keuper Claystone Member
4562	4600	Dolomitic Keuper Member
4600	4610	Red Keuper Claystone Member
4610	4654	Upper Muschelkalk Member
4654	4667	Middle Muschelkalk Marl Member
4667	4681	Muschelkalk Evaporite Member
4681	4727	Lower Muschelkalk Member
4727	4775	Röt Claystone Member
4775	4787	Main Röt Evaporite Member
4787	4796	Solling Claystone Member
4796	4800	Basal Solling Sandstone Member
4800	4836	Hardegsen Formation
4836	4918	Upper Detfurth Sandstone Member
4918	4928	Lower Detfurth Sandstone Member
4928	5040	Upper Volpriehausen Sandstone Member
5040	5123	Lower Volpriehausen Sandstone Member
5123	5230	Rogenstein Member

P18-A-07-S1

Kickoff Depth (m)	Bottom Hole Depth (m)	Stratigraphic Unit
0	548	Upper North Sea Group
548	609	Vessem Member
609	862	Dongen Formation
862	1001	Landen Formation
1001	1883	Ommelanden Formation
Sidetrack		
1045	2140	Ommelanden Formation
2140	2203	Texel Marlstone Member
2203	2310	Texel Greensand Member
2310	2510	Upper Holland Marl Member
2510	2617	Middle Holland Claystone Member
2617	2740	Holland Greensand Member
2740	2887	Lower Holland Marl Member
2887	3266	Vlieland Claystone Formation
3266	3299	Berkel Sandstone Member
3299	3384	Berkel Sand-Claystone Member
3384	3478	Rijn Member
3478	3798	Alblasserdam Member
3798	4121	Werkendam Formation
4121	4199	Posidonia Shale Formation
4199	4730	Aalburg Formation
4730	4783	Sleen Formation
4783	4877	Keuper Formation
4877	4944	Muschelkalk Formation
4944	4954	Röt Formation
4954	4971	Solling Formation
4971	5002	Hardegsen Formation
5002	5052	Upper Detfurth Sandstone Member
5052	5066	Lower Detfurth Sandstone Member

Q16-04

Kickoff Depth (m)	Bottom Hole Depth (m)	Stratigraphic Unit
0	483	Upper North Sea Group
483	510	Middle North Sea Group
510	751	Lower North Sea Group
751	770	Ekofisk Formation
770	1407	Ommelanden Formation
1407	1459	Texel Formation
1459	1510	Texel Greensand Member
1510	1688	Upper Holland Marl Member
1688	1759	Middle Holland Claystone Member
1759	1797	Holland Greensand Member
1797	1865	Lower Holland Marl Member
1865	2106	Vlieland Claystone Formation
2106	2158	Berkel Sand-Claystone Member
2158	2169	Rijswijk Member
2169	2350	Werkendam Formation
2350	2385	Posidonia Shale Formation
2385	2850	Aalburg Formation
2850	2896	Sleen Formation
2896	2910	Upper Keuper Claystone Member
2910	2933	Dolomitic Keuper Member
2933	2943	Red Keuper Claystone Member
2943	2962	Upper Muschelkalk Member
2962	2981	Middle Muschelkalk Marl Member
2981	2987	Muschelkalk Evaporite Member
2987	3039	Lower Muschelkalk Member
3039	3064	Röt Claystone Member
3064	3071	Solling Claystone Member
3071	3076	Basal Solling Sandstone Member
3076	3136	Hardegsen Formation
3136	3162	Detfurth Claystone Member
3162	3167	Lower Detfurth Sandstone Member
3167	3216	Volpriehausen Clay-Siltstone Member
3216	3276	Lower Volpriehausen Sandstone Member
3276	3360	Rogenstein Member
3360	3462	Main Claystone Member
3462	3467	Zechstein Upper Claystone Formation
3467	3475	Z3 Fringe Sandstone Member
3475	3496	Z2 Fringe Sandstone Member
3496	3508	Z1 Fringe Sandstone Member
3508	3515	Z1 Lower Claystone Member
3515	3517	Fringe Coppershale Member
3517	3525	Slochteren Formation
3525	3714	Hellevoetsluis Formation
3714	3839	Maurits Formation

Q16-FA-101-S1

Kickoff Depth (m)	Bottom Hole Depth (m)	Stratigraphic Unit
0	476	Upper North Sea Group
476	516	Rupel Formation
516	822	Ieper Member
822	844	Basal Dongen Tuffite Member
844	897	Landen Clay Member
897	1657	Ommelanden Formation
1657	1702	Texel Marlstone Member
1702	1731	Texel Greensand Member
1731	1857	Upper Holland Marl Member
1857	1911	Middle Holland Claystone Member
1911	1967	Holland Greensand Member
1967	2098	Lower Holland Marl Member
2098	2216	De Lier Member
2216	2338	Eemhaven Member
2338	2367	IJsselmonde Sandstone Member
2367	2415	IJsselmonde Claystone Member
2415	2460	Berkel Sandstone Member
2460	2467	Berkel Sand-Claystone Member
2467	2520	Rijswijk Member
2520	2699	Nieuwerkerk Formation
2699	2716	Posidonia Shale Formation
2716	3117	Aalburg Formation
3117	3148	Sleen Formation
3148	3158	Upper Keuper Claystone Member
3158	3185	Dolomitic Keuper Member
3185	3192	Red Keuper Claystone Member
3192	3210	Upper Muschelkalk Member
3210	3221	Middle Muschelkalk Marl Member
3221	3226	Muschelkalk Evaporite Member
3226	3271	Lower Muschelkalk Member
3271	3292	Röt Claystone Member
3292	3302	Solling Claystone Member
3302	3304	Basal Solling Sandstone Member
3304	3374	Hardegsen Formation
3374	3399	Detfurth Claystone Member
3399	3405	Lower Detfurth Sandstone Member
3405	3451	Volpriehausen Clay-Siltstone Member
3451	3508	Lower Volpriehausen Sandstone Member
3508	3570	Rogenstein Member
3570	3636	Main Claystone Member
3636	3645	Zechstein Upper Claystone Formation
3645	3651	Z3 Fringe Sandstone Member
3651	3655	Grey Salt Clay Member
3655	3668	Z2 Fringe Sandstone Member
3668	3686	Z1 Fringe Sandstone Member
3686	3690	Z1 Fringe Carbonate Member
3690	3701	Coppershale Member
3701	3705	Slochteren Formation
3705	3970	Strijen Formation
3970	4023	Hellevoetsluis Formation
4023	4060	Maurits Formation

Table 1: *Lithostratigraphy of wells P18-A-05 and P18-A-07 (considered for CO2 injection), and Q16-04 and Q16-FA-101-S1 (used for cap rock sampling in this study). Note the common stratigraphy but different depth ranges of the reservoir (Volpriehausen, Detfurth, Hardegsen formations) and cap rock (Solling and Röt formations) in the different wells.*

1.3. Strategy for acquisition of material

Core material, held by TNO (Zeist) includes cored intervals from wells P18-02-A01 (Detfurth sandstone) and P18-02 (Volpriehausen and Hardegsen formations) from the upper part of the reservoir and intervals of core Q16-4 (Solling and Röt formations) of the cap rock sequences, was kindly made available for observation and limited sampling. Some petrophysical data and characterisation was available in the accompanying reports from Amoco Core Analysis Reports (CAR).

A further set of offshore core material Q16-FA-101-S1 (Röt formation) was made available to us by the NAM at Assen. This material included the cap rock sequence a little above the reservoir seal boundary. The lowest part of this sequence is shown in Figure 2 and consists of dark marly mudstones that are expected to be similar to the cap rocks that form the P18 reservoir seal.

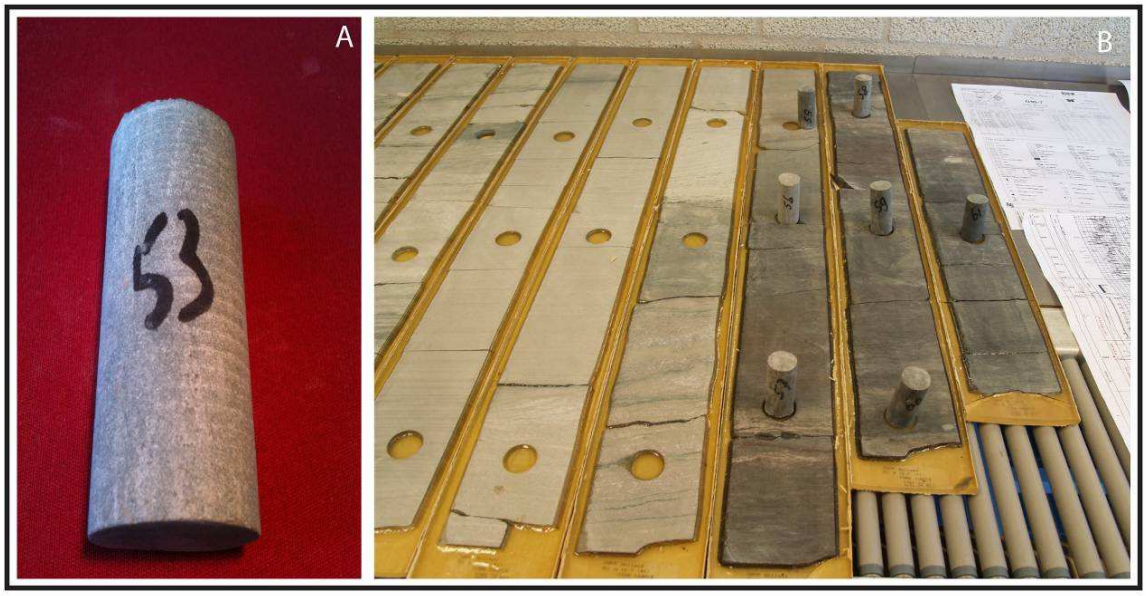

Figure 2: A. *Cap rock plug-core sample 53 with a diameter of roughly 25 mm.* ***B.*** *Complete well core retrieved from well Q-16-FA-101-S1, displayed at the NAM core repository in Assen. The dark cores standing upright, originating from the Röt formation, were sampled as cap rock material for this study.(Deepest material is on the right and up is away from the viewer)*

The material obtained from the NAM core store was sufficient for a few basic petrophysical and chemical tests but the need for larger samples, suitable for mechanical tests, remained. Therefore it was necessary to search for onshore equivalent material and a short field excursion was planned and executed in April 2010 to the Northern German Eifel area where the Buntsandstein, group of formations, outcrop in accessible quarries. The Buntsandstein formations (Volpriehausen, Detfurth and Hardegsen) that outcrop there are believed to be directly correlated with those of the P18 field (Ames and Farfan, 1996). These field observations and samples were used in comparison with the offshore reservoir data and material to assess their representative status.

Recently, material was also collected for us by colleagues at TU Delft from Eastern Germany and detailed characterisation of this material is yet to be performed. Preliminary assessment shows this to be too coarse grained and permeable to be a directly equivalent cap rock. The materials have a similar stratigraphy but different source area for the sediment.

1.4. Characterisation parameters required for CATO2 research

The composition and microstructure of the samples is an important quantity for any interpretation of CO_2 injection induced changes in the rock material. Likewise, the same information is required to validate the representative status or true equivalence of the onshore-collected material with respect to the *in situ*, site specific, rock formations. Basic optical microscopy and petrographical analysis of sample thin sections was performed together with X-ray diffraction (XRD) analysis of bulk mineralogy where required. Particular attention was given to the characteristics of grain cement and amount of chemical components likely to react with CO_2 rich fluids under the reservoir injection conditions (e.g. carbonate minerals and other less reactive but potentially useful longer term carbonate forming (carbon fixation) components such as feldspar (see Liteanu, 2009, and Hangx and Spiers, 2009).
In addition to microstructural analysis, the basic petrophysical properties such as permeability and porosity were measured to obtain the fluid transport properties, where not already available in core analysis reports. This was especially necessary for the newly collected material and cap rocks from the well cores.

2. Actual core material from offshore P18 field

2.1. Geological setting and stratigraphical position of material

The gas reservoirs in the P18 field are situated in the Lower Triassic Buntsandstein series. The geological setting for these highly porous reservoir sandstones and low permeability marl/mudstones forming the cap rock is comprehensively described by Geluk, 2007.

2.1.1. Basic geological history

During the Triassic and Jurassic the structural outline of the Netherlands progressively changed from one single, extensive basin, the Southern Permian Basin, into a complicated pattern of smaller, fault-bounded basins and highs (Figure 3; Wong, 2007). This change to a multi-basinal pattern is associated with the disintegration of Pangea (Ziegler, 1990) and occurred in several extensional phases (Wong, 2007): Hardegsen (Scythian), Early Kimmerian, Mid Kimmerian (Aalenian-Callovian/Oxfordian) and Late Kimmerian (Kimmeridgian-Ryazanian). The Hardegsen phase and Early Kimmerian phase took place during the Triassic and the Mid and Late Kimmerian phases during the Jurassic. The intervals in between these phases were characterized by regional, thermal subsidence that is recognized in the sedimentation pattern. It led to broad, regular facies patterns, interrupted locally by halokinesis which became widespread after the Early Triassic (de Jager, 2007).

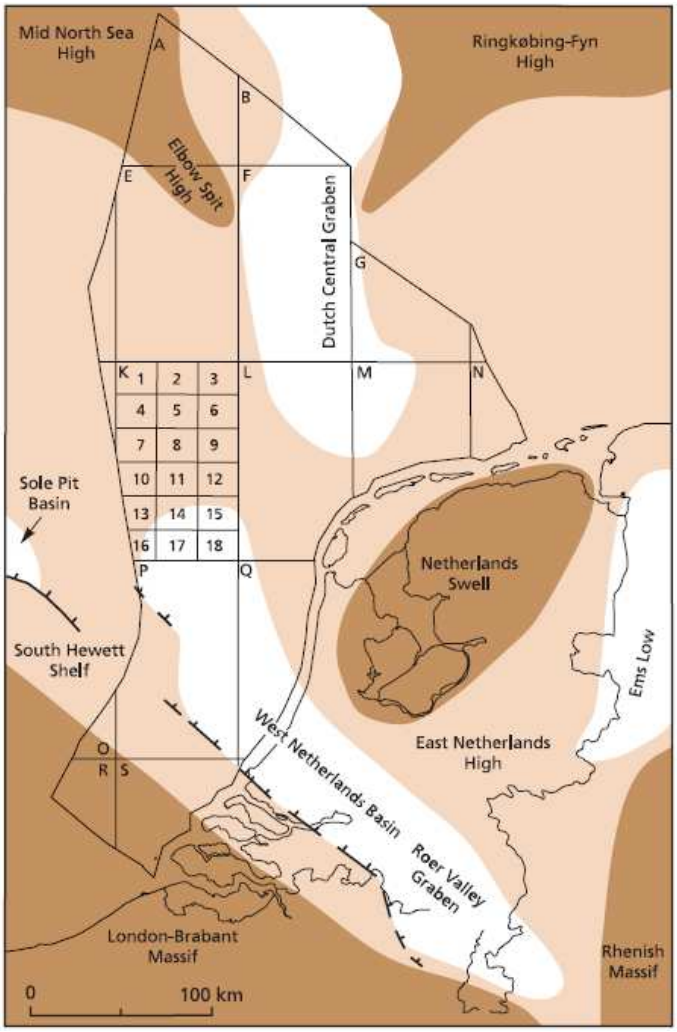

***Figure 3**: Map of the latest Triassic to Middle Jurassic structural elements in the Netherlands. Dark brown: structural high, partly subaerial landmass; light brown: platform, intermittently flooded; white: basin (Wong, 2007).*

2.1.2. Stratigraphical setting

The Triassic rocks can be subdivided into two groups (Table 2; Geluk, 2007), the *Lower Germanic Trias Group* - mainly fine-grained clastic deposits with sandstone and oolite intercalations and consisting at the southern basin margin predominantly of sandstones - and the *Upper Germanic Trias Group*, an alternation of fine-grained clastics, carbonates and evaporites with subordinate sandstones. The Lower Germanic Trias Group comprises widely distributed sandstones which form the second most important hydrocarbon reservoirs in the Netherlands. They originate from the south, containing progressively more shales towards the north and were deposited in fluvial and aeolian settings (de Jager & Geluk, 2007). Producing fields occur in the east Netherlands, in the West Netherlands Basin, and in the northern and western offshore (Figure 1). The top seal of these reservoirs is formed in most cases by the shales of the Upper Germanic Trias Group and where the Triassic is truncated, by shales of the Lower Cretaceous (de Jager & Geluk, 2007).

Lower Germanic Trias Group:

The Lower Germanic Trias Group is divided into the Lower and Main Buntsandstein. The Lower Buntsandstein formation is composed of a cyclic alternation of fine-grained lacustrine sandstone and clay-siltstones, which form stacked fining-upward sequences (Geluk, 2007). This formation is overlain by the Main Buntsandstein, which is subdivided into the Volpriehausen, Detfurth and Hardegsen formations. It displays a cyclic alternation of (sub-) arkosic sandstones and clayey siltstones organized in large scale fining upward sequences (Geluk, 2007). The original distribution and thickness of the Main Buntsandstein Formation was modified by two phases of erosion (Ames & Farfan, 1996). During the Early Triassic it was partly eroded and unconformably covered by the Late Triassic (Hardegsen phase). During this phase four short lived rift pulses occurred (Geluk & Röhling, 1999). The next phase of modification was the Kimmerian, during the Late Jurassic and Early Cretaceous. Uplifts partly or totally denuded some areas and fault blocks of the Triassic sediments (Ames & Farfan, 1996). This resulted in preservation of the Main Buntsandstein only in the central and western parts of the Broad Fourteens and West Netherland Basins (see Figure 1). The Main Buntsandstein in this area can be subdivided into two stratigraphic provinces according to the "zero salt line", an east-west line which broadly corresponds to the southern limit of underlying Zechstein evaporites. South of this line lithostratigraphic subdivision of the Main Buntsandstein is more difficult, as siltstone and claystone beds grade into sandstones (Ames & Farfan, 1996). However the Main Buntsandstein can still be subdivided into five members: the Volpriehausen Sandstone, the Volpriehausen Clay-siltstone, the Detfurth Sandstone, the Detfurth Claystone and the Hardegsen Sandstone (Table 2). In the southern Netherlands and the UK southern North Sea, the Main Buntsandstein Formation is entirely sandy (Geluk, 2007 on cit. Cameron et al., 1992; Johnson et al., 1994; Geluk et al., 1996). The sandstones are mainly fluvial in the south and grade northward into predominantly aeolian deposits (Geluk 2007, on cit., Fontaine et al., 1993, Ames & Farfan, 1996). The clay-siltstones are playa-lake deposits (Figure 4). The Main Buntsandstein reaches a thickness of 350 m offshore the western Netherlands (Geluk, 2007). Within the P quadrant it ranges between 100 and 300 m and in the P18 field it has a thickness of 100-250 m (Figure 5A).

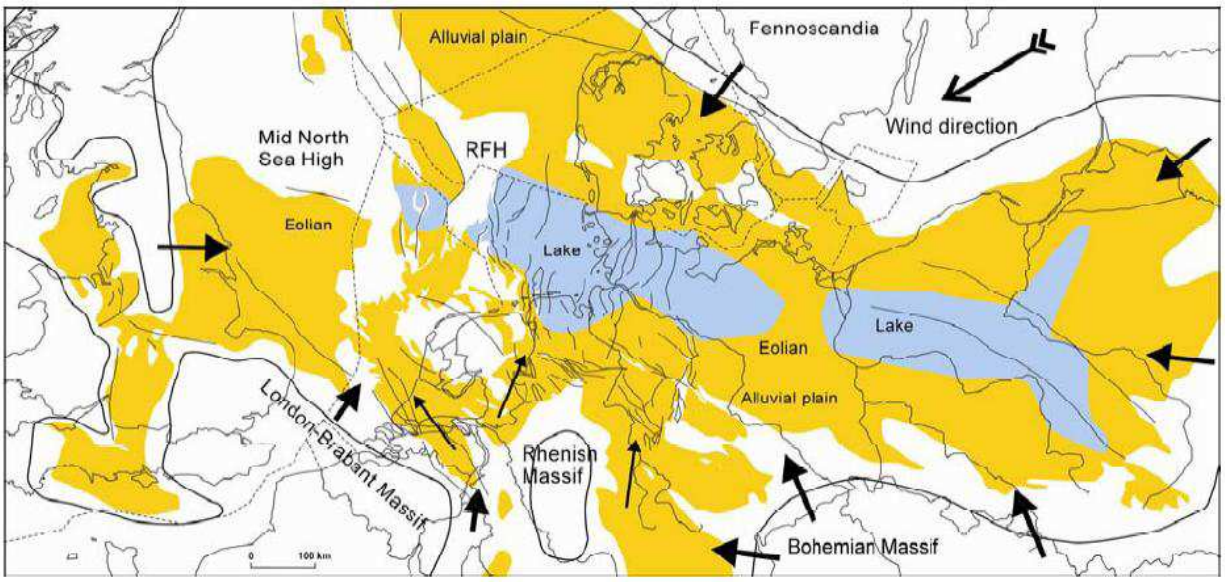

Figure 4: *Present-day distribution and facies map of the Main Buntsandstein. Extensive, sandy alluvial plains bordered a lake which occupied the deepest parts of the basin. The facies shown is approximately for the Volpriehausen Sandstone. Thick arrows represent clastic influx, thin arrows the approximate orientation of fluvial systems. The prevailing wind direction was from the north-east. Solid lines represent the reconstructed basin outline. Black lines represent active faults (Geluk, 2005).*

Stage	Age (Ma)	Sequence	UK southern North Sea	Netherlands Formation	Netherlands Member	NW Germany	Tectonics
Triassic Late Rhaetian	200		Penarth Group	Sleen Fm		Mittelrhät	EK II
Late Norian	204			upper Keuper	Upper Keuper Claystone Dolomitic Keuper Red Keuper Claystone	Unterrhät Steinmergelkeuper	
Late Carnian	218		Triton Fm	Keuper Fm			EK I
Middle Ladinian	228		Haisborough Group Dudgeon Fm	lower + middle Keuper	Red Keuper Evaporite Middle Keuper Claystone Main Keuper Evaporite Lower Keuper Claystone	Oberer Gipskeuper Schilfsandstein Unterer Gipskeuper Lettenkeuper	
Middle Anisian	237		Dowsing Fm	Muschelkalk Fm	Upper Muschelkalk *Middle Muschelkalk** Lower Muschelkalk	Oberer Muschelkalk Mittlerer Muschelkalk Unterer Muschelkalk	
Middle Anisian	245			Röt Fm	Upper Röt Claystone Upper Röt Evaporite Intermed. Röt Claystone Main Röt Evaporite	Pelitröt-Folge Salinarröt-Folge	
Middle Anisian				Solling Fm	Solling Claystone Basal Solling Sandstone	Solling-Folge	H
Early Olenekian			Bunter Sandstone Fm	Hardegsen Fm		Hardegsen-Folge	
Early (Scythian)		Milankovitch cycles	Bacton Group	Detfurth Fm	Detfurth Claystone Low. Detfurth Sandstone	Detfurth-Wechselfolge Detfurth-Sandstein	
Early (Scythian)				Volpriehausen Fm	Volpriehausen Clay-Siltstone Low. Volprieh. Sandstone	Volpriehausen-Wechself. Volpriehausen-Sandstein Quickborn-Folge	
Early Induan	251		Bunter Shale Fm	Lower Buntsandstein Fm	Rogenstein Main Claystone	Bernburg-Folge Calvörde-Folge	
Permian				Zechstein Upper Claystone Fm		Zechstein-Übergangsfolge	

Upper Germanic Trias Group; Lower Germanic Trias Group; Main Buntsandstein; Middle Buntsandstein

Table 2: *Stratigraphic subdivision of the Triassic in the Netherlands and adjacent countries (Geluk, 2007).*

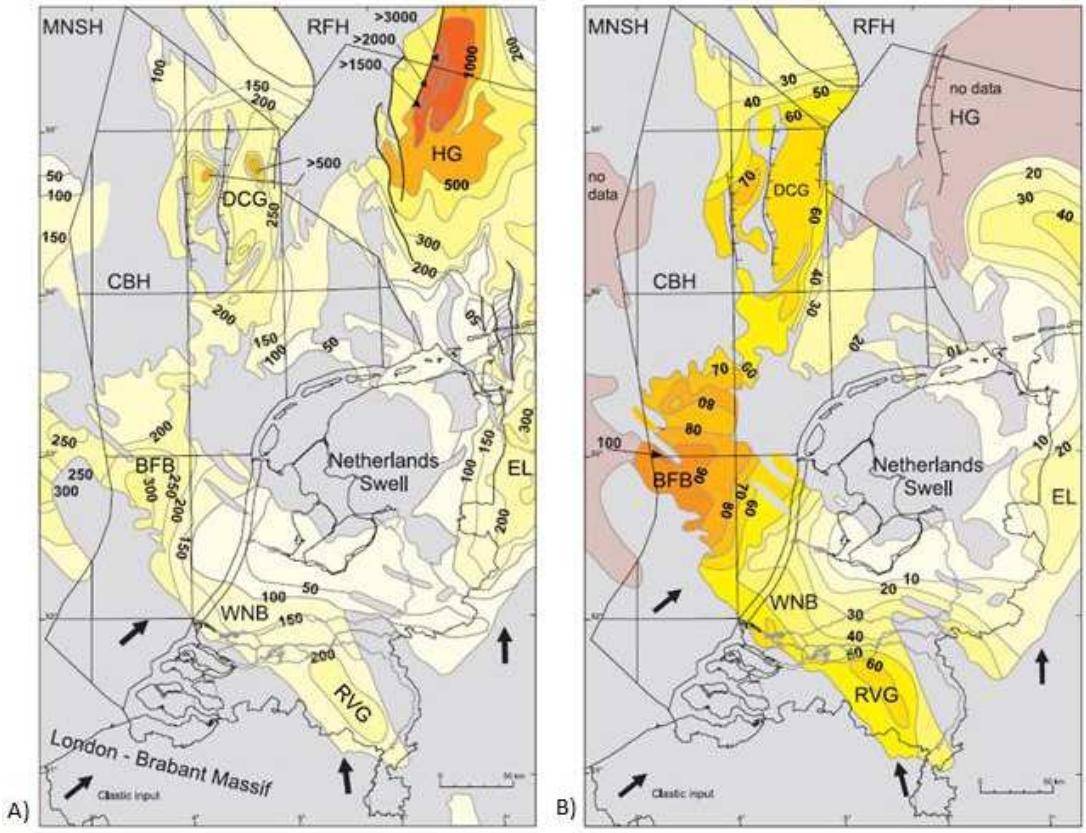

Figure 5: A) *Isopach map (in meters) of the Main Buntsandstein Formation.* ***B)*** *Isopach map (in meters) of the Lower Volpriehausen Sandstone. Abbrevations: BFB: Broad Fourteens Basin; CBH: Cleaverbank High; CNB: Central Netherlands Basin; CNG: Central North Sea Graben; DFZ: Dowsing Fault Zone; DCG: Dutch Central Graben; EL: Ems Low; HG: Horn Graben; LBM: London-Brabant Massif; MNFZ: Mid Netherlands Fault Zone; MNSH: Mid North Sea High; NDFZ: North Dogger Fault Zone; RFH: Ringkøbing-Fyn High; RM: Rhenish Massif; RVG: Roer Valley Graben; WNB: West Netherlands Basin. (Geluk, 2007).*

Volpriehausen formation:

This formation forms the base of the Main Buntsandstein group (Table 2). Its greatest thickness, over 200 m, can be found in the Dutch Central Graben and the Broad Fourteens Basin. It reaches 100 m in the Ems Low and 150 m in the Roer Valley Graben (Geluk, 2007). The Volpriehausen unconformity - related to the tectonic activity in the Triassic, locally cuts several meters through the Lower Buntsandstein Formation. As mentioned above the Volpriehausen can be subdivided in two members, the Lower Volpriehausen Sandstone and the Volpriehausen Clay-Siltstone. The sandstone member displays marked differences in thickness (Figure 5B). It varies between 50 and 100 m within the P quadrant offshore the Netherlands and displays a thickness of approximately 50 to 60 m in the P18 field (Figure 5B). The sandstone is arkosic, with a quartz-content slightly below 50%. It is cemented by high percentages of calcite and dolomite, especially in its lower part (Geluk, 2007). The second (clay-siltstone) member consists mainly of lacustrine siltstones and marls, with subordinate sandstones which are more fine-grained than the Lower Volpriehausen Sandstone and cemented by dolomite, calcite and ankerite. A number of carbonate oolite beds occur (Geluk, 2007). In the southern offshore the siltstones grade into fluvial and eolian sandstones (Ames and Farfan, 1996). Considerable variations in thickness are observed.

Detfurth formation:
The Volpriehausen is overlain by the Detfurth Formation, which is subdivided into the Detfurth Sandstone and the Detfurth Claystone. At the base, an unconformity cuts into the Volpriehausen Formation which was induced due to tectonic activity (Table 2). In the southern and western offshore areas of the Netherlands this unconformity is the most prominent one in the Buntsandstein (Geluk et al., 1996, Geluk & Rhöling, 1999). The sandstone member displays a relatively high quartz-grain content (>50%) and is loosely quartz-cemented (Geluk, 2007). In the basin margin area, the sandstone is one of the best hydrocarbon reservoirs in the Main Buntsandstein Formation. Within the P quadrant it displays a thickness of 10-30 m and the P18 field approximately 10-20m (Figure 6). The Claystone member follows the thickness trend of the Lower Detfurth Sandstone. It consists of claystones, with thin intercalations of siltstone (Geluk, 2007). These claystones grade laterally into aeolian sandstones in the southern offshore and onshore (Ames and Farfan, 1996).

Hardegsen formation:
The Hardegsen Formation forms the top of the Main Buntsandstein Formation. It is composed predominantly of siltstones with subordinate, thin sandstone beds (Geluk, 2007). Significant amounts of sandstone occur only in the basin-margin area. The distribution and thickness of this formation was strongly modified by pre-Solling erosion, which caused strong thickness variation. In the Broad Fourteens Basin, the West Netherlands Basin and the Roer Valley Graben, the thickness reaches up to 70 m (Geluk, 2007).

Upper Germanic Trias Group:
The Upper Germanic Trias Groups comprises the Solling, Röt, Muschelkalk and Keuper formations (Table 2). The base Solling Unconformity forms the base of the group and was induced by the last tectonic pulse of the Hardegsen phase (Figure 7; Geluk, 2007). The thickness of deposition of the Röt, Muschelkalk and Keuper formations is determined by the Early Kimmerian phase which comprises up to five tectonic pulses (Table 2; Wolburg, 1967, Beutler, 1995). This led to two unconformities; the first at the base of the Red Keuper Claystone (Early Kimmerian I; Table 2) and the second at the base of the Sleen Formation (Early Kimmerian II; Table 2). The Solling Formation consists of a basal-sandstone, overlain by a succession of siltstones and claystones (Table 2; Geluk, 2007). This is overlain by the Röt Formation which comprises a lower evaporitic part and an upper part dominated by clay and siltstones (Table 2; Geluk, 2007). The Röt Formation is overlain by the Muschelkalk Formation which is a more marine interval. It comprises a lower and upper carbonate part and in between an evaporitic part. The carbonates comprise a cyclic alternation of limestones and marls (Table 2; Geluk, 2007). On top lies the Keuper Formation which is marked by claystones at its base with a low sonic velocity (Geluk, 2007). The lower part of the Keuper Formation comprises reddish and dark-coloured claystones, alternating with thin layers of dolomite, fine grained sandstone and coal. The middle consists of reddish claystones followed by anhydrite. The Upper part of the Keuper Formation is separated by the Early Kimmerian I Unconformity from the underlying Triassic (Table 2; Geluk, 2007) and comprises variegated clay and siltstones, light coloured micritic carbonates and dark coloured marls and claystones (Geluk, 2007).

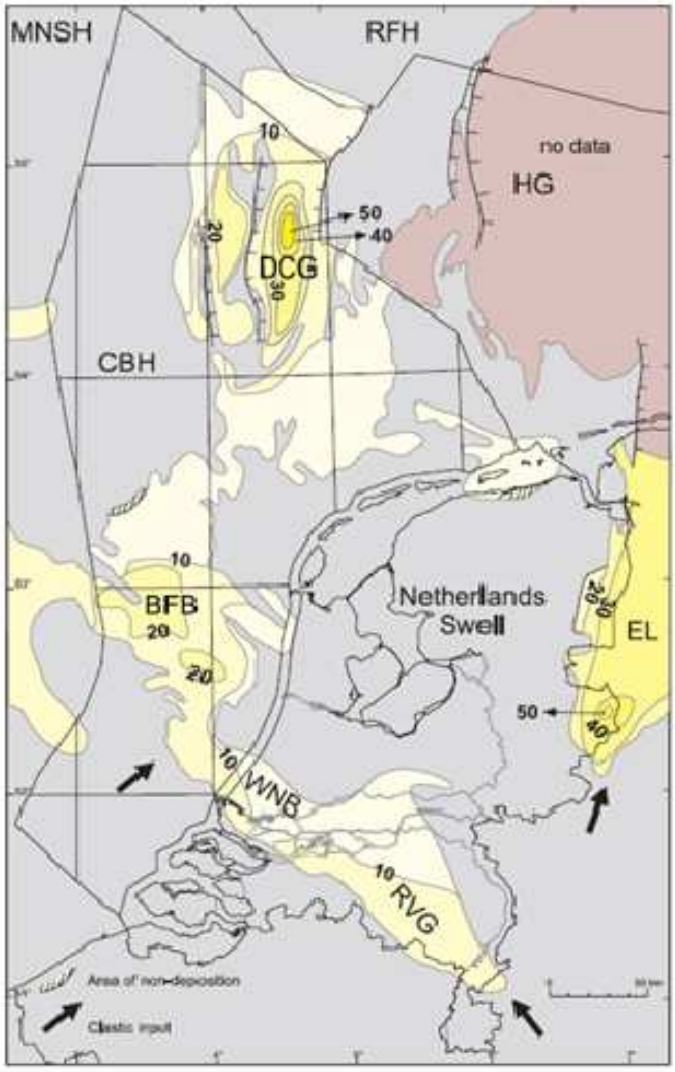

Figure 6: *Isopach map (in metres) of the Lower Detfurth Sandstone. Abbreviations as in Figure 5 (from Geluk, 2007).*

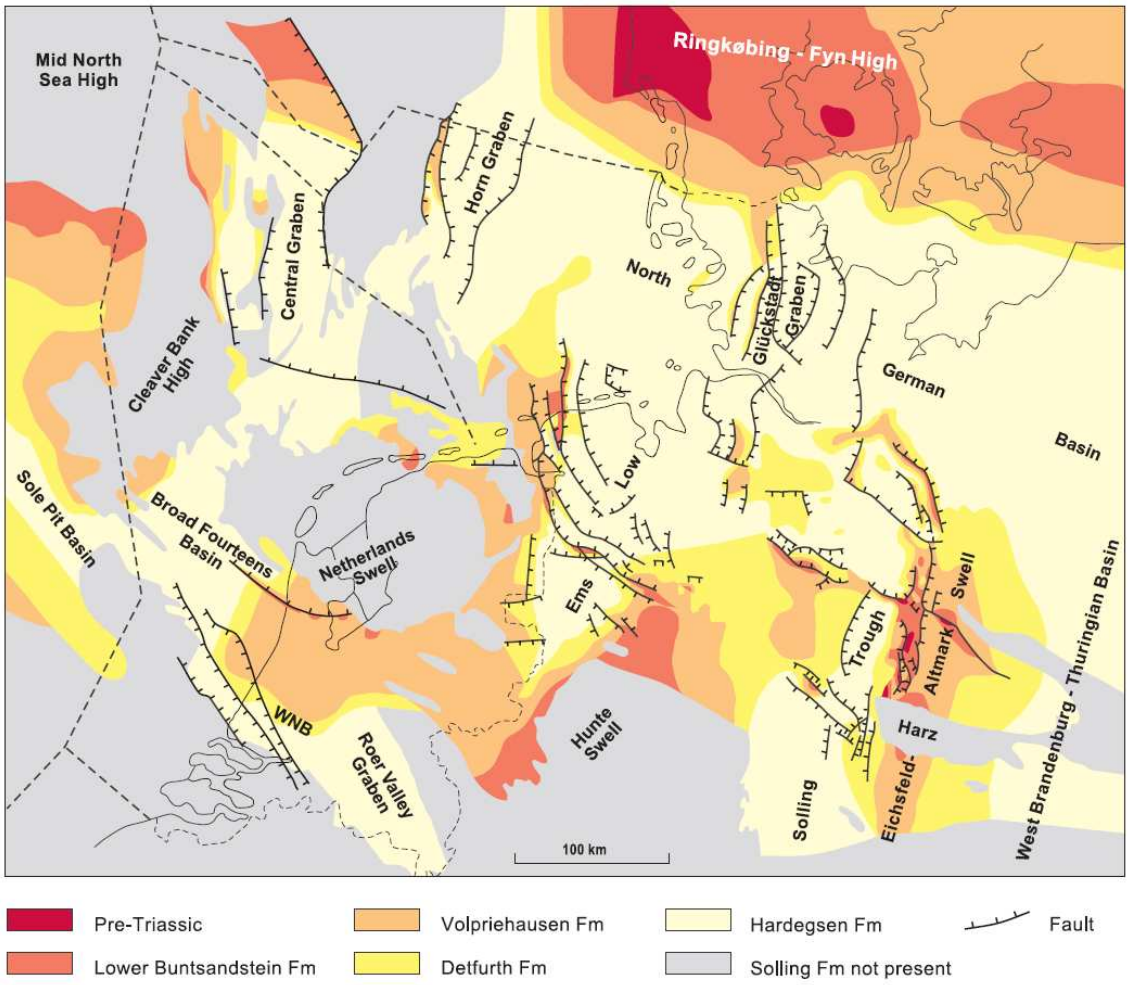

Figure 7: *Subcrop map of the Base Solling (= Hardegsen) Unconformity (Geluk, 2007).*

As can be seen from Figure 1 and Table 1, the P18 and Q16 gas fields are capped by the Solling formation at the base of the Upper Germanic Triassic group. The lithology is predominantly claystone of sufficiently low permeability to seal the high porosity/permeability aeolian reservoir sands of the Hardegsen formation. Further to the East, the sedimentary basin is continuous but the Solling becomes progressively sandier and more permeable so that the onshore reservoirs must be sealed by higher/younger shale formations such as the Muschelkalk Fm. This lateral variation makes the search for onshore equivalents of the P18 cap rock extremely difficult.

2.2. Description of cores and position of samples

Samples in the form of 25mm diameter plugs were drilled from the cores held at TNO (Zeist) and these were numbered "*n*a" or "*n*b" dependent upon whether the plugs were cored perpendicular or parallel to bedding, respectively. The remaining core material was returned to TNO. Core material from NAM (Assen) was plug sampled in a similar way although remaining material was retained for further experimentation. Such retained material carries the same sample number as its associated plug but without suffix (a or b). The interval depths and original descriptions of these well cores are documented in core analysis reports.

2.2.1. Core Analysis Reports (CAR); P18-field

At the time of original well drilling ~1989/90, Core Laboratories - Netherlands Branch - were requested by Amoco Netherlands Petroleum Company to perform a series of conventional core analysis measurements and services on several cores from the P18-02 and P18-02-A01 wells in the P quadrant offshore the western Netherlands. The results of these measurements were presented in two core analysis reports. Both reports include spectral core gamma, horizontal permeability - every 25 cm at 800, 2500, 4000 and 5300 psi confining pressure using the CMS 300, Vertical Permeability - every 1 meter at 800 psi confining pressure using CMS 300, Porosity - every 25 cm at 800, 2500, 4000 and 5300 psi confining pressure using CMS 300 and grain density measurements. The spectral core gamma system is capable of measuring the natural radioactivity from cores and enables accurate placement of the cored section within the well bore. CMS 300 - used for horizontal, vertical permeability and porosity is a core measurement system (model 300) which uses an integrated form of the combined Darcy, Klinkenberg and Forchheimer equations to accurately determine permeability from >1.48E-11 m^2 (15 Darcy) to <4.93E-20 m^2 (0.05 micro-Darcy). The permeability measurements made also include the Dykstra-Parsons Variation - a measure of the uniformity of permeability distribution throughout a zone and the Lorenz Coefficient - a value used for describing the permeability distribution within a zone. Both values can range from 0 to 1, with an exactly uniform set of data having a value of zero.
The permeability, Dykstra-Parson Variation, Lorenz Coefficient, porosity, mineralogy and lithology measurements of the different cores in the core analysis reports have been correlated - according to their depth with our samples obtained from the P18 field (Utrecht University (UU) samples 1-7), to give an indication of their characteristics (Tables 3-7). These materials are typical of the upper part of the gas reservoir. Similarly, samples from the Q16-4 and Q16-FA-101-S1 cores are represented by UU samples 8-15 and represent cap rock materials.

2.3. Previously known petrophysical data on correlated samples of reservoir rocks

Table 3 gives an overview of the UU reservoir rock samples from the P18 field and their correlated samples from the core analysis reports together with their core depths and formations. The core analysis reports comprise measurements of three cored intervals. Two from the P18-02 well (Hardegsen and Volpriehausen core) and one from the P18-02-A01 well (Detfurth core). The correlated results of the core analysis reports will be discussed per core.

UU Sample	*CAR sample*	*Well*	*Depth Interval (m)*	*CAR Core depth (m)*	*Formation*
1a	74 & 75	P18-02-A01	3644.33-3644.52	74: 3644,25	Detfurth
1b				75: 3644,5	
2a	59	P18-02-A01	3640.50-3640.61	3640,5	Detfurth
2b					
3a	2	P18-02-A01	3626.22-3626.38	3626,25	Detfurth
3b					
4b	97	P18-02	3442.53-3442.74	3442,69	Volpriehausen
5b	71	P18-02	3436.00-3436.36	3436,25	Volpriehausen
6b	46	P18-02	3295.00-3295.35	3295,25	Hardegsen
7b	14	P18-02	3287.00-3287.32	3287,25	Hardegsen

Table 3: *Overview of the UU reservoir rock samples that have been correlated with CAR report samples.*

2.3.1. Volpriehausen core

The approximately eight meter long core from the P18-02 well represents a part of the Volpriehausen formation (3434-3442.85 m). It has a porosity ranging from 3.1 to 7.4% and permeability between 9.87E-18 and 1.97E-15 m^2 with a median of 3.30E-15 m^2. The core has a Dykstra-Parsons Variation of 0.478 and a Lorenz Coefficient of 0.614 indicative for the heterogeneous character of the permeability distribution.
The core analysis measurements of this zone have been correlated with the UU samples - 4 and 5 from the P18 field (see Table 7). They show a relatively low porosity and permeability. The porosity ranges between approximately 4.7 to 6.8% and the permeability ranges from approximately 2.96E-17 to 1.14E-16 m^2 (Table 7). The permeability measurement of sample 4 is inaccurate as only one measurement at a confining pressure of 800 psi has been made. This had been done for a number of samples showing low permeability to speed up the data output. The correlated mineralogy of both samples seems to be similar, with a quartz content of 67% (Table 8). A description of the lithologies can be found in Table 5.

2.3.2. Detfurth core

From the P18-02-A01 well a core of approximately 25 m has been drilled (3626.00-3651.08 m) in the Bunter Sandstone Formation. According to the core analysis report, the core consists of very well cemented grey sandstone, very fine to fine grained and generally very well laminated. Abundant clay laminations and clay clasts occur in the bottom section of the core. Anhydrite occurs locally abundant in interval 3634.25-3634.55 m. A homogenous section occurs between 3637.00 and 3640.30 m, while a very heterogeneous section occurs between 3642.00 and 3646.75 m. This heterogeneous section shows a high variation in the permeability data, with a Dykstra-Parson Variation of 0.914 and a Lorenz Coefficient of 0.731. A red, very tight clay-rich section occurs at the bottom of the core between 3650.55 and 3651.08 m (CAR P18-02-A01, 1990). The core has a porosity ranging from 2.4 to 15.2% with a median of 9.5% and a permeability ranging from 1.48E-17 to 3.19E-13 m^2 with a median of 3.30E-15 m^2.
The core analysis measurements of this zone have been correlated with the samples - 1 through 3 from the P18 field (see Table 6). Sample 1 falls within the heterogeneous section of the Detfurth core. This makes correlation of the permeability difficult. When samples 1 is compared with the core photos of the core analysis report, permeability and porosity measurements of CAR sample 74 seem to give a better representation of the sample then CAR sample 75. Although CAR sample 74 does not fall within the depth interval. So to be more precise both results of CAR sample 74 and 75 are listed in Table 6. The correlation of sample 2 seems to be just below the homogenous section and sample 3 within the top of the core. The permeability for the three samples is between 8.49E-17 and 1.04E-14 m^2 and the porosity ranges between 7.4 and 13.5% (table 6). The correlated mineralogy of the samples seems to be approximately the same, with 67 to 78% quartz (see Table 8). For a description of the lithologies of the different samples see Table 5.

2.3.3. Hardegsen core

A core of approximately 15 m from the P18-02 well runs between 3284 and 3299 m. This has a porosity ranging from 4.7 to 23.1% with a median of 12.7%. The permeability is quite variable with tight and permeable bands ranging in the extremes from 4.84E-17 to 1.18E-11 m^2 (0.049 to 12000 md). The majority of the zone appears to be moderately permeable. It has

a Dykstra-Parsons Variation of 0.799 and a Lorenz Coefficient of 0.742, so the permeability throughout the core is quite heterogeneous.
The core analysis measurements of this core can be correlated with the samples - 6 and 7 from the P18 field (Table 7). UU sample 7 (CAR sample 14) shows the highest porosity and permeability. Although, it should be noted that according to the core analysis report, the samples directly above show a lower porosity (approximately two times smaller), the permeability changes approximately with one order of magnitude. Also, CAR sample 14 is reported with a K-berg permeability of 2.96E-12 m^2 (3000 md), however measurements indicate a higher permeability due to limitations in the CMS-300 software used. The report indicates that the K-berg permeability at 5.52 MPa confining pressure (800 psi) should be 1.22E-11 m^2 (12360 md), which is an order of magnitude higher than listed in Table 6. The correlated mineralogy of both samples is listed in Table 7, which are again alike and consistent with the samples of the other formations, although they show a slightly higher quartz content of 73 to 83%. For a description of the lithologies, see Table 4.

Lithological Description P18-02 & P18-02-A01 Well

Well	*Interval (m)/ Formation*	*UU Sample #*	*CAR Sample*	*CAR Core depth (m)*	*Lithological Description*
P18-02-A01	3644.33-3644.52 Detfurth	**1**	75	3644.5	Very well cemented grey sandstone, medium grained, siliceous/dolomitic and laminated
			74	3644.25	Very well cemented grey sandstone, fine to medium grained, siliceous/dolomitic and clay laminated
P18-02-A01	3640.50-3640.61 Detfurth	**2**	59	3640.5	Very well cemented dark grey sandstone, medium grained, siliceous/dolomitic and clay laminated
P18-02-A01	3626.22-3626.38 Detfurth	**3**	2	3626.25	Very well cemented grey sandstone, fine grained, siliceous/dolomitic and clay laminated
P18-02	3442.53-3442.74 Volpriehausen	**4**	97	3442.69	Very well cemented grey sandstone, very fine to fine grained, siliceous
P18-02	3436.00-3436.36 Volpriehausen	**5**	71	3436.25	Very well cemented grey sandstone, fine grained, siliceous
P18-02	3295.00-3295.35 Hardegsen	**6**	46	3295.25	Well cemented light grey sandstone, fine grained, siliceous
P18-02	3287.00-3287.32 Hardegsen	**7**	14	3287.25	Moderate cemented light grey sandstone, coarse grained, siliceous

Table 4: *Overview of the lithological descriptions according to the core analysis reports correlated with the new samples from the P18 field (sample 1-7). (CAR P18-02,1989 & CAR P18-02-A01,1990)*

Porosity & Permeability data P18-02-A01 Detfurth

CAR = Core Analysis Report. The data below is measured from cores taken in the past.

Well	Interval (m)/ Formation	UU Sample #	CAR Sample	CAR Core depth (m)	Conf. pressure		Porosity	K-berg permeability		Gas permeability		K-berg slip factor	
					PSI	MPa	%	mD	m2	mD	m2	PSI	MPa
P18-02-A01	3644.33-3644.52 Detfurth	**1**	75	3644.5	800	5.52	13.5	26.8	2.64E-14	28.3	2.8E-14	2.95	0.0203
					2500	17.24	13	24.8	2.45E-14	26.2	2.6E-14	2.88	0.0199
					4000	27.58	12.8	23.8	2.35E-14	25.1	2.5E-14	2.88	0.0199
					5475	37.75	12.7	23.2	2.29E-14	24.5	2.4E-14	2.85	0.0197
			74	3644.25	800	5.52	8.1	0.309	3.05E-16	0.44	4.3E-16	28.95	0.1996
					2500	17.24	7.7	0.198	1.95E-16	0.288	2.8E-16	30.75	0.212
					4000	27.58	7.5	0.168	1.66E-16	0.238	2.3E-16	28.27	0.1949
					5475	37.75	7.4	0.156	1.54E-16	0.216	2.1E-16	26.11	0.18
P18-02-A01	3640.50-3640.61 Detfurth	**2**	59	3640.5	800	5.52	9.3	12.9	1.27E-14	14	1.4E-14	4.34	0,0299
					2500	17.24	8.8	11.5	1.13E-14	12.3	1.2E-14	3.84	0.0265
					4000	27.58	8.6	10.9	1.08E-14	11.6	1.1E-14	3.53	0.0243
					5475	37.75	8.4	10.5	1.04E-14	11.2	1.1E-14	3.38	0.0233
P18-02-A01	3626.22-3626.38 Detfurth	**3**	2	3626.25	800	5.52	8.1	0.305	3.01E-16	0.466	4.6E-16	35.64	0.2457
					2500	17.24	7.6	0.150	1,48E-16	0.251	2.5E-16	46.19	0.3185
					4000	27.58	7.5	0.105	1.04E-16	0.18	1.8E-16	48.33	0.3332
					5475	37.75	7.4	0.086	8.49E-17	0.148	1.5E-16	49.08	0.3384

Table 5: *Overview of the porosity and permeability data of the P18-02-A01 Well for the Detfurth formation obtained from the Core Analysis Reports correlated with the new samples (1-7) from the P18 field (CAR P18-02-A01, 1990).*

Porosity & Permeability data P18-02
Hardegsen & Volpriehausen

CAR = Core Analysis Report. The data below is measured from cores taken in the past.

Well	Interval (m)/ Formation	UU Sample #	CAR sample	CAR Core depth (m)	Conf. pressure		Porosity	K-berg permeability		Gas permeability		K-berg slip factor	
					PSI	MPa	%	mD	m2	mD	m2	PSI	MPa
P18-02	3442.53-3442.74 Volpriehausen	**4**	97	3442.69	800	5.52	4.7	0.03	2.96E-17	0.04	3.9E-17	25.62	0.1766
P18-02	3436.00-3436.36 Volpriehausen	**5**	71	3436.25	800	5.52	6.8	0,299	2.95E-16	0.418	4.1E-16	27.08	0.1867
					2500	17.24	6.3	0.164	1.62E-16	0.237	2.3E-16	30.62	0.2111
					4000	27.58	6.1	0.129	1.27E-16	0.184	1.8E-16	29.18	0.2012
					5300	36.54	6	0.116	1.14E-16	0.164	1.6E-16	28.63	0.1974
P18-02	3295.00-3295.35 Hardegsen	**6**	46	3295.25	800	5.52	12.3	14.7	1.45E-14	16.3	1.6E-14	5.9	0.0407
					2500	17.24	12	13.4	1.32E-14	14.8	1.5E-14	5.73	0.0395
					4000	27.58	11.8	12.8	1.26E-14	14.2	1.4E-14	5.7	0.0393
					5300	36.54	11.7	12.6	1.24E-14	14	1.4E-14	5.68	0.0392
P18-02	3287.00-3287.32 Hardegsen	**7**	14	3287.25	800	5.52	23.1	3000	2.96E-12	3000	3E-12	0.5	0.0034
					2500	17.24	21.6	3000	2.96E-12	3000	3E-12	2.9	0.02
					4000	27.58	21	3000	2.96E-12	3000	3E-12	1.9	0.0131
					5300	36.54	20.7	3000	2.96E-12	3000	3E-12	0.5	0.0034

Table 6: *Overview of the porosity and permeability data of the P18-02 well for the Hardegsen and Volpriehausen formations obtained from the Core Analysis Reports correlated with the new samples (1-7) from the P18 field (CAR P18-02, 1989).*

Mineralogy

P18-02 & P18-02-A01 Well

CAR = Core Analysis Report. The data below is measured from cores taken in the past.

For CAR P18-02-A01, there is distinction between Plag and Alb; for CAR P18-02 only Plag is mentioned.

Well/ Formation	Interval (m)	UU Sample #	CAR Core depth (m)	Minerals (wt%)								
				Qtz	Plag	K-fsp	Alb	Calc	Dol	Chl	clays/mica	Total
P18-02-A01 Detfurth	3644.33-3644,52	**1**	3644,0	67	-	8	6	-	5	-	14	100
P18-02-A01 Detfurth	3640.30-3640,61	**2**	3640,0	78	4	2	-	-	4	3	9	100
P18-02-A01 Detfurth	3626.22-3626,38	**3**	3626,0	71	-	14	2	-	3	-	10	100
P18-02 Volpriehausen	3442.53-3442,74	**4**	3442,5	67	5	8	-	-	6	-	14	100
P18-02 Volpriehausen	3436.00-3436,36	**5**	3436,0	67	-	10	-	-	9	3	11	100
P18-02 Hardegsen	3295.00-3295,35	**6**	3295,0	73	3	7	-	-	3	4	10	100
P18-02 Hardegsen	3287.00-3287,32	**7**	3287,0	83	-	9	-	-	2	-	6	100

Table 7: *Overview of the reservoir rock mineralogy of the P18-02 & P18-02-A01 wells according to the core analysis reports correlated with the new UU samples (1-7) from the P18 field (CAR P18-02, 1989 & CAR P18-02-A01, 1990).*

2.4. Previously known petrophysical data on correlated samples of cap rocks

Samples 8-15 were taken from cores in the reservoir cap rock sealing formations Solling and Röt present in well cores Q16-4 and Q16-FA-101-S1. Figure 2 shows the core interval from which the samples 12-15 were derived. Dark reddish marly-claystone (Solling) is seen passing into the evaporitic sequence of the Röt. It is unfortunate that the base of the Solling and top of the Hardegsen are not present in the cored interval. Table 8 gives a summary of previously known data form CAR reports for these samples, correlated by depth.

UU Sample #*	Well	Depth Interval (m)	Form.	Klinkenberg (extrapolated) Permeability ** (mD)	Gas Permeability (mD)	Porosity (%)	Density (g/cm^3)
8a 8b	Q16-4	3056.90-- >3056.97	Röt	0.00045 mD	0.00089	0,2	2.77
9a 9b	Q16-4	3060.78-- >3060.87	Röt	0.0004 mD	0.00078	0.3	
10a 10b	Q16-4	3065.91-- >3065.97	Solling	0,002 mD	0.0061	1.1	2.73
11a 11b	Q16-4	3066.53-- >3066.71	Solling	0.0092 mD	0.0268	3.9	2.71
12 12b	Q16-FA-101-S1	3292.1	Solling		secondary porosity?	3.4	2.808
13 13b	Q16-FA-101-S1	3291.2	Solling		<0.01 mD	2,1	2.805
14 14b	Q16-FA-101-S1	3290.05	Röt		0.08 mD	5.3	2.67
15b	Q16-FA-101-S1	3278.65	Röt		0.02 mD	1.8	2.747

Table 8: *CAR report data for caprock samples*
**) "a" implies the plug is taken perpendicular to the bedding; "b" implies the plug is taken parallel to the bedding. Without specification implies a large chunk of original core is still available. For thin section optical microscopy we use the 'b' plugs where possible.*
***) Klinkenberg permeability measured at ±36-38 MPa*

2.5. Analyses of cap rock samples using XRD

The results of our ongoing analysis of the mineralogy of the cap rock in the Q16 oil field, using X-ray diffraction analysis (XRD), show high phyllosillicate (Muscovite) and carbonate (Dolomite/ Ankerite) content (Table 9). It is interesting to note that the mineralogy of samples 8 and 9, both from the Röt formation in well Q16-04 is very rich in Muscovite (42-45%) with

more modest amounts of Ankerite (20-29%) whereas sample 13, extracted from the Q16-FA-101-S1 well, show the reverse, 52.5% Ankerite and only 17.5% Muscovite. Sample 12 is the only sample evaluated thus far that lies within the Solling formation, as defined by the lithostratigraphy (Fig. 1), and it shows significantly different mineralogy from the Röt formation samples, dominated by Dolomite (54%) and Muscovite (39.7%), with very little Quartz (3.3%) and Ankerite (3%).

UU Sample I.D.	Well I.D.	Depth (m)	Formation	XRD Results
8⊥ & 8//	Q16-04	3056.90 - 3056.97	Röt	45.1% - Muscovite - $KAl_2(AlSi_3O_{10})(OH)_2$ 28.6% - Ankerite - $Ca(Fe,Mg,Mn)(CO_3)_2$ 26.3% - Quartz - SiO_2
9⊥ & 9//	Q16-04	3060.78 - 3060.87	Röt	42.7% - Muscovite - $KAl_2(AlSi_3O_{10})(OH)_2$
				37.1% - Quartz - SiO_2
				20.3% - Ankerite - $Ca(Fe,Mg,Mn)(CO_3)_2$
10⊥ & 10//	Q16-04	3065.91 - 3065.97	Solling	Not yet evaluated
11⊥ & 11//	Q16-04	3066.53 - 3066.71	Solling	Not yet evaluated
12⊥ & 12//	Q16-FA-101-S1	3292,1	Röt/Solling	54.0% - Dolomite - $CaMg(CO_3)_2$ 39.7% - Muscovite - $KAl_2(AlSi_3O_{10})(OH)_2$ 3.3% - Quartz - SiO_2 3.0% - Ankerite - $Ca(Fe,Mg,Mn)(CO_3)_2$
13⊥ & 13//	Q16-FA-101-S1	3291,2	Röt	52.5% - Ankerite - $Ca(Fe,Mg,Mn)(CO_3)_2$ 30.4% - Quartz - SiO_2 17.1% - Muscovite - $KAl_2(AlSi_3O_{10})(OH)_2$
14⊥ & 14//	Q16-FA-101-S1	3290,05	Röt	Not yet evaluated
15//	Q16-FA-101-S1	3278,65	Röt	Not yet evaluated
53//	Q16-FA-101-S1	3289,75	Röt	Not yet evaluated
55//	Q16-FA-101-S1	3290,35	Röt	Not yet evaluated
56//	Q16-FA-101-S1	3290,6	Röt	Not yet evaluated
57//	Q16-FA-101-S1	3290,9	Röt	Not yet evaluated
59//	Q16-FA-101-S1	3291,5	Röt	Not yet evaluated
60//	Q16-FA-101-S1	3291,8	Röt/Solling	Not yet evaluated

Table 9: *Samples used in this study, including XRD data obtained thus far. ⊥ implies the sample is cored perpendicular to sedimentary layering. // implies the sample is cored parallel to the sedimentary layering. Sample numbers >50 are plug numbers from the CAR for the Q16-FA-101-S1 well.*

2.6. Microstructural description of samples

This section describes the characterisation of mineralogical and textural features, such as mineral content, cementation, grain dissolution by compaction (pressure solution) and grain overgrowth seen in the thin sections using optical microscopy. These features are important as they determine the reservoir potential for CO_2 storage. The presence of certain minerals such as feldspars and micas, are likely to be more reactive to CO_2 as well as the presence of calcite

cement which is expected to dissolve as it interacts with CO_2, jeopardizing the structure of the reservoir. The reactions might alter the porosity, permeability and the cementation strength of the reservoir rock leading to compaction of the reservoir or a decrease in porosity and permeability. On the other hand, dissolving the calcite cement could lead to an increased porosity if the structure holds and possibly assist the injection process.

The thin sections were studied under an optical microscope in plane and crossed polarized light at different objective magnifications (2,5x and 10x). Of each thin section several photographs have been made to clarify some of the features observed (Figures 8-18). Table 10 gives an overview of the porosity of the thin sections which was estimated with the line intercept stereological method, assuming that volume per unit volume = area per unit area = line per unit line. From the core analysis reports it has become clear that for the Detfurth, the porosity ranges between 2.4 and 15.2%, the Volpriehausen between 3.6 and 7.4% and for the Hardegsen between 4.7 and 23.1% which seem to be consistent with the estimated porosities of the thin sections from the P18 field.

P18 field		
UU Sample#	**Formation**	**Porosity (%)***
1a	Detfurth	15
1b	Detfurth	12
2a	Detfurth	12
2b	Detfurth	10
3a	Detfurth	12
3b	Detfurth	10
4b	Volpriehausen	5
5b	Volpriehausen	8
6b	Hardegsen	10
7b	Hardegsen	25

***Table 10**: Estimations of porosity made by a line intercept stereological method. These porosities compare favourably with previous data from the CAR.*

2.6.1. Optical microscopy: P18 reservoir rock thin sections

From the Volpriehausen, Detfurth and Hardegsen formation plugs, a total of ten thin sections were made - sample 1a through 7b. All thin sections were made perpendicular to the bedding without a cover glass. Beforehand, sample 6b and 7b were first impregnated with a blue resin to clarify the porosity. Table 11 gives an overview of the mineralogical and textural features observed in each thin section. Below, the ten thin sections will be discussed organized per formation, starting with the Detfurth.

P18 field									
UU Sample#	Formation	Grainshape	Grainsize*	Mineral content (%)**				Pressure solution	Over-growth
				Qtz	Fsp	Rock frag.	Calc. Cem.		
1a	Detfurth	subrounded	fine to medium	75	7.5	7.5	10	yes	yes
1b	Detfurth	subrounded	fine to medium	70	7.5	7.5	15	yes	yes
2a	Detfurth	subrounded	fine to medium	70	7.5	10	12.5	yes	yes
2b	Detfurth	subrounded	fine to medium	75	7,5	7.5	10	yes	yes
3a	Detfurth	subrounded	fine to medium	75	7,5	7.5	10	yes	yes
3b	Detfurth	subrounded	fine to medium	75	7.5	7,5	10	yes	yes
4b	Volpriehausen	subrounded	fine to medium	65	5	20	10	yes	yes
5b	Volpriehausen	subrounded	fine to medium	65	5	20	10	yes	yes
6b	Hardegsen	subrounded	fine	75-80	5	5	10-15	yes	yes
7b	Hardegsen	well-rounded	medium	90	2.5	2.5	5	yes	yes

Table 11: *Overview of the grainshape, grainsize, mineral content, pressure solution and overgrowth features of the ten P18-field samples that were analysed under an optical microscope. *: fine grained represents 125-250 μm and medium grained 250-500 μm.**: The mineral content of the thin sections was roughly estimated with the line per unit line method, assuming: volume per unit volume = area per unit area = line per unit line. Abbreviations: qtz; quartz, fsp; feldspar, rock frag.; rock fragments, calc. cem.; calcite cement.*

2.6.2. Detfurth samples; 1a-3b

Most of the thin sections of this formation display bands which differ in grain size, porosity and compaction (Figure 8-10). The bands are either with a smaller grainsize, higher porosity and looser compaction or with a larger grain size, lower porosity and tighter compaction. In some of the thin sections the distinction between these two bands is easier than others. For example, sample 1a (Figure 8A, B) clearly shows the different bands as well as sample 1b and 3b (Figure 8C-E and Figure 10E-F). Apart from the banding, each thin section displays signs of calcite cementation, pressure solution - the process whereby sediment under load is subject to selective solution, and overgrowth. The calcite cement shows high order pink and green interference colours and has a patchy structure. A good example can be observed in Figure 8E. At many of the contacts between grains, one grain has undergone solution leading to the penetration of one grain by another (concave-convex). This is the first stage of pressure solution. Where pressure solution is more intense, the contact between the grains become sutured giving grain contacts an irregular and wavy structure (Figure 10E). Silica dissolved during the process may be precipitated as cement away from grain contact, leading to destruction (occlusion) of porosity. A good example of overgrowth can be observed at the bottom of Figure 8B. Roughly estimated, the thin sections have a quartz content of approximately 70-75%, 7.5% Feldspar, 7.5% rock fragments and 10-15% calcite cement. Rock fragments, in particular metamorphic rock fragments, are important contributors to many detrital sediments. Good examples of these fragments can be seen in Figure 10B (the

darker "dotted" minerals). The Detfurth interval is generally described as poorly to moderately sorted, tight and well cemented, despite some porosity.

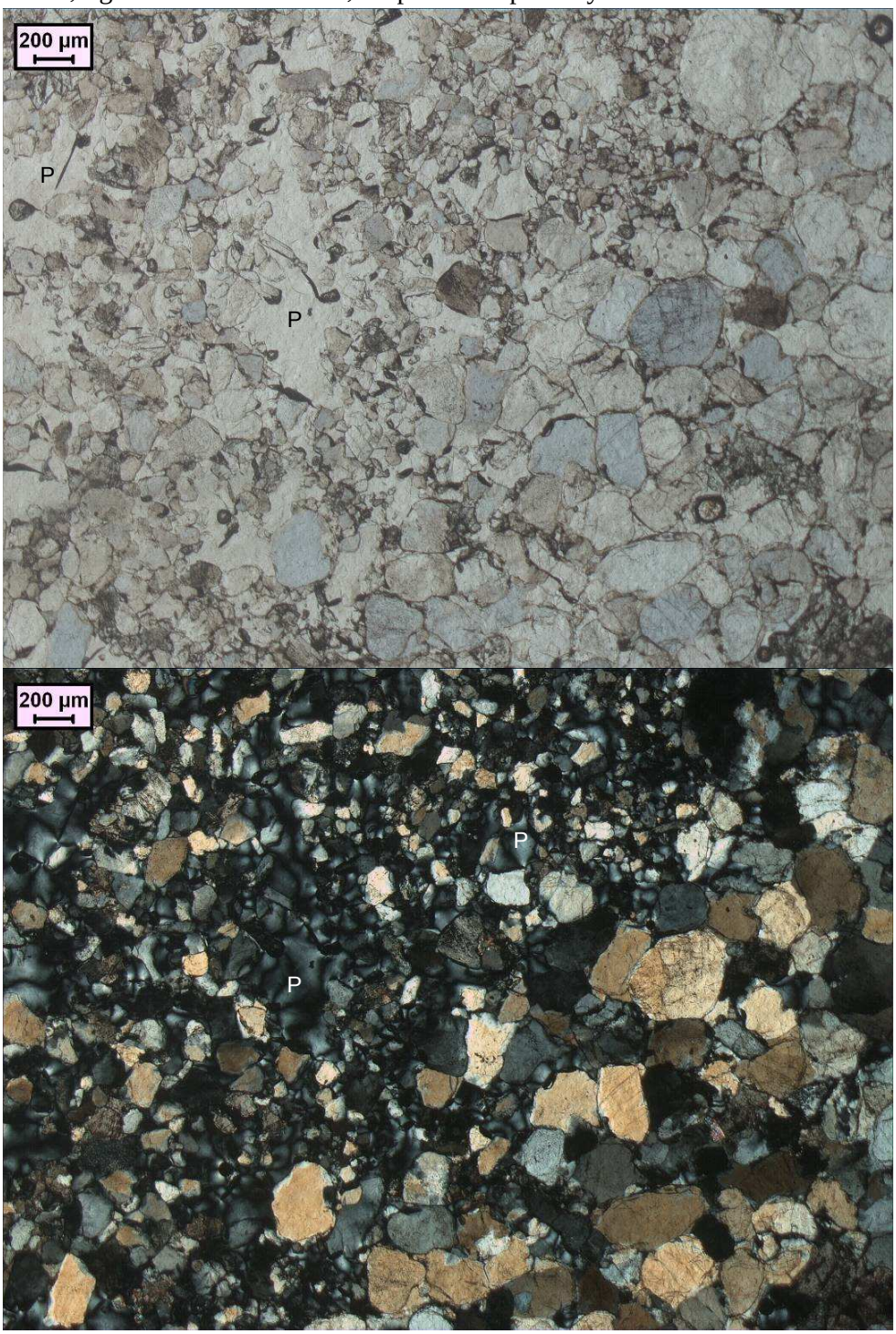

Figure 8*: Detfurth sst.* ***A)*** *Sample 1a, plane polarized light, Bedding layers.* ***B)*** *Sample 1a, crossed polarized light, One layer with a smaller grainsize, higher porosity and looser compaction against another layer with a larger grainsize, lower porosity and tighter compaction.(Prominent pores marked* P).

C

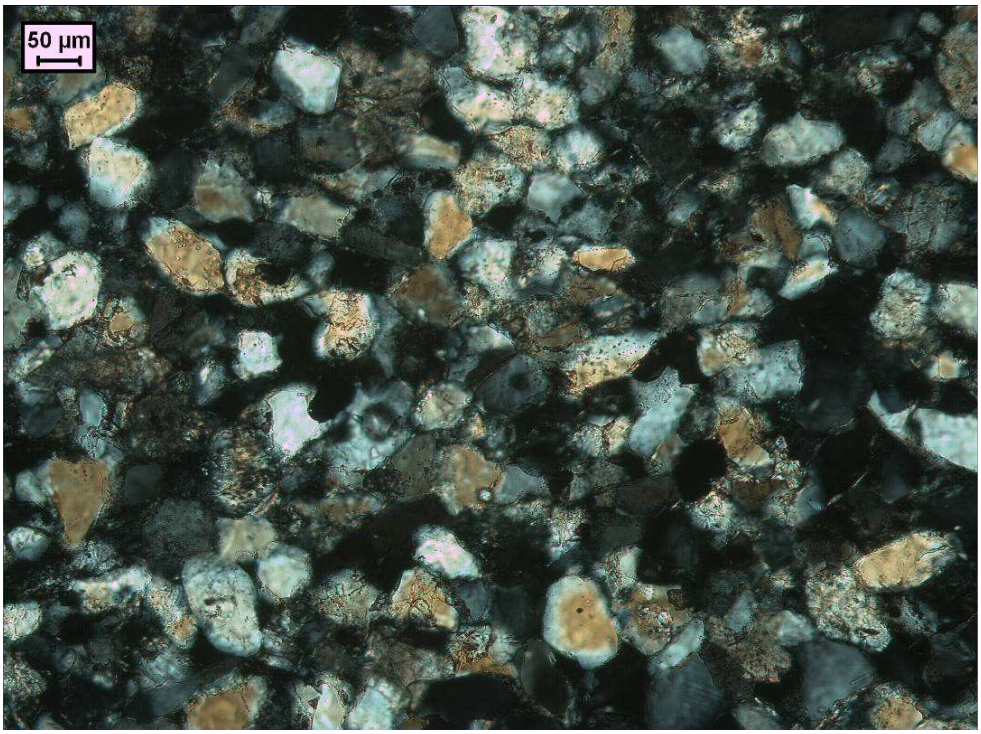

D

Figure 8: *Detfurth sst.* ***C)*** *Sample 1b, crossed polarized light. One layer with a finer grainsize, higher porosity and looser compaction between layers with a coarser grainsize, lower porosity and tighter compaction.*
D) *Sample 1b, crossed polarized light, magnification of the middle layer in Figure 8C.*

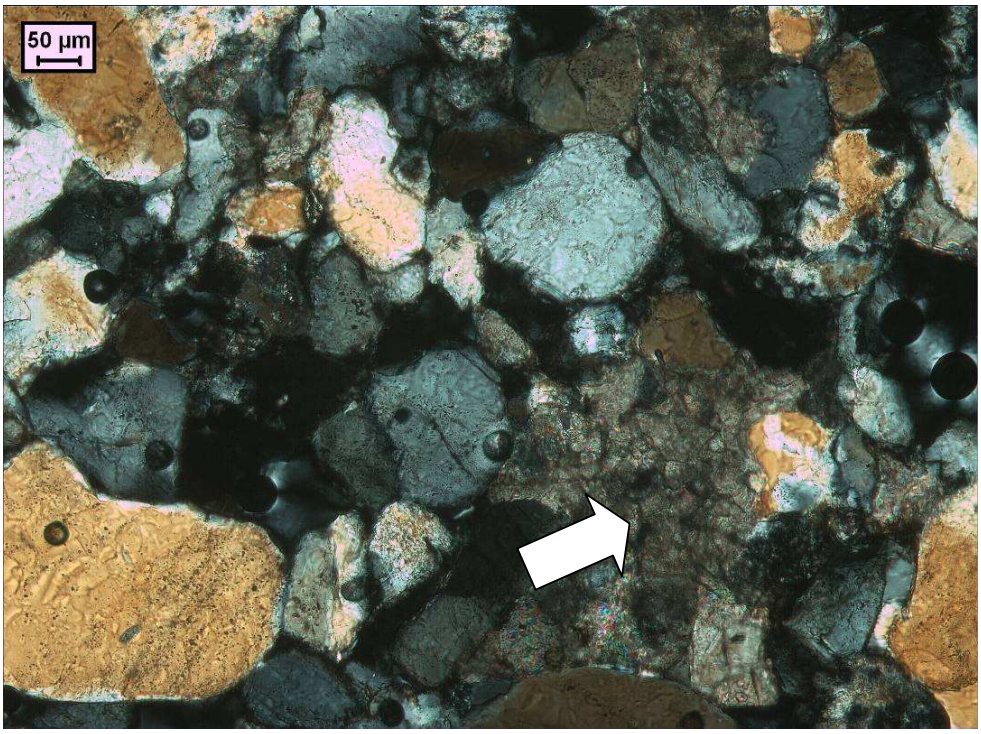

E

Figure 8: D*etfurth sst.* ***E)*** *Sample 1b, crossed polarized light, magnification of the coarser layer in Figure 8C (bottom right). Note calcite infill (arrowed).*

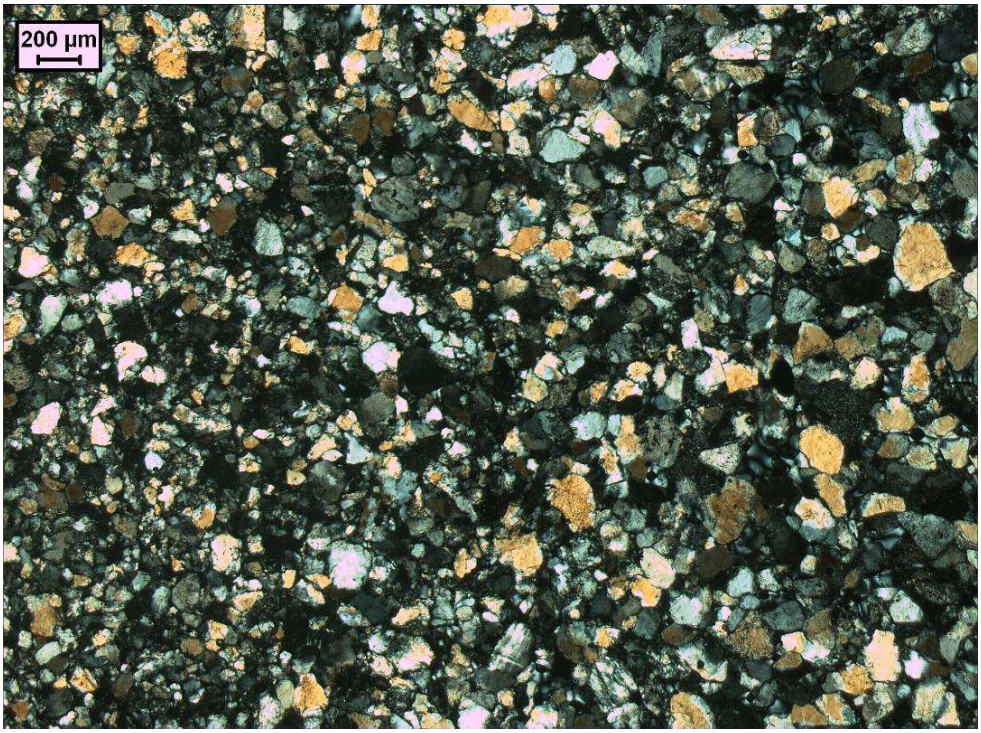

A

Figure 9: *Detfurth sst.* ***A)*** *Sample 2a, crossed polarized light. One layer with a slightly smaller grainsize, higher porosity and looser compaction and one layer with a larger grainsize, lower porosity and tighter compaction.*

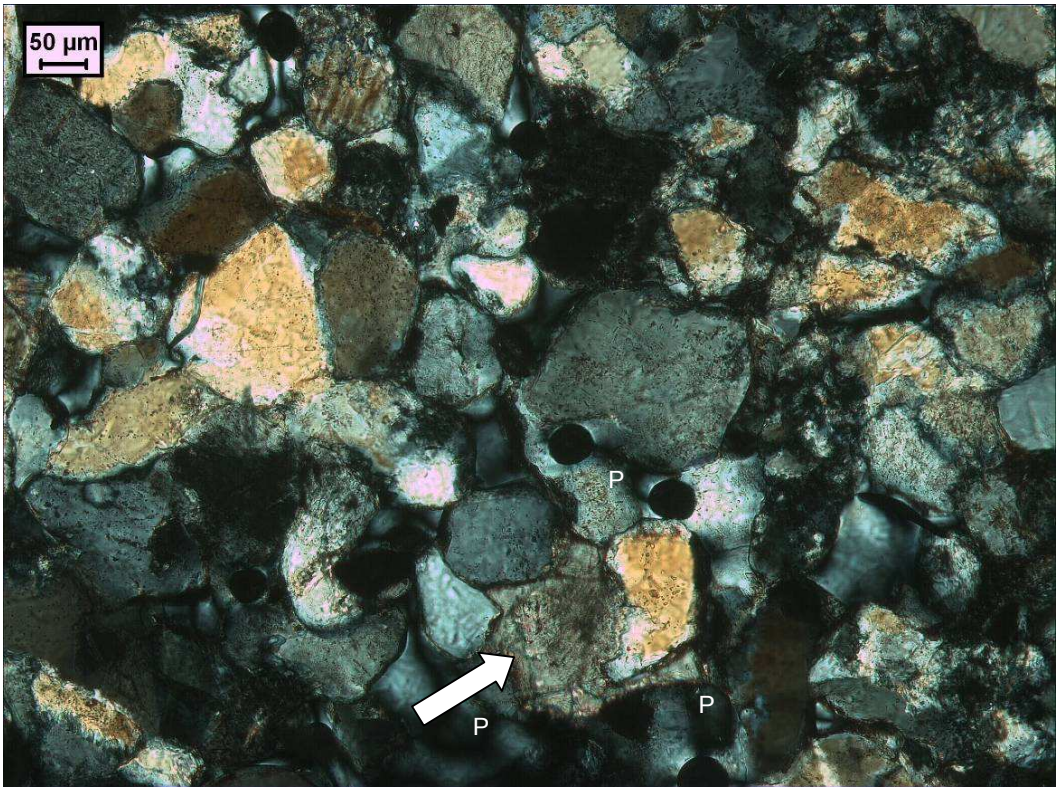

B

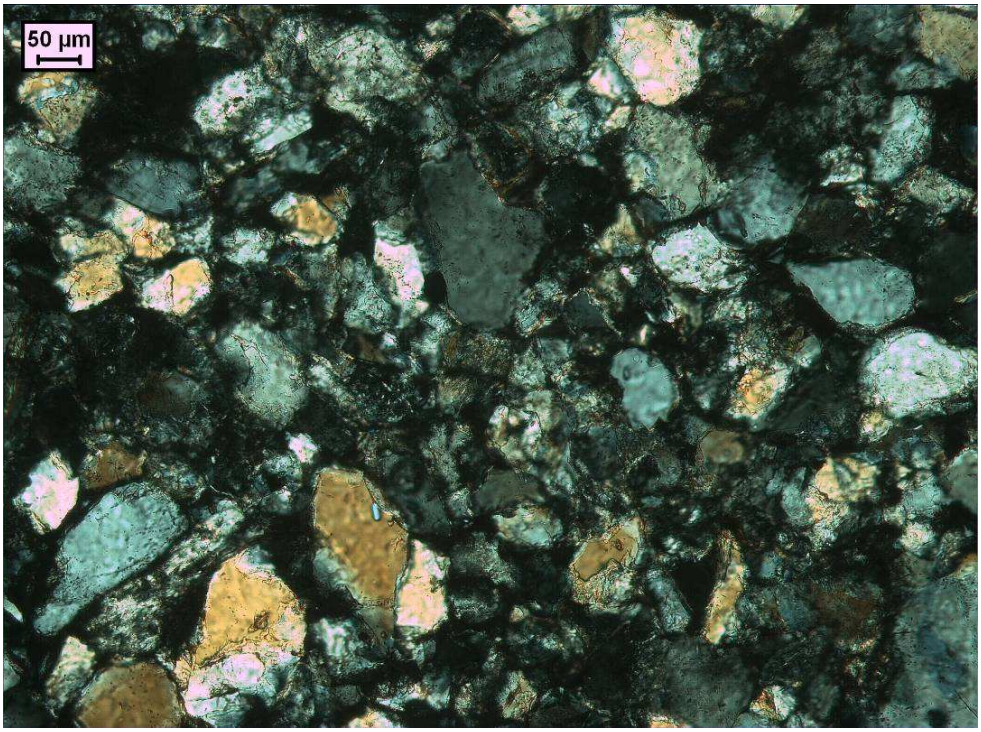

C

Figure 9: *Detfurth sst.* ***B)*** *Sample 2a, crossed polarized light, magnification of the layer with higher porosity. Calcite infill (arrowed)* ***C)*** *Sample 2a, crossed polarized light, magnification of the layer with lower porosity.*

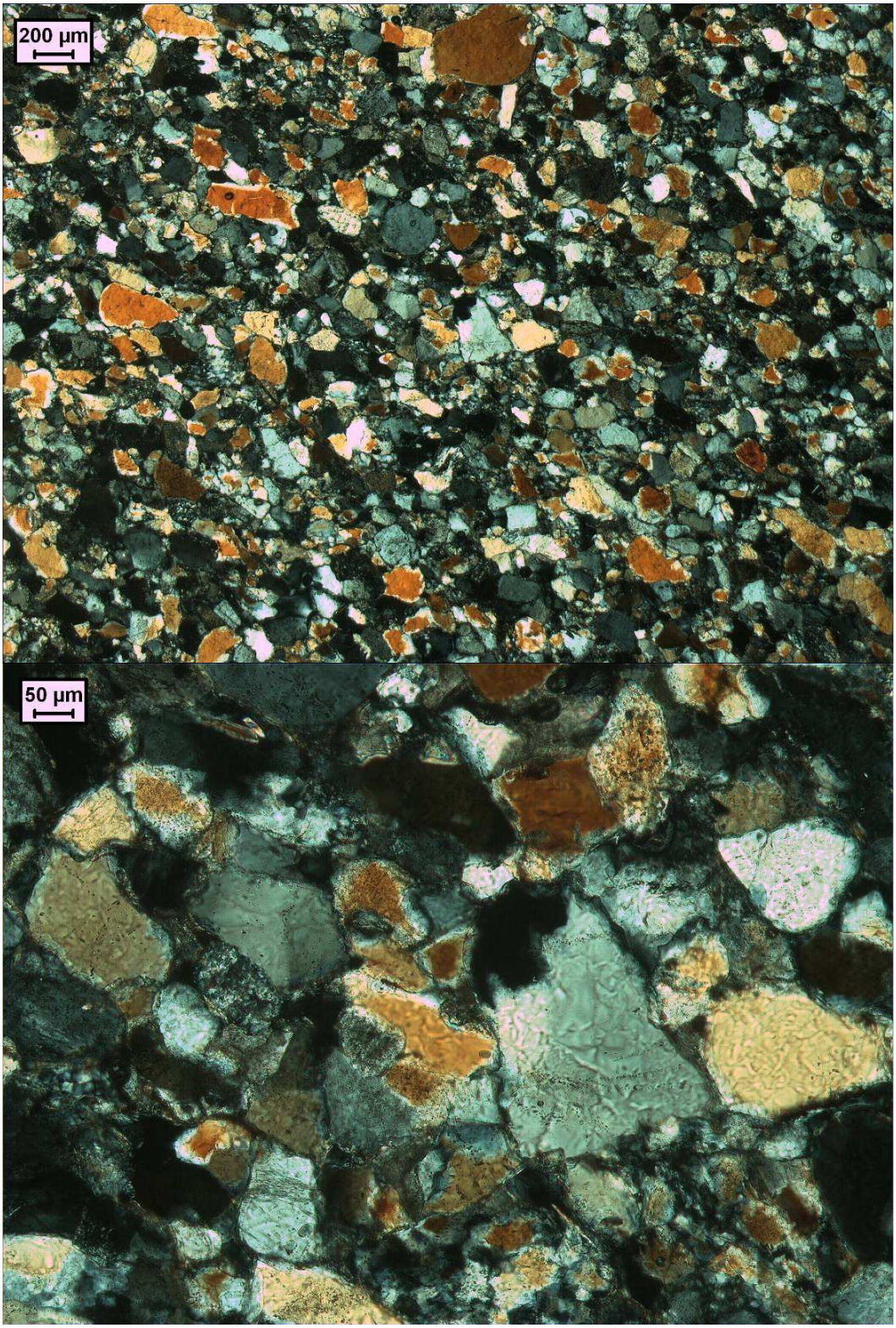

D

E

Figure 9: *Detfurth sst.* ***D)*** *Sample 2b, crossed polarized light,* ***E)*** *Sample 2b, crossed polarized light. Tightly compacted angular quartz.*

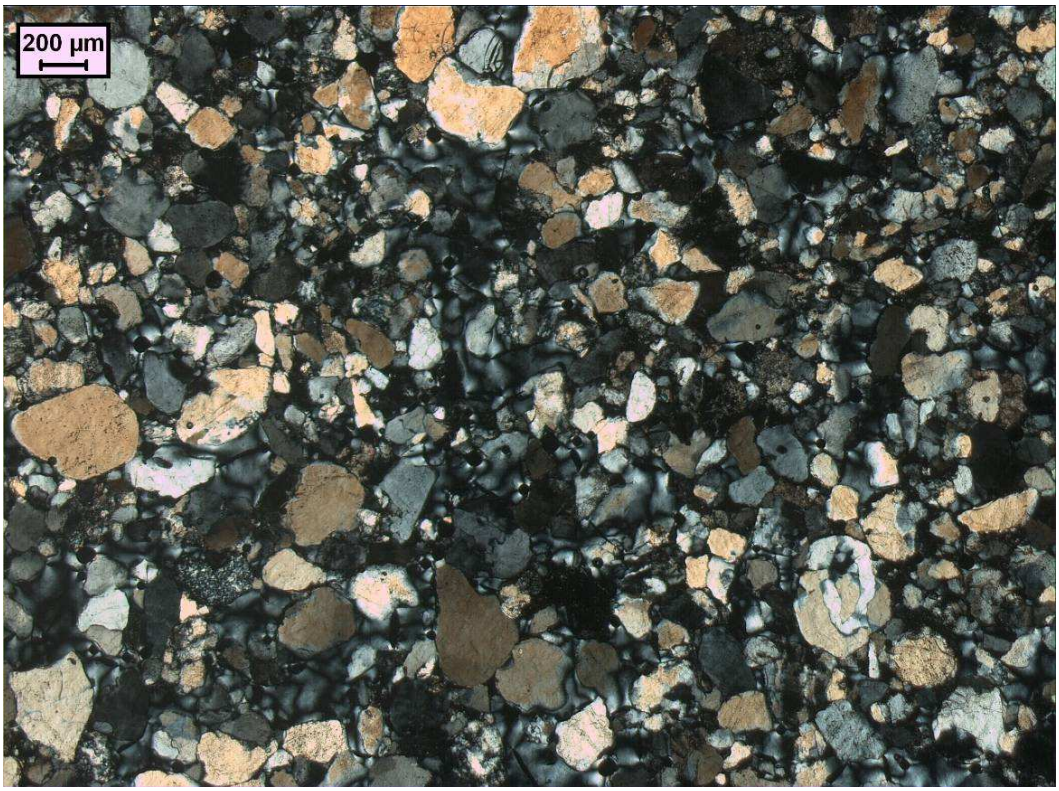

A

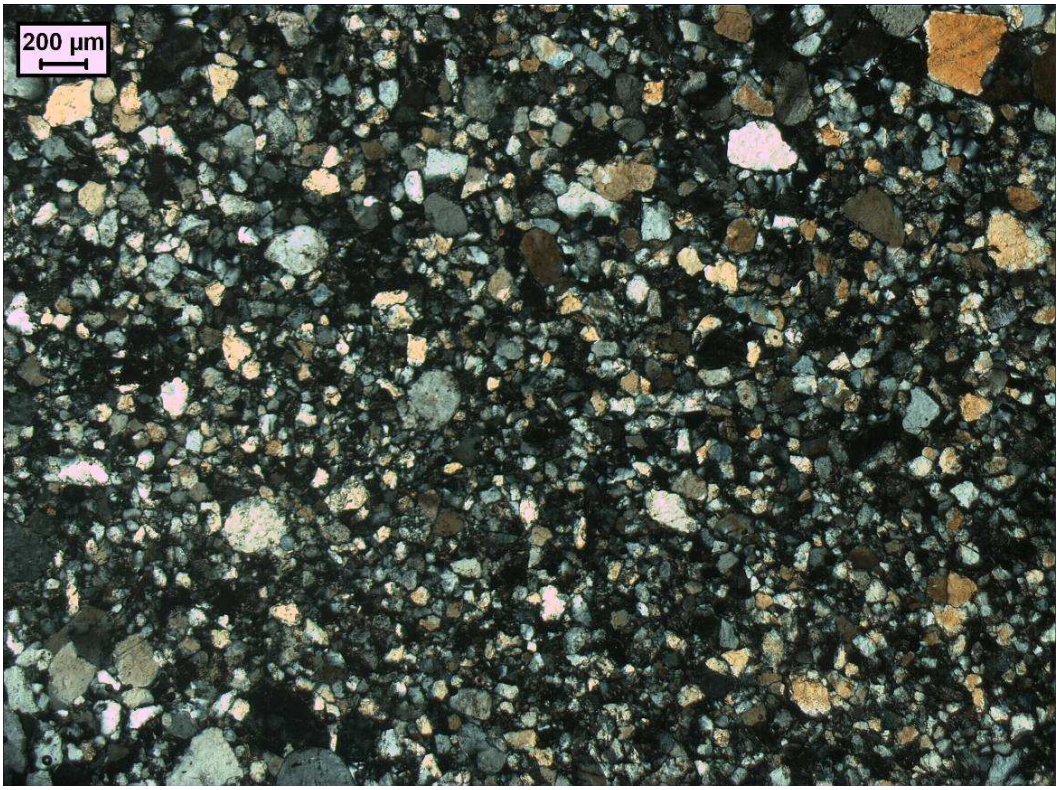

B

Figure 10: *Detfurth sst.* ***A)*** *Sample 3a, crossed polarized light, higher porosity zone,* ***B)*** *Sample 3a, crossed polarized light, lower porosity zone.*

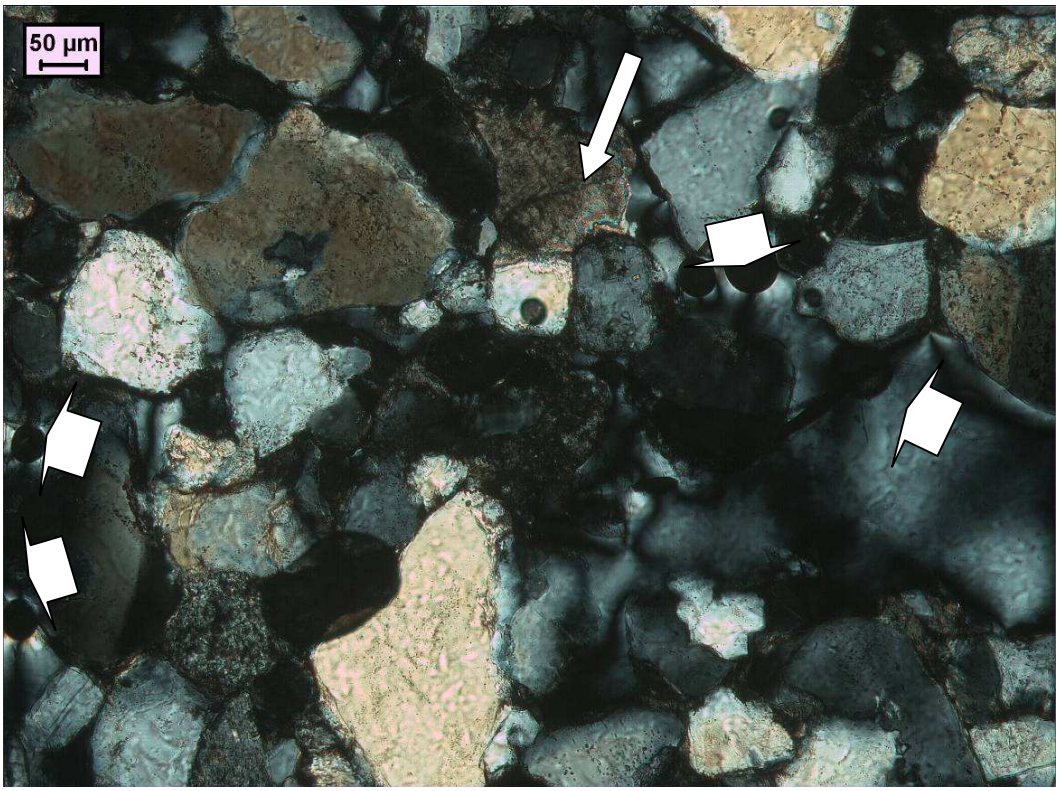

C

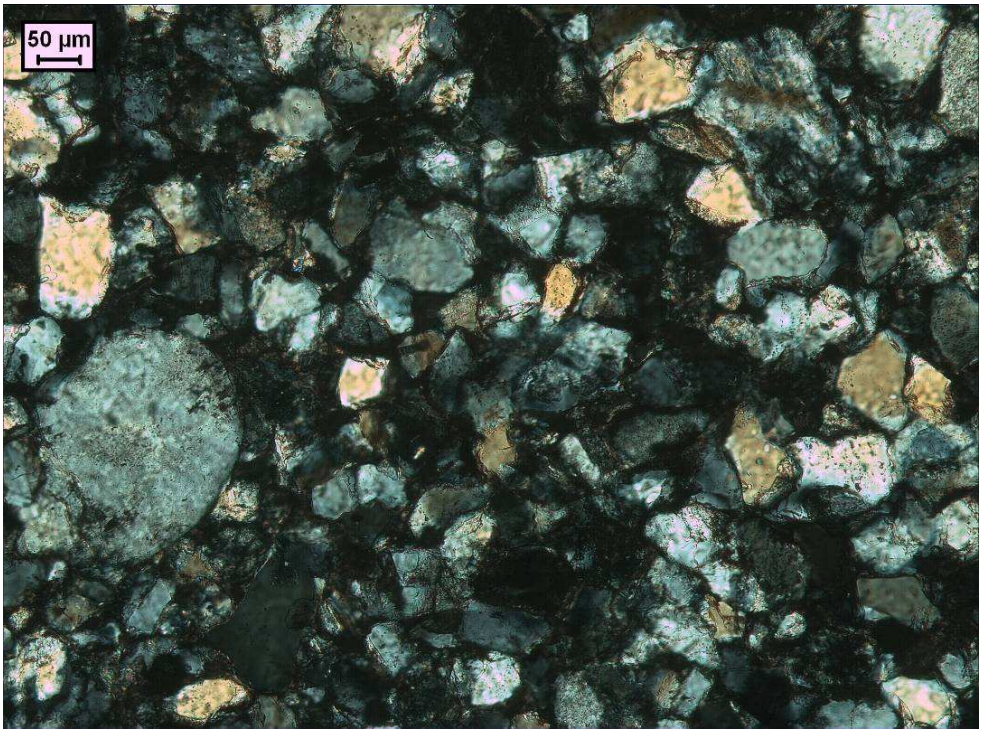

D

Figure 10: *Detfurth sst.* ***C)*** *Sample 3a, crossed polarized light, higher porosity zone. Broad arrows indicate resin filled pores. Narrow arrow indicates calcite cement,* ***D)*** *Sample 3a, crossed polarized light, lower porosity zone.*

E

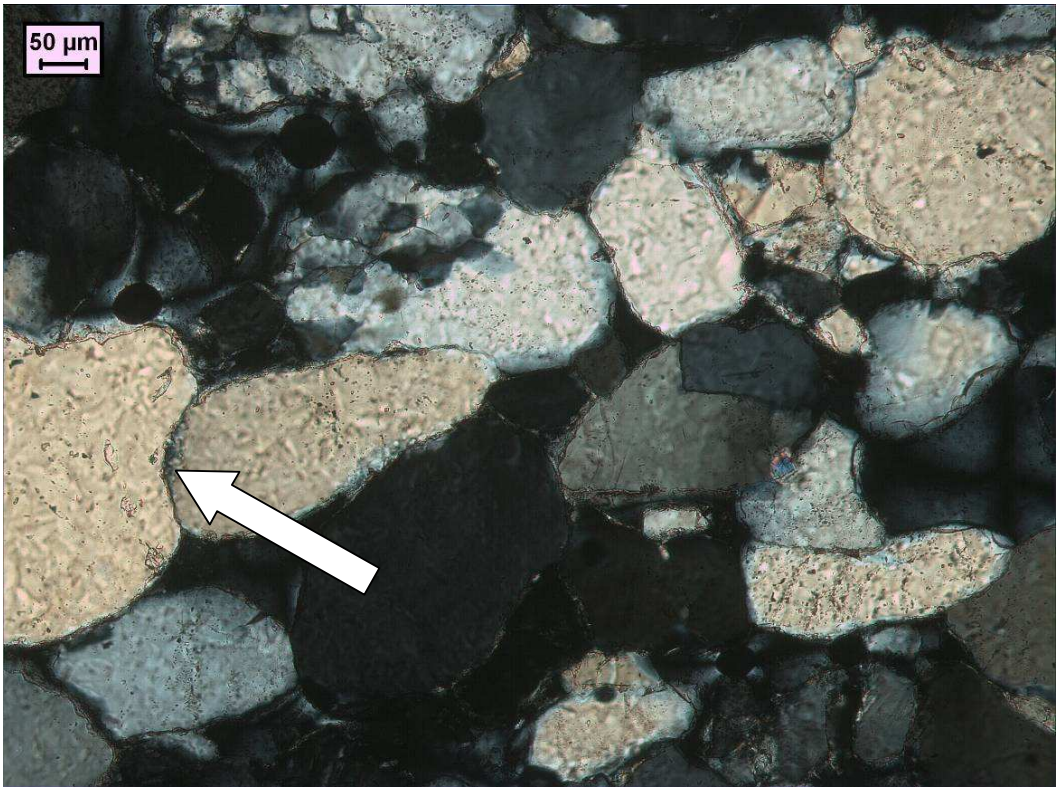

F

Figure 10 *Detfurth sst.* ***E)*** *Sample 3b, crossed polarized light, banding.* ***F)*** *Sample 3b, crossed polarized light, tighter band with lower porosity. Indented grain contacts (arrowed) indicative of pressure solution*

2.6.3. Volpriehausen samples; 4b&5b

In contrast to the Detfurth interval, the thin sections of the Volpriehausen are moderately sorted and display no fine banding (Figures 11&12). The thin sections have a more uniform structure and therefore a more equally distributed porosity which is relatively low. Both samples display pressure solution where one grain has undergone solution leading to the penetration of one grain by another (Figures 11B&12B). The contacts are sutured giving them an irregular and wavy structure, indicative for a more intense compaction. Figure 11B and 12B also display precipitated cement (caused by pressure solution), overgrowths and calcite cement. Roughly estimated, both thin sections have a quartz content of approximately 65%, 5% Feldspar, 20% rock fragments and 10% calcite cement.
The Volpriehausen interval is generally described as moderately sorted, tight and very well cemented.

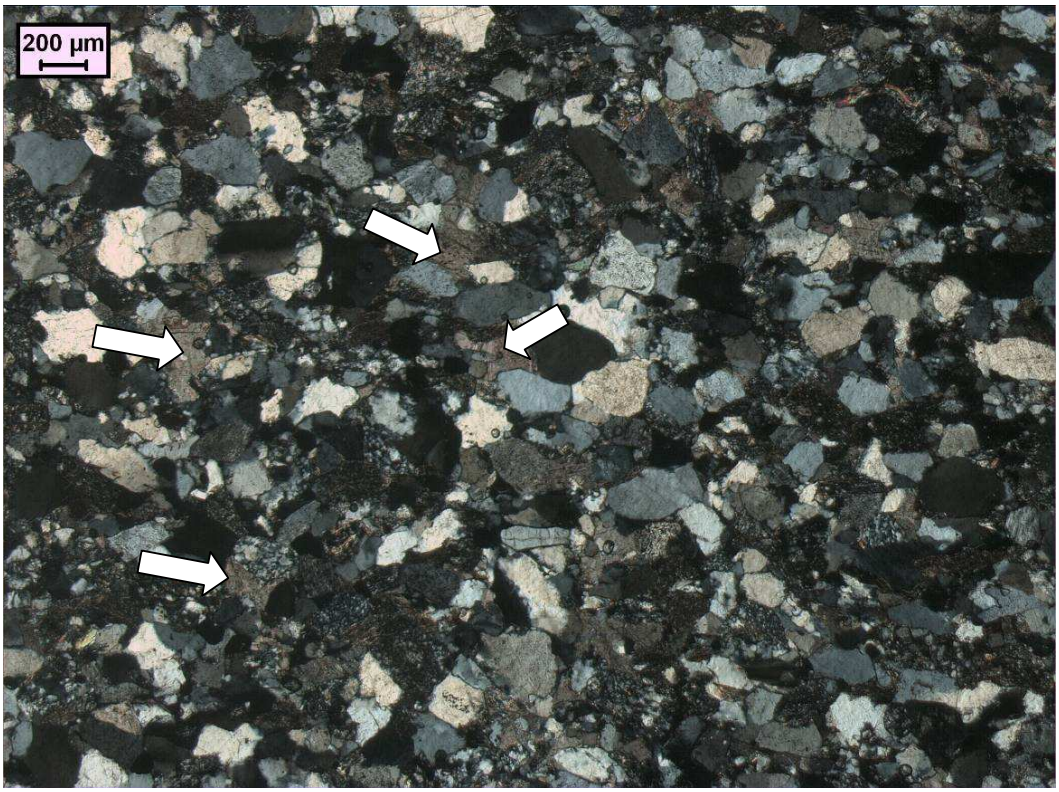

A

Figure 11: *Volpriehausen sst.* ***A)*** *Sample 4b, crossed polarized light. White arrows show areas of calcite cement.*

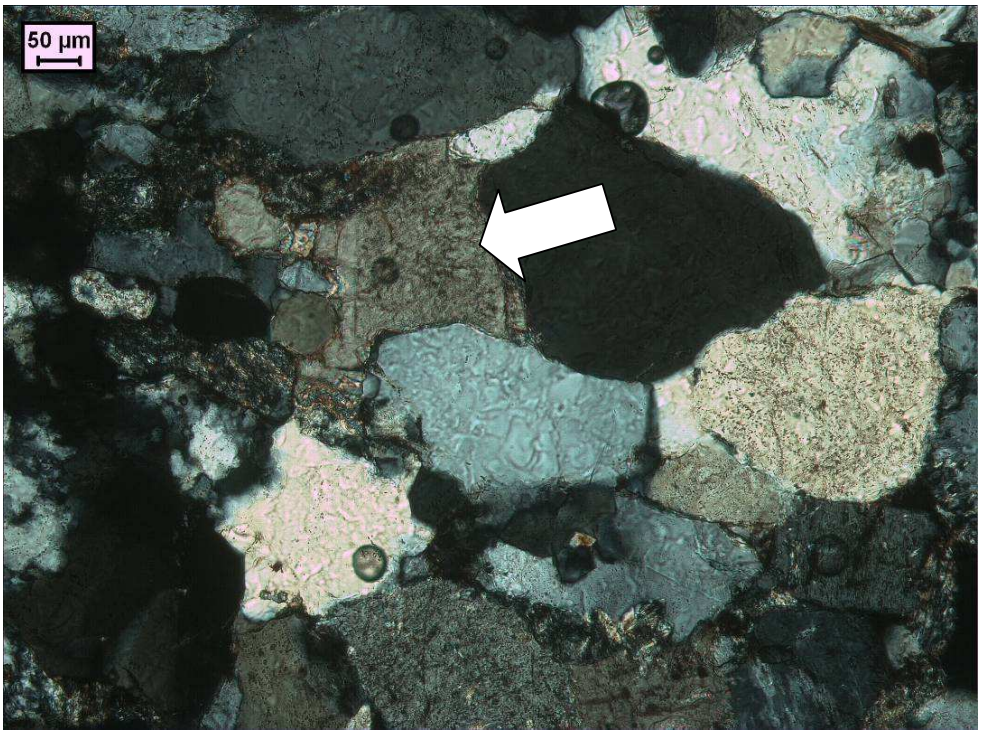

B

Figure 11: *Volpriehausen sst.* ***B)*** *Sample 4b, crossed polarized light, Calcite infill (arrowed)*

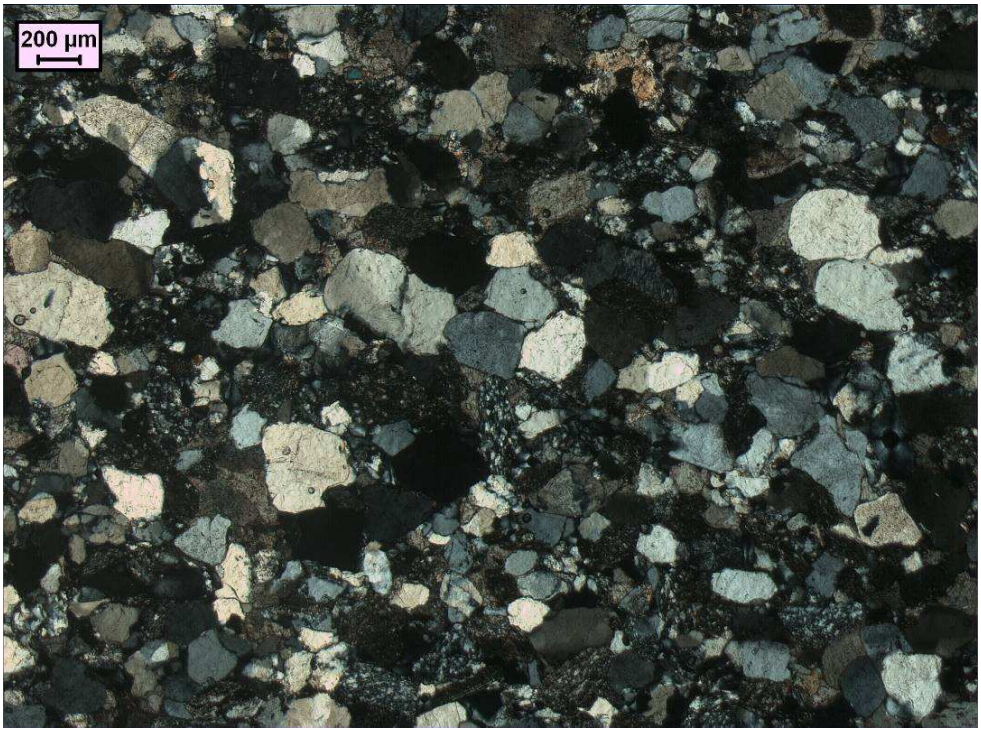

A

Figure 12: *Volpriehausen sst.* ***A)*** *Sample 5b, crossed polarized light,* ***B)*** *Sample 5b, crossed polarized light,*
(Next page)

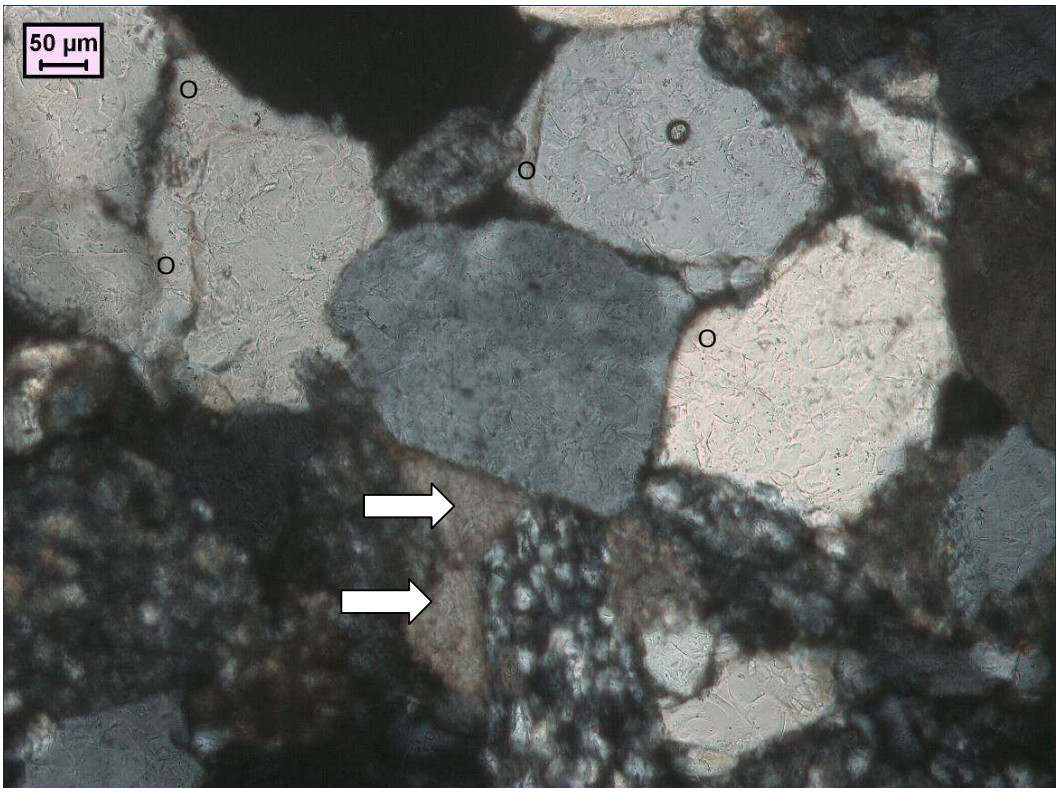

B

Figure 12: *Volpriehausen sst.* ***B)*** *Sample 5b, crossed polarized light, indented grain contacts with quartz overgrowth (O) and calcite cement infills (arrowed)*

2.6.4. Hardegsen samples; 6b&7b

In contrast to the other formations, both thin sections seem to be quite different. Although comprising a loose fabric of grains sample 7b is well-cemented by secondary quartz in the form of overgrowth on the grains (Figure 14C&D). Sample 6b displays a much higher amount of calcite cement (Figures 13C&D; 14A&B). Both samples display pressure solution where one grain has undergone dissolution at stressed grain contacts, leading to the penetration of one grain by another. The contacts of sample 7b are more sutured giving an irregular and wavy structure, indicative for a more intense compaction. Roughly estimated, sample 6b has a quartz content of approximately 75-80%, 5% feldspar, 5% rock fragments and 10-15% calcite cement and sample 7b a quartz content of 90%, 2,5% feldspar, 2,5% rock fragments and 5% calcite cement.
The Hardegsen interval is generally described as moderately to well sorted, loose to tight and well cemented with a high porosity consisting mostly of quartz.

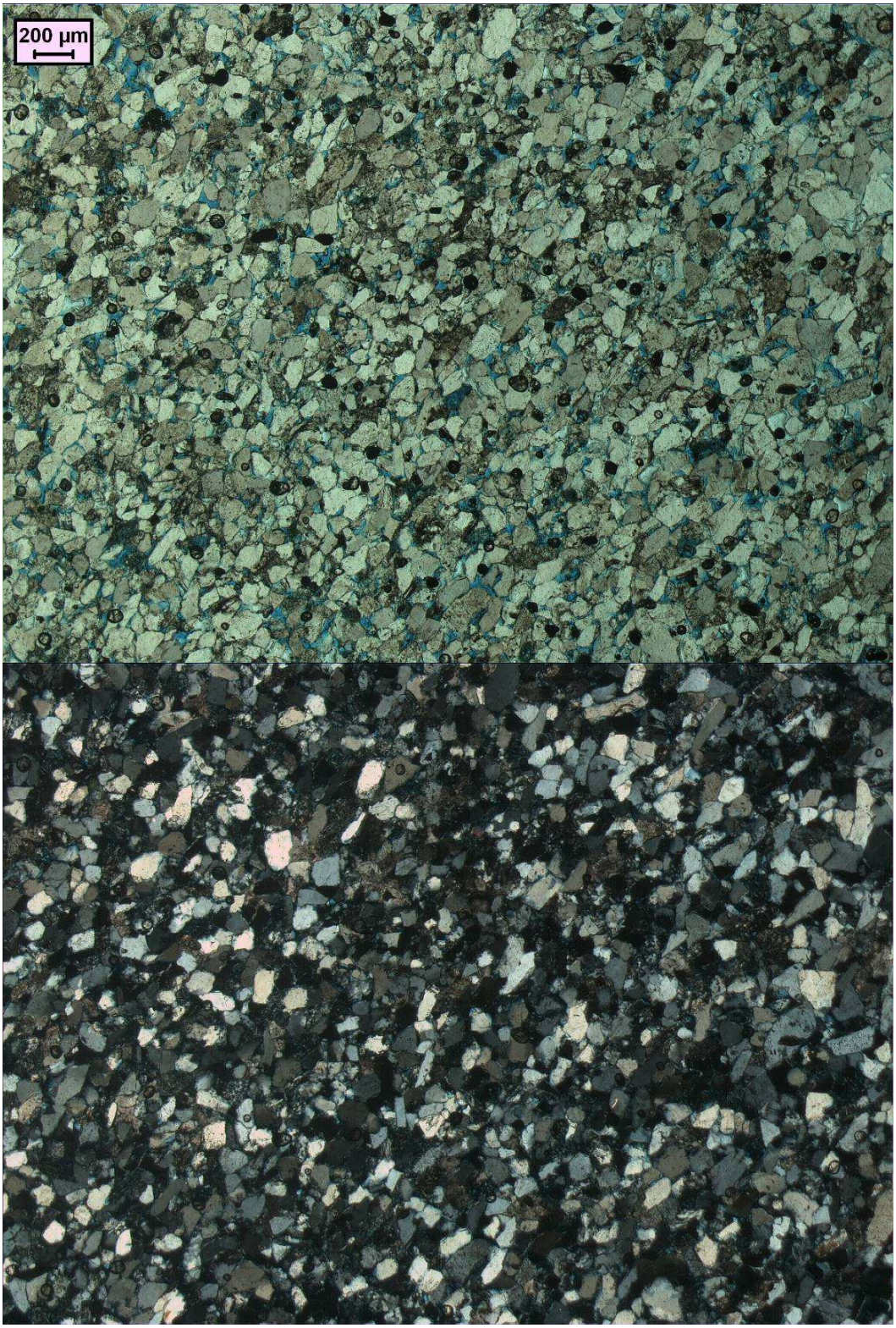

Figure 13: *Hardegsen sst.* ***A)*** *Sample 6b, plane polarized light, blue areas are porosity,* ***B)*** *Sample 6b, crossed polarized light, (same scale bar as A).*

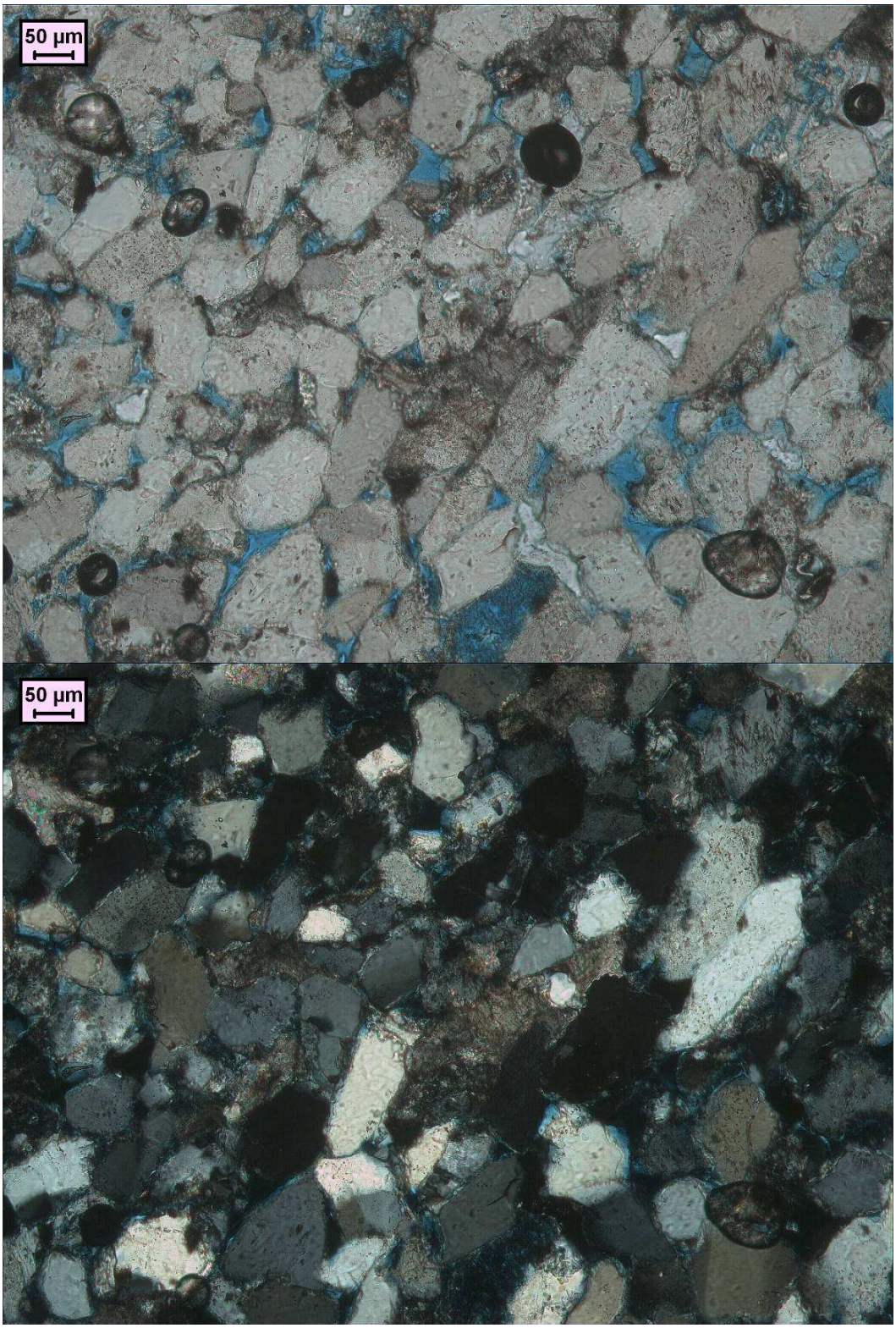

Figure 13: *Hardegsen sst.* ***C)*** *Sample 6b, plane polarized light, blue areas are porosity,* ***D)*** *Sample 6b, crossed polarized light..*

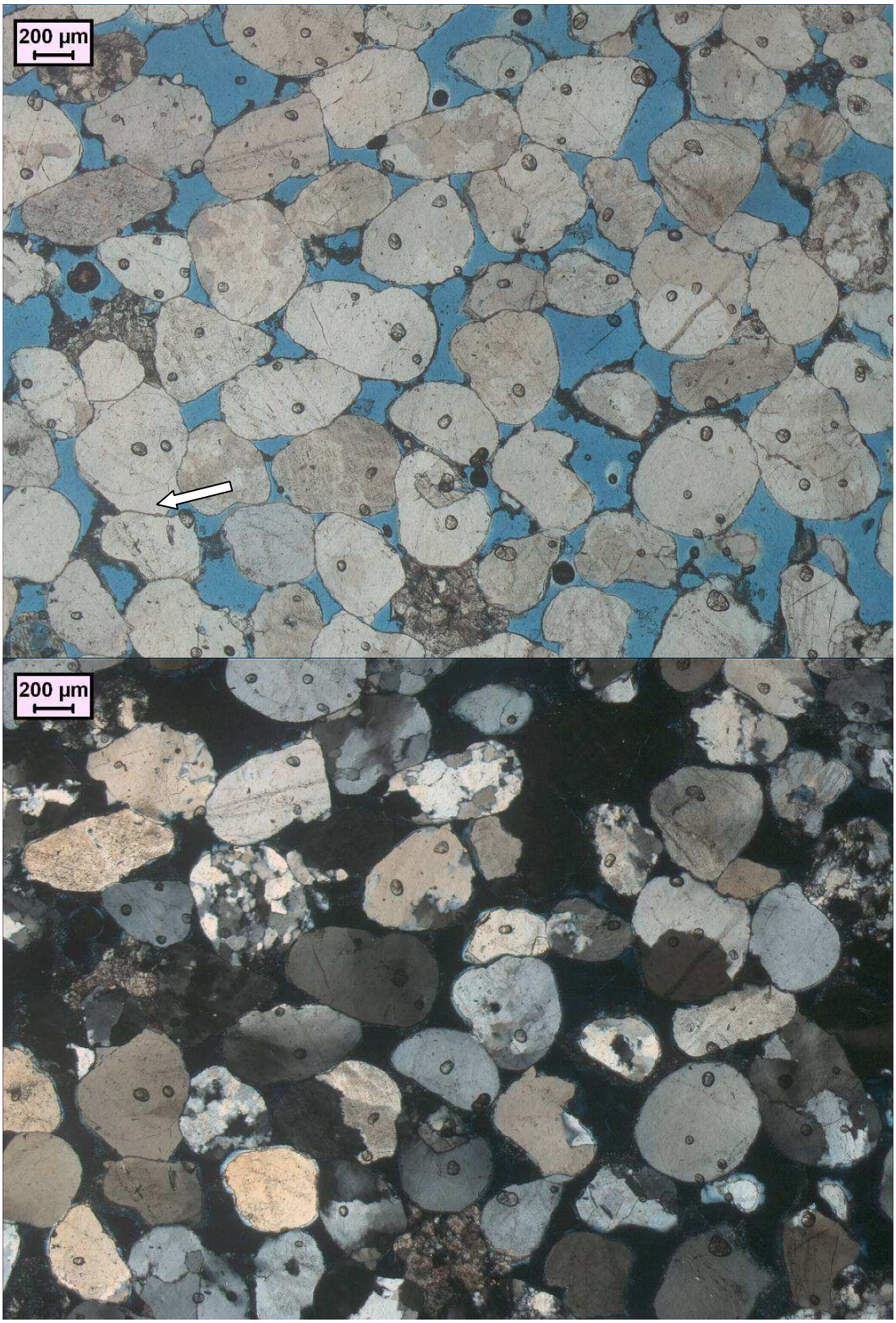

Figure 14: *Hardegsen sst.* ***A)*** *Sample 7b, plane polarized light, (blue areas are porosity, quartz cement overgrowth arrowed)* ***B)*** *Sample 7b, crossed polarized light.*

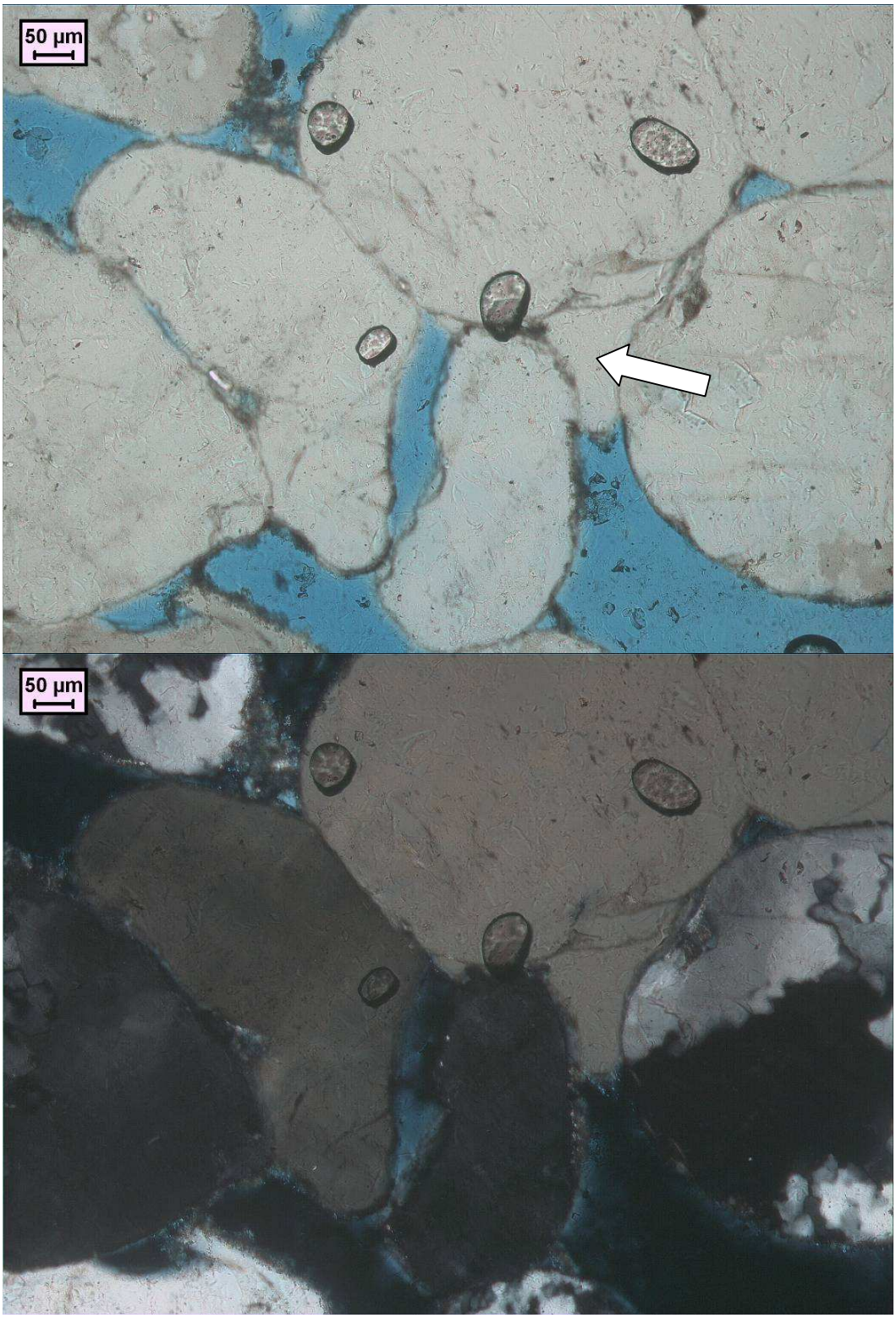

Figure 14: *Hardegsen sst.* ***C)*** *Sample 7b, plane polarized light, showing quartz overgrowth cement (arrowed). Blue areas are porosity.* ***D)*** *Sample 7b, crossed polarized light, view of same area showing optical continuity of cement with upper grain.*

2.6.5. Cap rock samples; 8-15

The samples of cap rock were taken from two cores in the Q quadrant nearby the P18 wells. The Q16-4 material in the interval containing the Röt and Solling Formations is less carbonate rich and coarser grained (sandier) than the similar material from Q16-FA-101-S1 where finer marl-mudstones dominate. Both sets of material contain low porosity and low permeability mudstones capable of sealing a reservoir.

Core Q16-4	**Sample 8 Röt Fm.**	**Sample 9 Röt Fm.**	**Sample 10 Solling Fm.**	**Sample 11 Solling Fm.**
Lithology	Siltstone	Siltstone	Siltstone	Sandstone
Mineral Content (estimate)	Quartz (25%), calcite (25%), micas (50%)	Quartz (25%), calcite (25%), micas (50%)	Quartz (20%), calcite (30%), micas (50%)	Quartz (20%), calcite (30%), micas (50%)
Grainsize (estimate)	very fine grained (5-15 µm)	very fine grained (5-15 µm)	very fine grained (5-15 µm)	fine grained (50-300 µm)
Porosity (estimate)	very low porosity	very low porosity	low porosity	very low porosity
Sorting	moderately sorted	moderately sorted	moderately to well sorted	poorly sorted
Cement	very well cemented	very well cemented by dolomite	very well cemented by dolomite	well cemented

Table 12: *Summary of observations on cap rock samples 8-11 from Core Q16-A*

Core Q16-FA-101-S1	**Sample 12 Röt/Solling Fm.**	**Sample 13 Solling Fm.**	**Sample 14 Röt Fm.**	**Sample 15 Röt Fm.**
Lithology	Mudstone	Sandstone	Sandstone	Sandstone
Mineral Content (estimate)	Quartz (10%), calcite (60%), micas (30%)	Quartz (30%), calcite (50%), micas (20%)	Quartz (40%), calcite (40%), micas (20%)	Quartz (50%), calcite (40%), micas (10%)
Grainsize (estimate)	very fine grained (1-5 µm)	very fine to fine grained (10-30 µm)	fine grained (25-100 µm)	fine grained (50-300 µm)
Porosity (estimate)	very low porosity	low porosity	medium porosity	low to medium porosity
Sorting	moderately to well sorted	moderately sorted	poorly sorted	poorly to moderately sorted
Cement	very well cemented by dolomite	well cemented by dolomite	poorly cemented	moderately cemented

Table 12: *Summary of observations on cap rock samples 12-15 from Core Q16-FA-101_S1.*

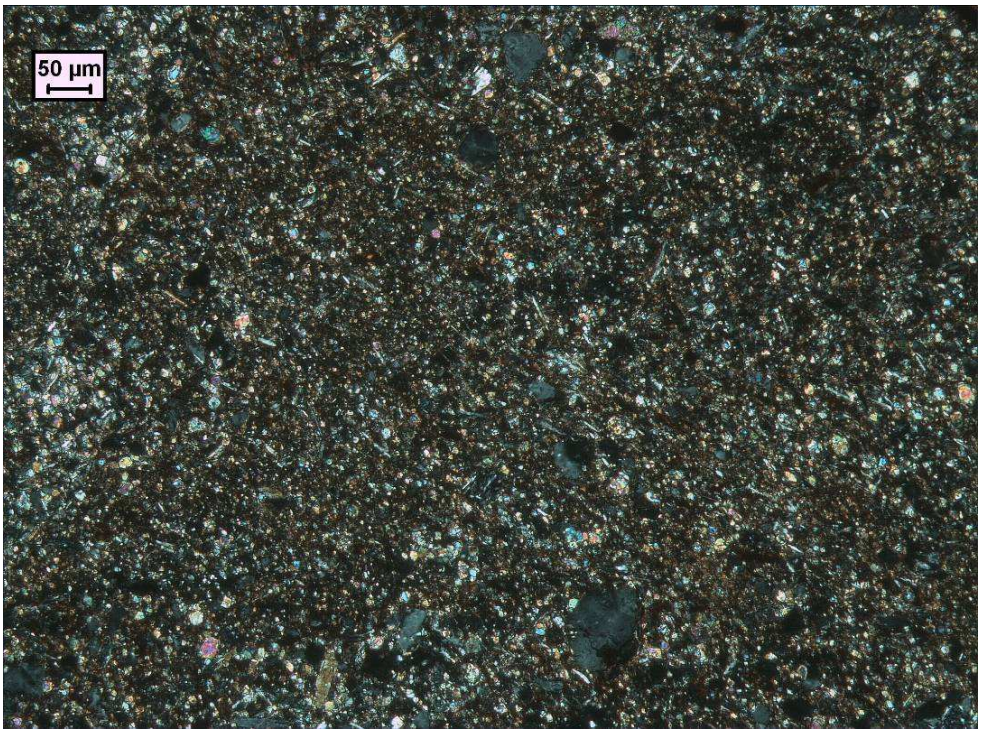

A

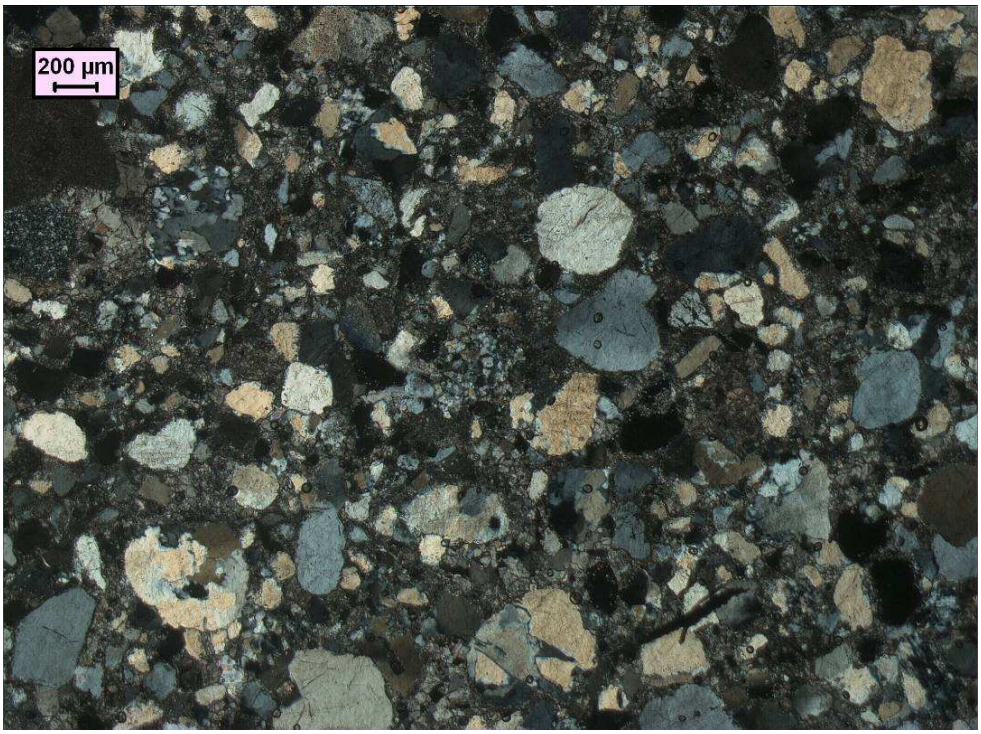

B

Figure15: A) *Photomicrograph of sample 9: silty-mudstone from the Rot Fm. Core Q16-4 Small mica flakes and some fine carbonate grains with coarser isolated quartz grains (crossed polarized light)* ***B)****:Sample 11; an impure sandstone from the Solling Fm. Core Q16-4 (crossed polarized light).*

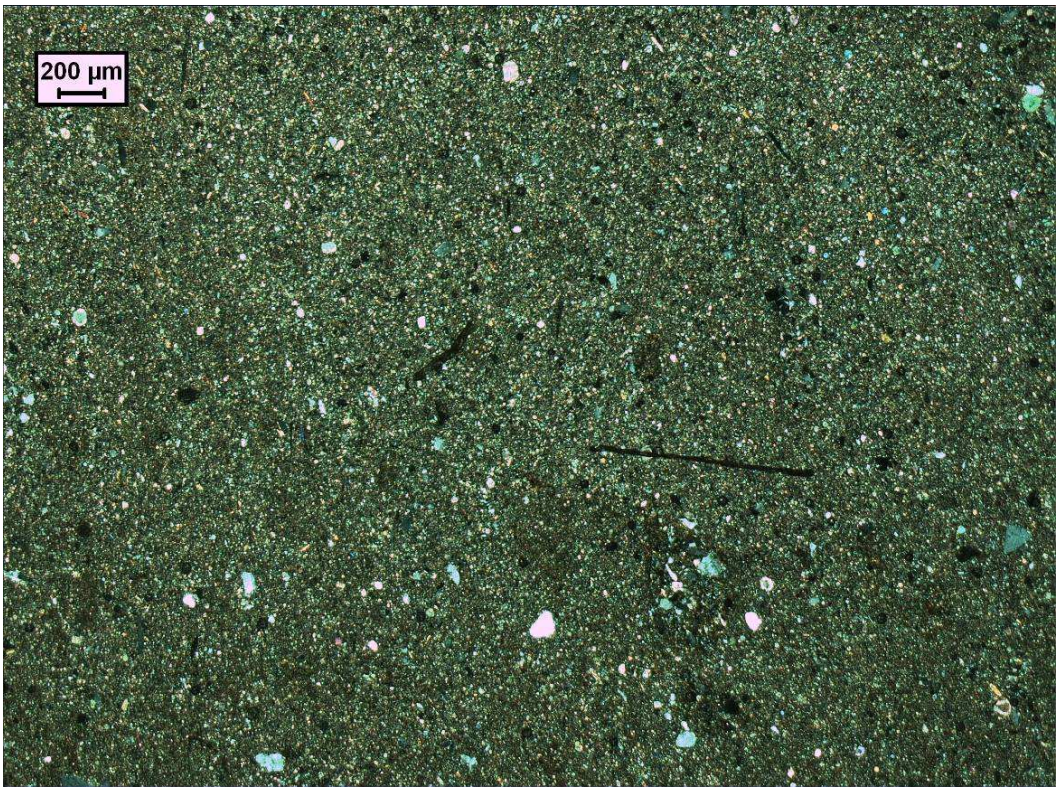

A

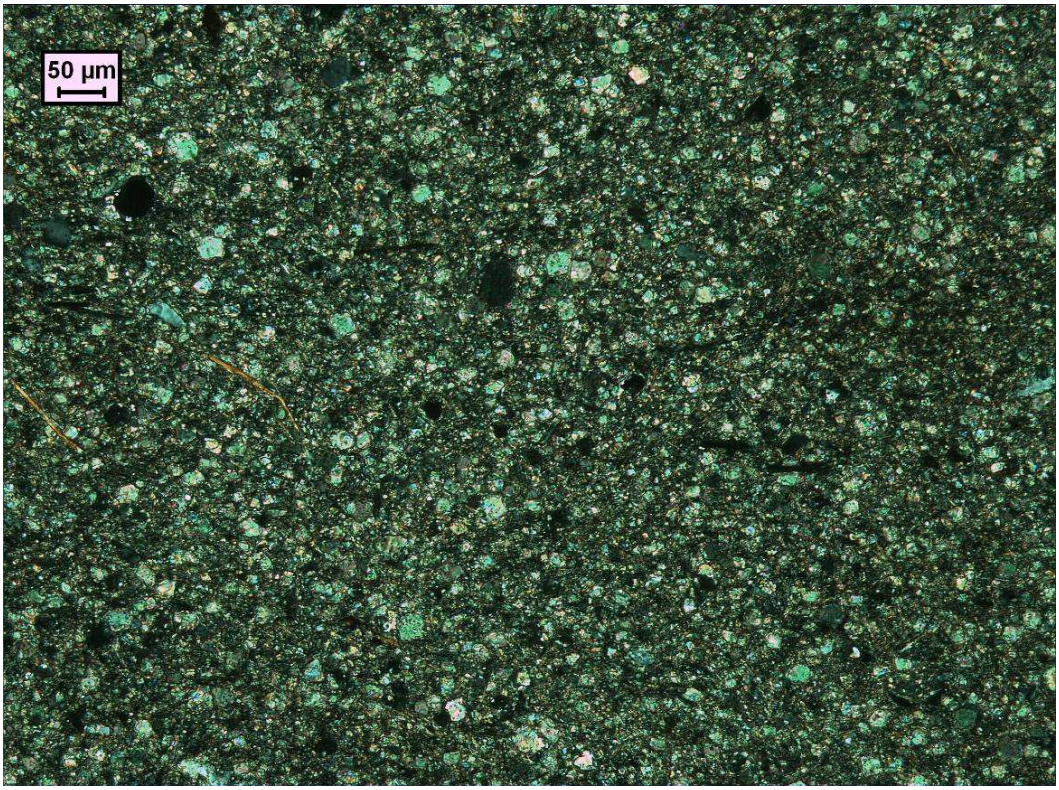

B

Figure 16: A) *crossed polarized micrographs of Sample 12; Marl-mudstone from the Solling Fm.(Q16-FA-101-S1 core). The higher magnification image* ***(B)*** *shows ubiquitous calcite grains and a few muscovite flakes.*

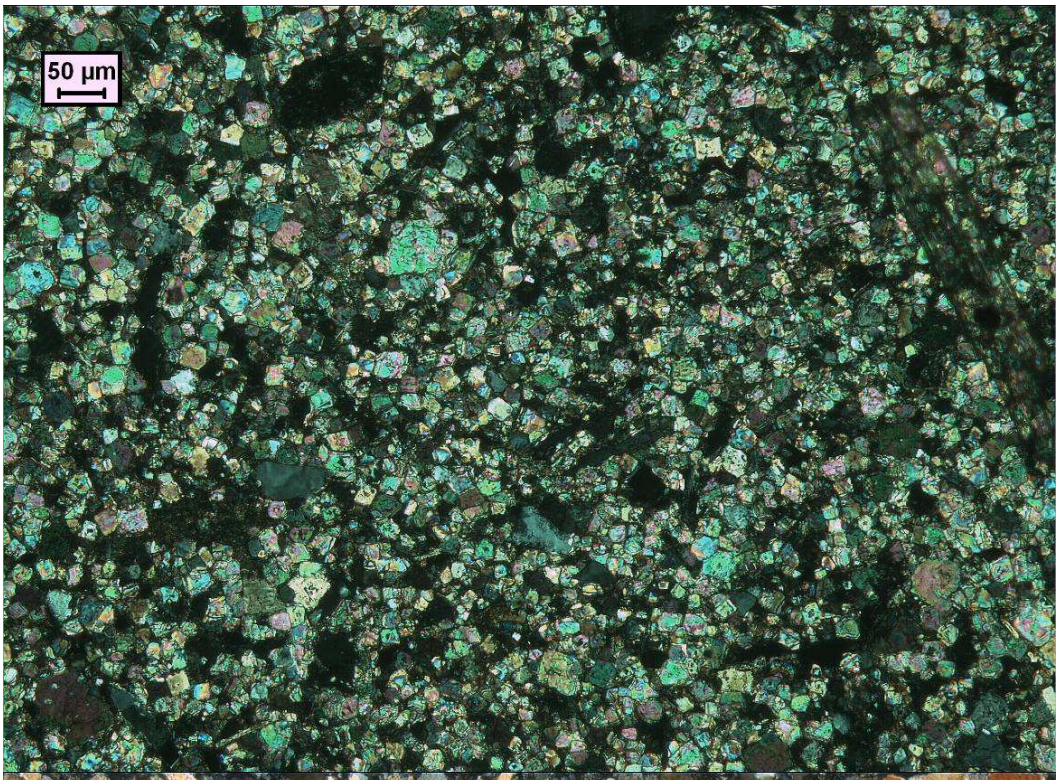

A

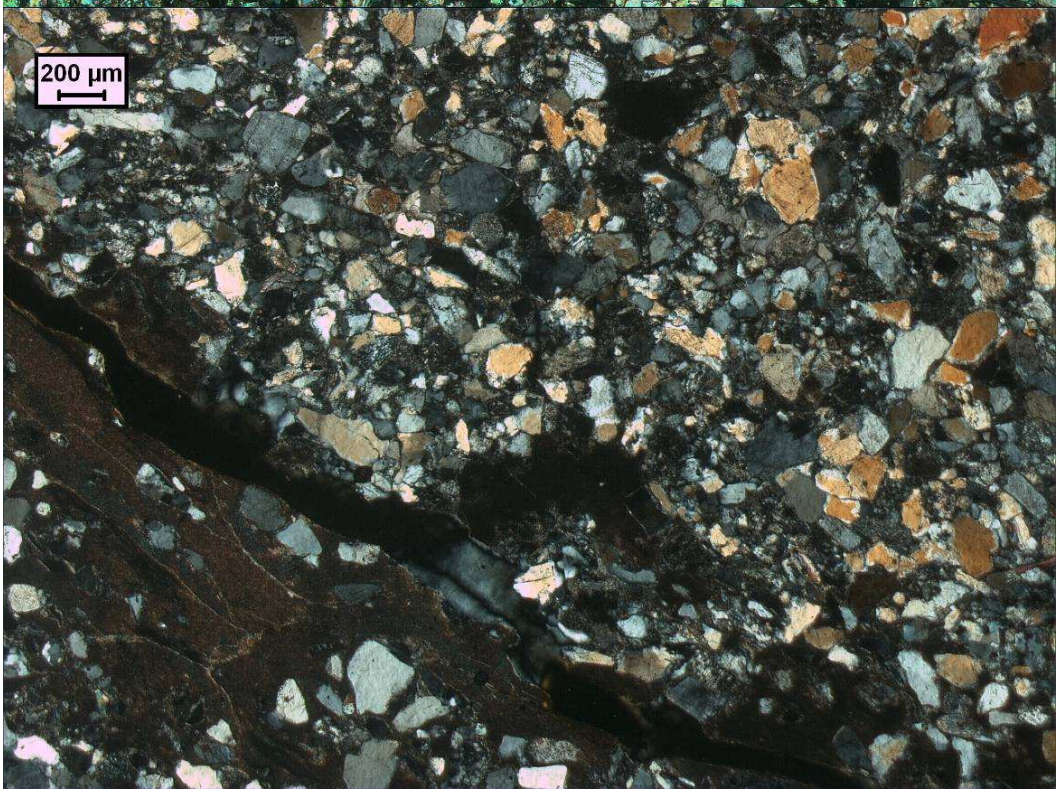

B

Figure 17: A): *Crossed polarized micrograph of sample 13, (Solling Fm., Q16-FA-101-S1 core) marly-silt contains at least 50% carbonate (bright coloured grains).* ***B):*** *Crossed polarized micrograph of sample 14, (Röt Fm., Q16-FA-101-S1 core) impure sandstone with shale partings.*

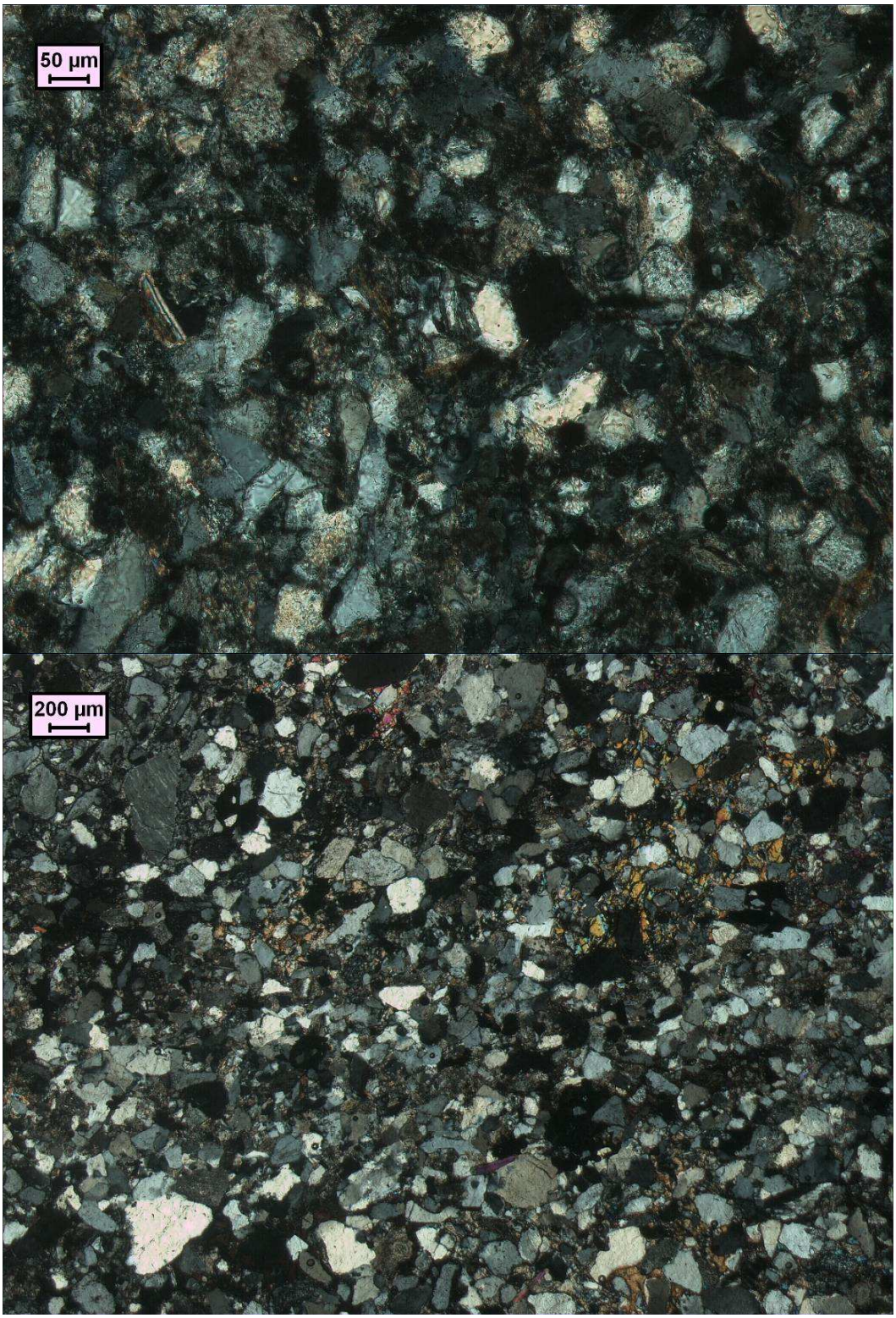

A

B

Figure 18: A) *Crossed polarized micrograph of sample 14, (Röt Fm., Q16-FA-101-S1 core) impure calcite cemented sandstone* ***B)*** *Crossed polarized micrograph of sample 15, (Röt Fm., Q16-FA-101-S1 core) impure sandstone moderately well cemented by calcite.*

2.7. New petrophysical measurements

2.7.1. Permeability measurements P18-field samples

The permeability of samples 1-5 of the P18 field have been measured by the constant-head flow-through permeability test method, using water. These measurements were made to see if they are consistent with the core analysis report (CAR) measurements. The constant head permeability method is a common laboratory testing method used to determine the permeability of granular soils like sands and gravels containing little or no silt and permeabilities > $10^{-18}m^2$. It involves the flow of water through a cylindrical sample under a constant pressure difference (head). The test is carried out in a permeability cell, or permeameter, which can apply a confining pressure to ensure that the rubber jacket seals around the cylinder of rock. For the samples 1-5 the permeability was measured at a confining pressure of 1 MPa (Table 12).
Against expectation, the samples show a relatively low permeability compared to the correlated permeability measurements which were measured historically at pressures ranging between 5 and 37 MPa (Tables 5&6). However the error in the measurements is large. This is probably caused by air bubbles which were trapped within the cylindrical sample, blocking the flow of water and influencing the permeability measurements.
The samples were also measured dry with the Argon gas transient step method. This method involves the transient flow of Argon gas through a cylindrical sample achieved by application of a sudden step change in pressure difference between each end of the sample. The logarithm of pressure decay with time is used to obtain the permeability (Peach, 1991)

UU Sample#	Constant head H_2O flow-through*			Argon transient step**			CAR***
	Head (m)	κ (m^2)	Best range κ (m^2)	Mean P_{Ar} (MPa)	κ (m^2)	Best range κ (m^2)	κ (m^2)
1a Detfurth	2.2	$1{,}8 \cdot 10^{-17}$	$1.8 – 5.0 \cdot 10^{-17}$	1.5	$7.2 \cdot 10^{-16}$	$3.4 – 7.2 \cdot 10^{-16}$	-
	1.7	$2.2 \cdot 10^{-17}$		1	$3.6 \cdot 10^{-16}$		
	1.4	$2.7 \cdot 10^{-17}$		0.5	$3.4 \cdot 10^{-16}$		
	0.2	$5.0 \cdot 10^{-17}$					
1b Detfurth	2.2	$4.8 \cdot 10^{-17}$	$4.8 – 6.5 \cdot 10^{-17}$	1.5	$1.7 \cdot 10^{-15}$	$1.7 – 2.0 \cdot 10^{-15}$	
	1.7	$5.5 \cdot 10^{-17}$		1	$2.0 \cdot 10^{-15}$		
	1.4	$6.5 \cdot 10^{-17}$		0.5	$1.9 \cdot 10^{-15}$		
	0.3	$5.2 \cdot 10^{-17}$					
2a Detfurth	2.2	$7.4 \cdot 10^{-18}$	$7.4 – 8.8 \cdot 10^{-18}$	1.5	$1.8 \cdot 10^{-16}$	$1.1 – 1.8 \cdot 10^{-15}$	-
	1.7	$8.1 \cdot 10^{-18}$		1	$1.1 \cdot 10^{-16}$		
	1.4	$8.8 \cdot 10^{-18}$		0.5	$1.1 \cdot 10^{-16}$		
2b Detfurth	2.2	$2.8 \cdot 10^{-17}$	$2.0 \cdot 10^{-16}$	1.5	$2.1 \cdot 10^{-15}$	$2.1 – 5.0 \cdot 10^{-15}$	
	1.7	$3.4 \cdot 10^{-17}$		1	$3.9 \cdot 10^{-15}$		
	1.4	$5.2 \cdot 10^{-17}$		0.5	$5.0 \cdot 10^{-15}$		
	0.2	$2.0 \cdot 10^{-16}$					
3a	2.2	$2.7 \cdot 10^{-17}$	$3.6 \cdot 10^{-16}$	1.5	$1.5 \cdot 10^{-16}$	$3.6 \cdot 10^{-17}$	-

Detfurth	1.8	$2.5 \cdot 10^{-17}$		1	$3.6 \cdot 10^{-17}$		
	1.4	$2.9 \cdot 10^{-17}$		0.5	$3.6 \cdot 10^{-17}$		
	0.2	$3.6 \cdot 10^{-16}$					
3b Detfurth	2.2	$2.3 \cdot 10^{-17}$	$2.3 – 4.4 \cdot 10^{-17}$	1.5	$4.6 \cdot 10^{-16}$	$1.6 – 4.6 \cdot 10^{-16}$	
	1.7	$2.4 \cdot 10^{-17}$		1	$1.7 \cdot 10^{-16}$		
	1.4	$4.4 \cdot 10^{-17}$		0.5	$1.6 \cdot 10^{-16}$		
4b Volprie-hausen	2.2	$2.7 \cdot 10^{-17}$	$2.7 – 4.4 \cdot 10^{-17}$	1.5	$6.1 \cdot 10^{-17}$	$2.7 – 6.1 \cdot 10^{-17}$	-
	1.7	$2.9 \cdot 10^{-17}$		1	$2.7 \cdot 10^{-17}$		
	1.4	$4.4 \cdot 10^{-17}$		0.5	$3.0 \cdot 10^{-17}$		
5b Volprie-hausen	2.2	$3.2 \cdot 10^{-17}$	$3.2 – 9.0 \cdot 10^{-17}$	1.5	$6.8 \cdot 10^{-16}$	$6.2 – 6.8 \cdot 10^{-16}$	-
	1.7	$3.4 \cdot 10^{-17}$		1	$6.2 \cdot 10^{-16}$		
	1.4	$4.2 \cdot 10^{-17}$		0.5	$6.3 \cdot 10^{-16}$		
	0.2	$9.0 \cdot 10^{-17}$					
6b Hardegsen							$1.4 \cdot 10^{-14}$
7b Hardegsen							$3.0 \cdot 10^{-12}$

Table 12: *Permeability data on unreacted cylinders of P18 reservoir rock (Table 3). Sample 6b and 7b are taken from the Core Analysis Report (CAR). * Measured at 1MPa confining pressure. ** Measured at 2MPa confining pressure. *** Core Analysis Report.*

Clearly for the reservoir materials (Table 12) the Detfurth Fm. sandstones offers considerable permeability and the main reservoir sandstone of the Hardegsen is extremely permeable with a high storage potential.

The cap rock material from cores Q16-4 and Q16-FA-101-S1 shows that the finer materials have low permeabilities of ~10^{-18} m^2 and are capable of sealing the reservoir, see Table 13.

Cap Rock Sample	Argon transient step*			CAR** permeability (m^2)
	Mean Pressure (MPa)	*Permeability (m^2)*	*Range (m^2)*	
8a	1.5	$9.73x10^{-18}$	**$2.2 - 9.7x10^{-18}$**	$<1x10^{-17}$
	1.0	$2.15x10^{-18}$		
8b	*Sample broken*			
9a	1.5	$2.18x10^{-18}$	**$2.2x10^{-18}$**	?
9b	1.5	$7.75x10^{-17}$	**$7.8x10^{-17}$**	
	1.0	-		
10a	1.5	$5.50x10^{-18}$	**$1.0 - 5.5x10^{-18}$**	$2x10^{-18}$
	1.5	$4.50x10^{-18}$		
	1.0	$1.00x10^{-18}$		
	0.5	$4.30x10^{-18}$		
10b	1.5	$4.37x10^{-17}$	**$3.1 - 4.4x10^{-17}$**	
	1.0	$3.31x10^{-17}$		
	0.5	$3.13x10^{-17}$		
11a	1.5	$4.37x10^{-18}$	**$1.5 - 4.4x10^{-18}$**	$<1x10^{-17}$
	1.0	$1.50x10^{-18}$		
	0.5	-		
11b	1.5	$2.70x10^{-18}$	**$1.7 - 2.7x10^{-18}$**	
	1.0	$2.60x10^{-18}$		
	0.5	$1.70x10^{-18}$		

Cap Rock Sample	Argon transient step			CAR* permeability (m^2)
	Mean Pressure (MPa)	*Permeability (m^2)*	*Range (m^2)*	
12a	1.5	$4.16x10^{-18}$	**$5.0x10^{-19}$**	?
	1.0	$5.03x10^{-19}$		
12b	1.5	-	-	
13a	1.5	$7.36x10^{-18}$	**$1.0-7.4x10^{-18}$**	$<1x10^{-17}$
	1.0	$1.01x10^{-18}$		
13b	1.5	$4.90x10^{-18}$	**$4.9x10^{-18}$**	
14a	1.5	$1.30x10^{-17}$	**$4.7-4.9x10^{-18}$**	$8.0x10^{-17}$
	1.5	$1.08x10^{-17}$		
	1.0	$4.80x10^{-18}$		
	1.0	$4.68x10^{-18}$		
	0.5	$4.93x10^{-18}$		
14b	1.5	$5.35x10^{-16}$	**$2.1-5.4x10^{-16}$**	
	1.0	$2.71x10^{-16}$		
	0.5	$2.10x10^{-16}$		
15b	1.5	$5.40x10^{-18}$	**$4.9-5.4x10^{-18}$**	$2.0x10^{-17}$
	1.0	$4.11x10^{-18}$		
	0.5	$4.88x10^{-18}$		

* Measured at 2 MPa confining pressure

**Core Analysis Report, for comparison

Comments:

1) For samples 12a and 14a, we assumed that either a leak or an opened crack disturbed the measurement at the highest mean pressure

2) Due to limitations in the software, measurements that lasted >24 hrs could not be processed. These 'data' are indicated with a bar ('-')

3) Sample 8b was broken and couldn't be fixed; samples 9b and 10b were split along a fracture more the less parallel to the sample central axis, and were fixed with inert super glue.

***Table 13**: Permeability data on plug cores of cap rock material determined by Argon gas transient step permeametry (to date)*

2.8. Discussion of properties regarding CO_2 storage

The suitability of a depleted gas reservoir for storage of CO_2 rich fluids is dependent on both mineral-compositional (chemically sensitive) and grain-structural (mechanically sensitive) features of the host rock. The injection of CO_2 rich fluids will change the chemical environment and may also alter the thermo-mechanical loading. Clean well cemented quartz sandstone is less likely to be affected by this change in pore fluid. However, the presence of reactive and more soluble components such as carbonate grains (calcite) and cement will be much more likely to be affected and give rise to changes in porosity, permeability and through corrosion of cement to changes in mechanical strength. The presence of less reactive minerals, such as feldspar, mica or clay, also has an important role in the longer term. Such minerals can be sources of cations which can react to form low solubility carbonate products capable of fixing CO_2 via mineralization. These processes are the core problem for the research currently underway by UU and others under the CATO2 framework. Identification of potential

reactants in this preliminary study of site specific materials is one of the aims in the characterization study.

The Hardegsen sandstone reservoir rock examined in the P18 cores is a remarkably clean well rounded aeolian quartz sand with a quartz cement and evidence of compaction by pressure solution (indented grain contacts and quartz overgrowths/cement). The colour in the reservoir cores is white whereas onshore, in the absence of hydrocarbons the colour is usually deep red from iron rich coatings (original sedimentary desert environmental patina). This suggests that some chemical leaching occurs below ground in the hydrocarbon rich (reducing) environment. The cement remains intact and is probably more developed underground than observed in outcrop in the German Eifel. The equivalent sandstones are weakly cemented and crumble to the touch. The simple composition of the main reservoir sandstone does not suggest any great changes will occur during injection of CO_2. The lack of impurities can also be a disadvantage in that very little opportunity is available for mineralization and long term fixation of the CO_2 fluids.

The Detfurth and Volpriehausen sandstones in the reservoir core are both finer grained and contain many more impurities. In particular they both have extensive calcite cements. This will be reactive with CO_2 rich fluids and their behaviour during injection may be seriously affected. This is probably not a sealing problem but may affect reservoir compaction under load.

The cap rocks so far investigated are essentially carbonate rich mudstones of the Solling Fm. and lower Röt. This presence of carbonate (up to 60% by volume) will be reactive if exposed to the CO_2 rich fluids. The permeability is low and currently these rocks form a good hydrocarbon seal but may become modified by dissolution. Above the Solling Fm., the Röt formation contains evaporitic sequences with anhydrite and dolomite these are not likely to act as a secondary barrier, since they too contain reactive components. The need for more samples of cap rock to allow mechanical and fluid rock interaction experiments is vital. So far we have not been successful in finding similar material onshore, and the core material is severely limited.

2.9. Conclusions

Site-specific material from the wells nearest to the CO_2 injection-targeted and TAQA operated, P18A-05 and P18A-07 wells, has been obtained and examined as part of this preliminary characterization. The material is naturally limited in quantity due to the need to preserve core in the national archives. The material has allowed access to the main rock types expected in the upper part of the existing gas reservoir in the Buntsandstein series. The exact seal (reservoir sandstone to cap rock mudstone transition) was not available but core from very near in the sequence was available in the Solling Fm. and overlying Röt. The character of these materials would certainly constitute a cap rock seal. The need for larger volumes of material led us to search laterally onshore and it is clear that due to facies variation in the Lower Triassic Buntsandstein series the chance of finding exact equivalent material onshore is low. Indeed the character of the Solling in the Northern Eifel turned out to be permeable and even conglomeratic in exposures. The onshore material cannot be called a “cap rock”, and

indeed many of the onshore gas reservoirs to the East of P18 have cap rock seals much higher in the litostratigraphy (U. Trias - Muschelkalk or even rocks in the Cretaceous)
We are currently investigating alternative sites to obtain an equivalent cap rock.
The reservoir material is less of a problem and we have suitable material from onshore in sufficient quantity fro mechanical testing.

The occurrence of large amounts of carbonate in the P18 field cap rock is an important finding regarding the performance of the Solling cap rock seal during CO_2 injection. The material should be exhaustively tested to assess its performance. However, the limitation of material supply could present a serious problem to achieving that aim.

3. Representative material from onshore localities

3.1. Geological setting and stratigraphic equivalence

3.1.1. Triassic exposed in the Northern Eifel

The Buntsandstein Formation exposed at the surface in the Eifel region in Germany is assumed to be correlative and comparable with the Main Buntsandstein Formation in the southern parts of the P quadrant offshore the Netherlands (Ames & Farfan, 1996). According to Ames and Farfan both areas were affected by similar changes in climatic conditions; fluvial sedimentation of the lower Main Buntsandstein (Volpriehausen) was superceded by predominantly aeolian deposition of the middle Main Buntsandstein (Detfurth and Hardegsen sandstones). For the purpose of this research a short field trip to the Northern Eifel was organized to sample fresh specimens of the Volpriehausen, Detfurth and Hardegsen sandstones, the Röt and Solling claystones and to analyse the Hardegsen/Solling contact. However, the Röt and Solling claystones were not present in the outcrops visited. Likewise the Hardegsen/Solling contact proved elusive. A brief literature research was done (by B. Verberne) to locate several outcrops which were expected to contain the rocks of interest (Figure 19).

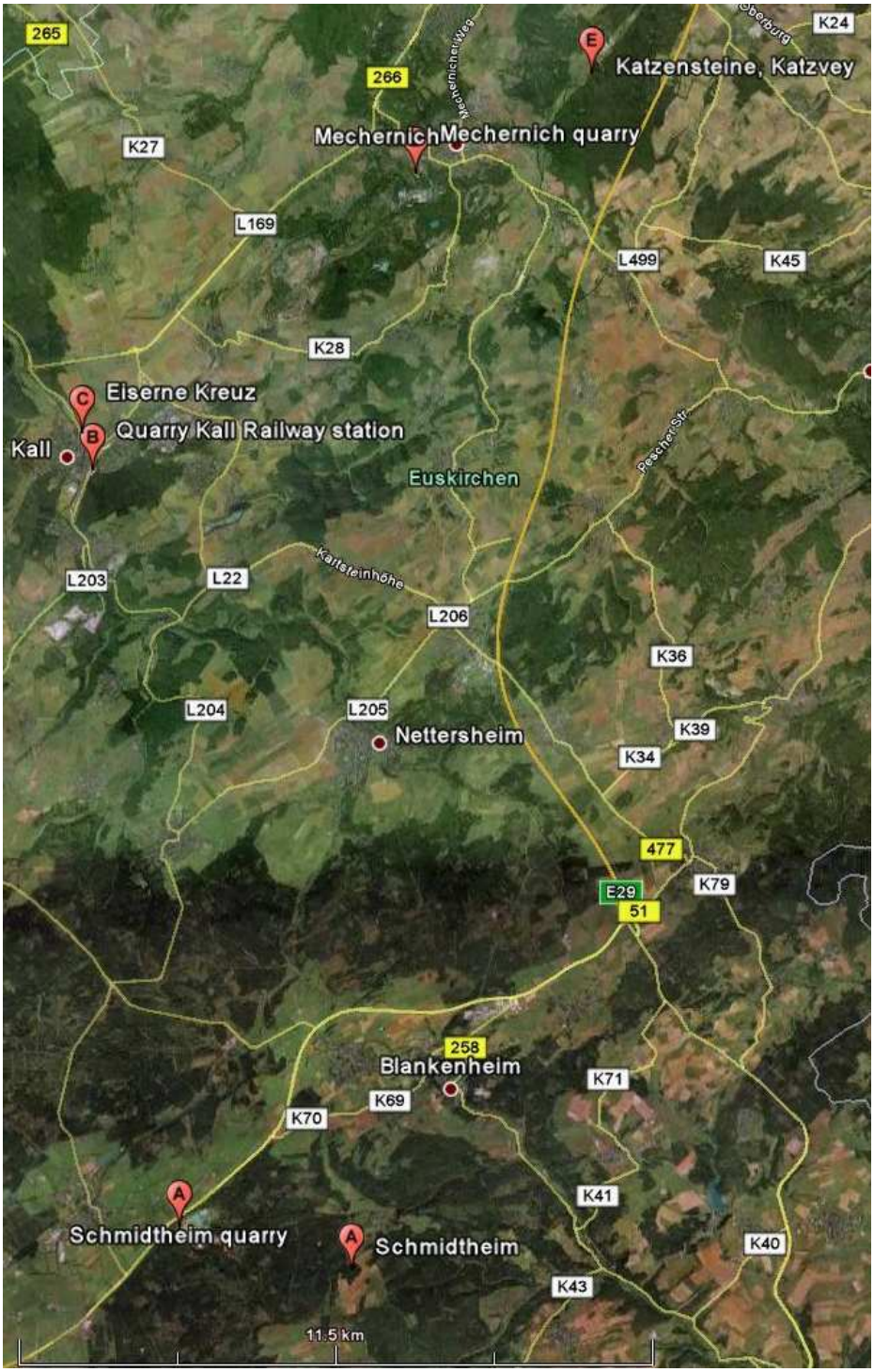

Figure 19: *An overview of the different sites visited during the short field trip in the Northern Eifel, Germany. Site 1: Schmidtheim quarry + Schmidtheim, Site 2: Old quarry at the Kall railway station, Site 3: "Eiserne Kreuz" along the road from Kall to Gemünd, Site 4: quarry in Mechernich, Site 5: Katzensteine, Katzvey. (Google Earth, 2010).*

3.2. Location of samples

3.2.1. Old quarry at the Kall railway station

This quarry is located just east of the Kall railway station (50°32'15.50"N, 6°33'29.27"E). In this quarry, the top of the Middle Buntsandstein is exposed, i.e. the Hardegsen and/or the Solling sandstones. The exposure displays the uppermost conglomerate, which is considered to represent the Solling Formation. The conglomerates consist mainly of quartzites of unknown provenance (Figure 20C). Further, limestone and dolomite pebbles of Lower Carboniferous origin occur, which are considered typical for the East-Belgium Paleozoic (Geluk et al, 1997). Within this sequence of conglomerates, sandstone layers of a few meters occur. The sandstone layers are fine to medium grained, have a slightly reddish colour and seem to be of fluvial origin (Figure 20B). Higher in the sequence the sandstone layer seems to get thicker and are more fine-grained (Figure 20D).

3.2.2. "Eiserne Kreuz" along the road from Kall to Gemünd

The "Eiserne Kreuz" - a military monument is located along the L204/B266 from Kall to Gemünd (50°32'38.06"N, 6°33'19.56"E). This exposure shows the boundary between the Middle and Upper Buntsandstein (Solling and Röt Formations). The coarse conglomeratic sediments alternate with sandstones; a NE transport direction can be concluded from the pebble imbrications (Figure 21A&B; Geluk et al., 1997).

3.2.3. Quarry in Mechernich

A small quarry located near Peterheide, Mechernich (50°35'11.56"N, 6°38'29.18"E). The exposed rocks consist of eolian Middle Buntsandstein, i.e. the Detfurth and/or the Hardegsen sandstones. The sequence displays mature sandstone layers of approximately 2 m thick, which are fine to medium grained and again have a slightly reddish colour (Figure 22A). It also consists of some conglomerate layers, with pebbles of unknown provenance and one sandstone layer of a few meters thick with a high amount of spherical objects which share the colour of the sandstone beds, (Figure 22B). These spherical objects are probably iron concretions.

3.2.4. Katzenstein, Katzvey

A sequence of fine to medium grained sandstones of the Middle Buntsandstein is exposed along the L61 from Mechernich to Satzvey (50°36'11.21"N, 6°41'13.18"E). The exposure displays peculiar pillar rock formations that are strongly eroded (Figure 23A&B). The outcrops comprise a sequence of sandstone layers which display sets of cross-strata, typical for an aeolian environment.

A

B

Figure 20: A) *Overview of the old quarry at the Kall railway station. It shows the uppermost 40 m of the Middle Buntsandstein comprising a large sequence of conglomerates with an alternation of sandstone beds (car for scale)* ***B)*** *Zoomed in on the middle of the exposure, showing a large conglomerate layer and a smaller sandstone layer at the base (person for scale).*

C

D

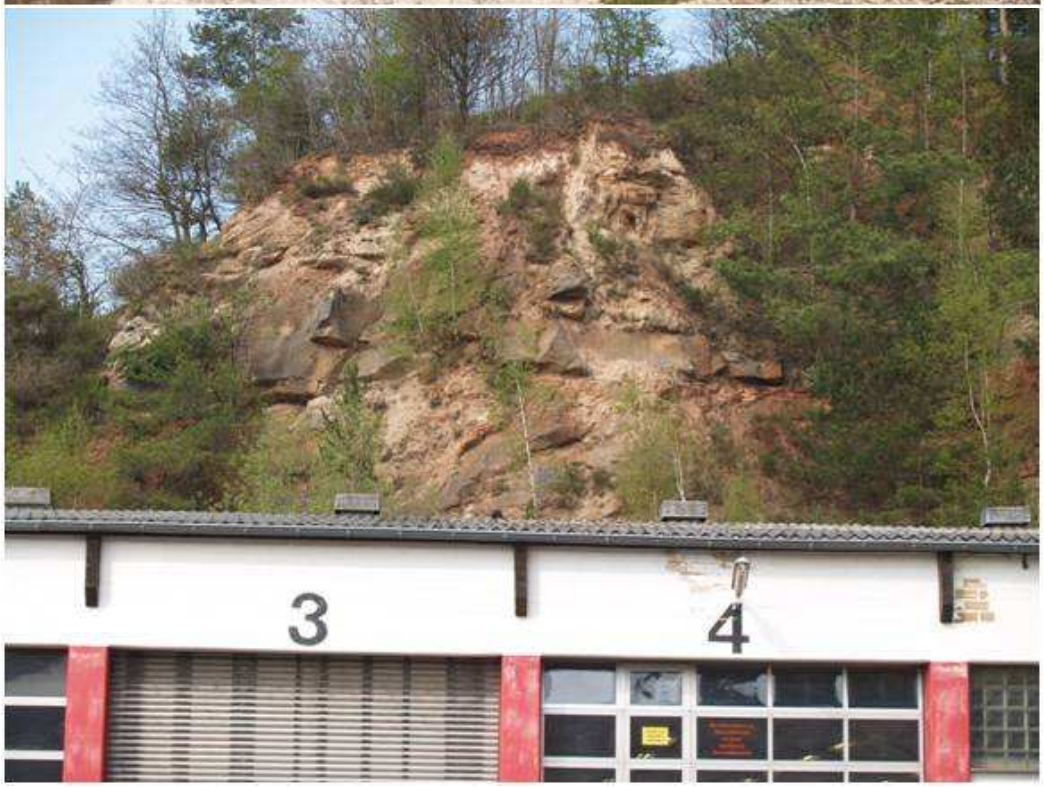

Figure 20: C) *Close-up of a conglomerate layer (bag for scale).* ***D)*** *Larger sandstone beds at the top of the sequence (building for scale).*

A

Figure 21: A) *Conglomerate and sandstone layers from the Upper Buntsandstein at the "Eiserne Kreuz" along the road to Gemünd (bench for scale).* ***B)*** *Picture which displays the sandstone and conglomerate alternation (hammer for scale).*

B

A

B

Figure 22: A) *The quarry in Mechernich. It displays a sequence of sandstones with some conglomerate beds and one sandstone layer with a high amount of concretions (bag for scale)* ***B)*** *Close-up of the sandstone layer with the concretions (lens cap for scale).*

A

B

Figure 23: A) *Picture showing the sequence of fine to medium grained sandstones (person for scale).* ***B)*** *Close-up of the sandstone layers showing a set of cross-strata (lens cap for scale).*

3.3. Preliminary petrophysical measurements

The porosity of the two samples obtained from the northern Eifel (16E&17E), seem to be consistent with the porosity measurement from the Hardegsen formation. Permeametry has concentrated on the offshore material so far. Future measurements will be made as required and suitable material is selected.

3.4. Microstructural description of samples

Sample 16E has a smaller grainsize (Table 11), is moderately sorted and is more cemented giving a tighter structure and lower porosity (Figure 24 A, B, C &D). Sample 17E has a larger grainsize (Table 11), is well sorted and less cemented giving a looser structure and higher porosity (Figure 25A, B, C &D).

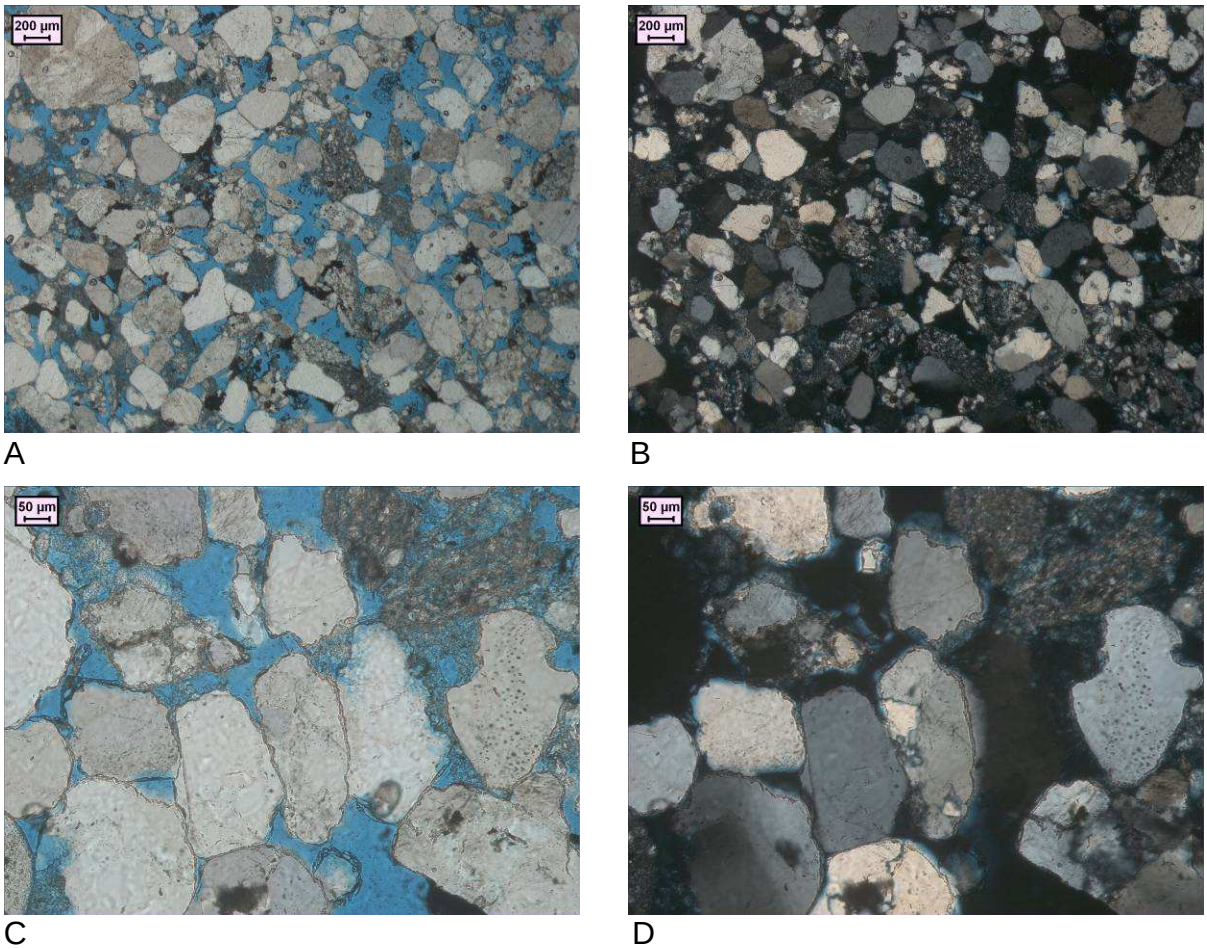

Figure 24: A): *Sample 16E in plane polarized light,* ***B):*** *Sample 16E, crossed polarized light,****C):*** *Close-up of grains showing cement overgrowth and grain indentations (blue are is porosity),* ***D)****: Same as C: crossed polarized light*

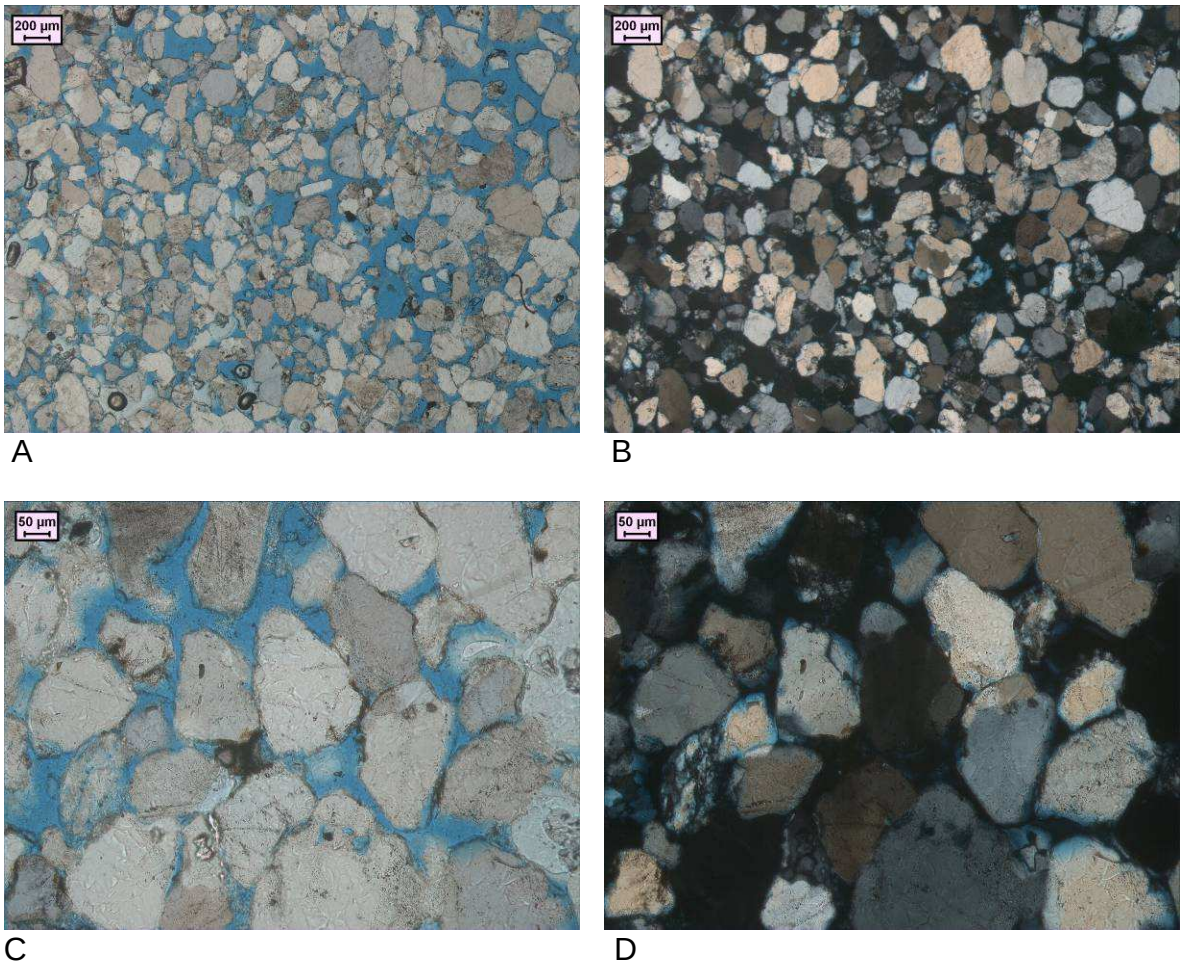

Figure 25: A): *Sample 17E plane polarized light (blue area is porosity),* ***B):*** *same as A but crossed polarized light,* ***C):*** *close-up of sample 17E in plane polarized light showing porosity in blue and grain contacts with less quartz cement than sample 16E,* ***D):*** *Same as C but in crossed polarized light.*

3.5. Discussion of equivalence to P18 material

The collection of Buntsandstein material from the Northern Eifel proved useful in allowing a clear observation of the sedimentary features and facies differences in this series. The offshore reservoir rocks from the P18 and adjacent fields all share a similar cap rock seal, in the Solling Fm., which consists of low permeability calc-mudstones (marls) and fine grained marly-silts. This facies of the Solling Fm. does not persist along the sedimentary basin as one travels eastward. Although the sedimentary basin is continuous, there is general coarsening of the sediments towards their source regions. These also change from the London Brabant Massif to the south, for the P18 field and the

Rhenish massif to the east for the Northern Eifel. It is unfortunate but the changes although subtle are more than enough to affect the seal horizon, so that the onshore gas fields have cap rock seals much higher in the stratigraphy (i.e. Upper Trias Muschelkalk, etc.). For this reason the Solling of the N Eiffel has not provided us with suitable cap rock equivalent material.

The reservoir sandstones are well represented in the Northern Eifel and we were able to collect material with very similar features to the offshore Hardegsen other than its colour and oxidation state. The quartz grains and their cement is very similar, in both onshore and offshore material.

3.6. Conclusions

We have investigated the availability of onshore equivalent material to the P18 reservoir and cap rock. We have found that good reservoir-compatible sandstone occurs in the Northern Eifel at the quarry at Mechernich and have collected samples suitable for mechanical testing. The sandstone is similar to that of the offshore P18 Hardegsen formation but the cement is a little less well developed and will probably mean a lower crushing strength for this material. Chemically it is similar.

The need for a good equivalent for the P18 cap rock remains and the search for suitable onshore material continues. If more offshore well-core material becomes available then of course we will use it in the CATO2 research.

4. General conclusions and next steps

The specific aim of deliverable D06 of WP3.03 is the acquisition, characterization and mutual comparison of geological materials from the reservoir-caprock-fault system that either directly come from the wells considered for CO2 injection in the P18 field or come from elsewhere but can be regarded as equivalent to the rocks encountered in the P18 wells.

Sealing caprocks are claystones from the Upper Triassic Solling formation, and evaporites and claystones from the Röt formation positioned directly above the Solling. Reservoir rocks are sandstones and clay-siltstones of Lower Triassic age from the so-called Main Buntsandstein. This unit is subdivided in three formations; Volpriehausen, Detfurth and Hardegsen. Fault rocks can be expected to contain components of the reservoir and/or caprocks.

- Material of all cap rock and reservoir formations (P18 and nearby Q16) has been acquired from core material held by TNO (Zeist) and NAM (Assen). Sample quantities, though, were limited.
- No fault rock material has yet been encountered in the cores.
- Fresh specimens of Volpriehousen, Detfurth and Hardegsen sandstones were collected in the Eifel region, Germany.
- Microstructural, petrographical and X-ray diffraction of samples has shown that the material from the Eifel forms a good equivalent for the P18 reservoir rocks, providing enough material for future mechanical testing.
- No rocks, equivalent to the cap rocks of P18, are exposed in the Eifel area; the trends in facies from the western part of the Netherlands towards the east are such that the sealing capacity is reduced.
- The Solling and lower Röt cap rocks investigated are essentially carbonate rich mudstones. They have low porosities and low permeabilities, confirming their sealing capacity with respect to hydrocarbons. However, the sealing characteristics may become modified by dissolution of calcite related to the injection of CO2.
- The Hardegsen sandstone reservoir rock is a clean, well rounded aeolian quartz sand with a quartz cement and evidence for compaction by pressure solution. Porosity lies in the range 5-23%, permeability runs up to 3000 mD. Some calcite, feldspar and rock fragments are present, but the simple composition (up to 90% quartz) of the sandstone does not suggest any great changes will occur during CO2 injection.
- The Detfurth and Volpriehausen sandstone reservoirs are finer grained, contain lower amounts of quartz (65-75%) and have relatively high amounts of calcite cement (up to 15%). Porosities range 2-15%, permeabilities are substantially lower than in Hardegsen. These reservoir rocks can be expected to be reactive with CO2 rich fluids, which may affect reservoir compaction under load as well as development of faults.

In order to come to a full characterization and comparison of relevant rock materials, more samples of cap rocks are needed. As one of the next steps, the search for cap rock equivalent material exposed onshore will be intensified. After obtaining suitable material, new petrographic analysis as well as permeability measurements can be made.

Further, more work is needed in order to locate suitable samples of faulted reservoir rock and caprock.

5. Acknowledgements

We wish to thank TNO (Zeist) for their help with the retrieval of core material and likewise the NAM (Assen) for their assistance in viewing and sampling the cores in their repository.

6. References

Ames, R. and Farfan, P.F., 1996. *The environment of deposition of the Triassic Main Buntsandstein Formation in the P and Q quadrants, offshore the Netherlands*. *In*: Rondeel, H.E., Batjes, D.A.J. & Nieuwenhuijs, W.H. (eds): Geology of gas and oil under the Netherlands. Kluwer (Dordrecht): 167–178.

Beutler, G., 1995. Stratigraphie des Keupers. Bundesanstalt fur Geowissenschaften und Rohstoffe (Hannover), Archive number 113087 (unpublished report): 147 pp.

CAR: *Core Analysis Report for AMOCO Netherlands Petroleum Company*, P18-02, The Netherlands, 1989.

CAR*: Core Analysis Report for AMOCO Netherlands Petroleum Company*, P18-02-A01 (P18-03), The Netherlands, 1990.

Egmond, van, S., Hendriks, C, Lysen, E. Visser, de, E. & Vos, de, R., 2009. Ecofys Netherlands. *Catching carbon to clear the skies: Experience and highlights of the Dutch R&D programme on CCS, 2009: 27-31*.

Fontaine, J.M., Guastella, G., Jouault, P. & De la Vega, P., 1993. *F15-A: a Triassic gas field on the eastern limit of the Dutch Central Graben*. *In*: Parker J.R. (ed.): Petroleum Geology of Northwest Europe. Proceedings of the 4th Conference, Geological Society (London): 583–593.

Geluk, M.C., 2005. Stratigraphy and tectonics of Permo-Triassic basins in the Netherlands and surrounding areas. PhD thesis, Utrecht University: 111 pp.

Geluk, M.C., 2007. *Triassic. In:* Wong, Th.E., Batjes, D.A.J. & de Jager, J. *Geology of the Netherlands. Royal Netherlands Academy of Arts and Sciences, 2007: 85-106*

Geluk, M.C., Albas, L. & Pagnier, H., 1997. *PGK Field seminar to the Buntsandstein of the Northern Eiffel (Germany), Mechernich area.*

Geluk, M.C. & Rohling, H.-G., 1999. *High-resolution sequence stratigraphy of the Lower Triassic Buntsandstein: a new tool for basin analysis. In*: Bachmann, G.H. & Lerche, I. (eds): The Epicontinental Triassic. Zentralblatt fur Geologie und Palaeontologie 7-8: 545–570.

Geluk, M.C., Plomp, A. & Van Doorn, Th.H.M., 1996. *Development of the Permo-Triassic succession in the basin fringe area, southern Netherlands. In*: Rondeel, H.E., Batjes, D.A.J. & Nieuwenhuijs, W.H. (eds): Geology of gas and oil under the Netherlands. Kluwer (Dordrecht): 57–78.

Hangx, S.J.T., 2008. *Geological storage of CO_2: Mechanical and chemical effects on host and seal formations. In:* Geologica Ultraiectina, no. 311

Hangx, S.J.T. and Spiers, C.J., 2009. Reaction of plagioclase feldspars with CO2 under hydrothermal conditions, Chemical Geology 265 (1-2) , 88-98.

Jager, de, J., 2007. Geological development. *In:* Wong, Th.E., Batjes, D.A.J. & de Jager, J. *Geology of the Netherlands. Royal Netherlands Academy of Arts and Sciences, 2007: 5-26.*

Jager, de, J. & Geluk, M.C., 2007. Petroleum geology. *In:* Wong, Th.E., Batjes, D.A.J. & de Jager, J. *Geology of the Netherlands. Royal Netherlands Academy of Arts and Sciences, 2007: 241-264.*

Johnson, H., Warrington, G. & Stoker, S.J., 1994. 6. Permian and Triassic of the Southern North Sea. *In*: Knox, R.W.O'B. & Cordey, W.G. (eds): Lithostratigraphic nomenclature of the UK North Sea. British Geological Survey (Nottingham).

Liteanu, E., 2009. *Subsurface impact of CO2*, PhD Thesis, 188pp, Geologica Ultraiectina, Utrecht University, Utrecht.

Peach, C. J., 1991.*Influence of deformation on the fluid transport properties of salt rocks.* Phd Thesis, 238 pp. Geologica Ultraiectina, Utrecht University, Utrecht.

Wolburg, J., 1967. Zum Wesen der Altkimmerischen Hebung, mit einem Uberblick uber die Muschelkalk- und Keuper- Entwicklung in Nordwest-Deutschland. Zeitschrift der deutschen Geologischen Gesellschaft 119: 516–523.

Wong, Th.E., 2007. *Jurassic. In:* Wong, Th.E., Batjes, D.A.J. & de Jager, J. *Geology of the Netherlands. Royal Netherlands Academy of Arts and Sciences, 2007: 107-125.*

Ziegler, P.A., 1990. *Geological Atlas of Western and Central Europe*. Shell Internationale Petroleum Maatschappij, 2nd edition. Geological Society Publishing House (Bath): 239 pp.

Deliverable WP3.03 D06

Progress report on: Site-representative cap rock and fault rock samples acquired and characterised.

Part 2: Contribution from Delft University of Technology

Characterisation of Carboniferous and Cretaceous Cap Rock: Petrography and Geochemistry

CATO-2A: WP3.3, D06: Site representative caprock samples

K-H.A.A. Wolf

Delft University of Technology, Dept. of Geotechnology, POB 5028, 2600 GA Delft
Stevinweg 1, Room 3.01, 2628 CN, Delft The Netherlands, k.h.a.a.wolf@tudelft.nl

Abstract

Rock samples of representative caprocks are collect over the past decades in underground and open cast coal mines. An inventory on the literature, lab reports and storage records provided information about majorly Carboniferous and to lesser extent Cretaceous roof rock. These samples are all of sedimentary origin and representative examples of caprock. The Carboniferous samples are all from depths over 700 m and by that not affected by (near surface) erosion effects. However, under in-situ conditions these rocks were under stress. Over the years they became stress-free and dried out, which caused (micro-) fracking. The major (Carboniferous) part of the collection can be used for the DSM-storage site. The samples are categorized on their petrographical and mineralogical properties and representative specimens are analyzed by thin section, XRD and XRF. For objective results of the mineral content, all XRD/XRF-data have been used to create a synthetical mineral composition. For a petrological point of view, the samples are plotted in a series of ternary diagrams. This alternative presentation may help to recognize the caprock quality of the different sedimentary rocks. Many of the analysis are performed under earlier research programs within the framework of CO2-ECBM, Coal Fires and In-situ Coal Combustion.

Introduction

Characterization of original sedimentary cap rocks and their depositional environments provide information on common vertical and lateral continuities, rock compositions and rock textures. It adds to the understanding of its permittivity for CO_2 as a function of varying mechanical behaviour. In other words, how does rock change in strength and volume by CO_2-charging and which minerals are representative for the contaminated zones.

For our purposes two types of coal-related roof rock sediments are sampled. Originally these are studied for an analogous objective, i.e. roof rock behaviour during in-situ coal conversion (Wolf et al. 1987, 1990, 1995, 1996, 1997, 2006). The samples are gathered from:

1. Westphalian coal and coal associated sediments of Northwest European origin. Most of the rocks are collected in the former Campina coalmines of Beringen and Zolder (Belgium), at depths in between 650 m and 950 m. The samples are acquired from fresh coal overburden rock at working faces and on the fronts of tunnel excavations. In addition, exploration drillings in Joppe, Lutte-6 and Kemperkoul (the Netherlands) provide cores of coal roof from depths between 566 m and 1403 m (Pagnier et al. 1996, RGD, 1993).
2. Albian-age coal-related roof rock sediments from Teruel (Spain). They are sampled in the Corta Barabassa and La Pitara open pit mines at depths of up to 120 m, and from outcrops in the vicinity of the former El Tremedal coalmine and EC in-situ coal gasification test site.

Sample blocks of at least 1000 cm^3 are collected and analysed on mineral content and micro-textures. The results of the original samples are presented in this chapter. The blocks are used for:

- The visualization of rock textures before and after experiments.
- The preparation of laboratory samples, i.e.; cylindrical cores and grain aggregates.

Stratigraphical columns and geochemical results of the samples are presented in the Appendix.

Rock Samples: Textures and Minerals

The petrographical data of the roof rocks of coal seams is collected from cores, slabs and thin sections. The distinctive petrography and geochemistry of the thermally and mechanically undisturbed samples is discussed in the following parts. The mineralogical information and results of X-ray diffraction (XRD) and X-ray fluorescence (XRF) are collected in the appendices. They are, among others, used for the determination of the fine grained mineral content, which is difficult to determine by polarization microscope.

The Carboniferous Samples

Many Carboniferous coal roof rocks are studied in-situ during underground sampling trips in Beringen and Zolder. The roofs of several Westphalian production fronts and shafts showed a variety of abrupt to gradational contacts between the coal seam and roof rock. During these visits, discordant coal-roof contacts were not observed and samples not collected. As an alternative washouts filled with distributary channel fills, crevasse channels and crevasse splays are sampled. They also show abrupt contacts, due to a sudden change in depositional conditions. The sandstones and siltstones in this study represent this situation. Many rock samples in this study are laminated sediments. Consequently, we use the textural expressions in accordance

with the “laminite-terminology” suggested by Diessel (1992). As a modification, (Table 1), the term “clay-laminated” is replaced by “shale-laminated” since diagenesis partly transformed clay minerals and organic matter into a shaly texture. In addition, diagenetic alterations, such as the formation of secondary chemical minerals (carbonates, oxides and transformed clay minerals, feldspar and quartz overgrowth), are mentioned as a part of the general mineral content.

About 120 cores and slabs and 17 thin sections have been characterised for their textures and associated mineral phases by polarization-, fluorescence-, and binocular microscopy, XRD, XRF, SEM and were classified into seven different textures in the next sections. The codes of the Carboniferous samples are associated to the layer numbers in the Campina Basin Stratigraphy (See appendix). The summarised rock types are illustrated with photos of slabs and thin sections.

Table 1: **Classification of the (laminated) Carboniferous sandstone, siltstones and shales, as used in our experiments (After Diessel, 1992).**

Sediment type		**Description of the content**
I	Sandstone	Sandstone with no or sparse laminites
II	Sandstone/siltstone – shale-laminite	Approximately equal proportions of sand/silt and shale (40% to 60%)
III	Shale-laminated siltstone	10% to 40% shale laminae alternate with at least 60% sand/silt laminae
IV	Silt-laminated shale	10% to 40% sand/silt laminae interchange with at least 60% shale laminae
V	Coal-laminated shale	10% to 40% coal laminae alternate with at least 60% shale laminae.
VI	Carbonaceous shale	10% to 40% organic matter not laminated with at least 60% shale minerals
VII	Shale	Shale with sparse laminites

Sandstones (I)

Macroscopic structure: Light grey parallel to cross-laminated layering. The cross-bedding shows fining upward, which ends in top sets of grey-brownish silty to shaly lamina (Figure 1.A). Black coal streaks are often observed. Massive parts have a vertical homogeneous sand grain distribution. The width of these massive bands is centimetres or more.

Microscopic description: The grain framework consists of quartz feldspar and muscovite flakes and is well-sorted with a grain size smaller than 200 μm (Figure 1.B). They are compacted with evidence of fracturing of quartz and feldspar grains. At the contacts the grains show pressure solution and weathering/leaching. The laminae consist of the clay minerals illite, chlorite, kaolinite and organic matter. Illite and kaolinite are also abundant present as weathering products of feldspars and muscovite. Secondary carbonates are present as crystallised calcite cement in fissures and as ankerite or siderite in the clay rich parts. In two cases, dolomite was recognised by XRD analysis. Fe-carbonates are abundant as fine-grained aggregates in the vicinity of clay and organic matter rich zones. Siderite is also present in sub-rounded brown coloured concretions (Figure 1.B). Dispersed pyrite is present in clay and organic rich zones. Rutile, tourmaline (schörl) and zircon are recognised in quartz/feldspar-rich areas.

Mineralogy: Quartz (65-75 %), feldspar (5-10%), muscovite flakes (accessory), chlorite (2-9 %), illite (4-10 %), kaolinite (3-5 %), summed carbonates (2-35 %), organic matter (4-6 %), accessory minerals: pyrite, rutile, tourmaline, and zircon.

Sandstone/Siltstone - Shale Laminites (II), Shale Laminated Siltstone (III) and Silt Laminated Shale (IV)

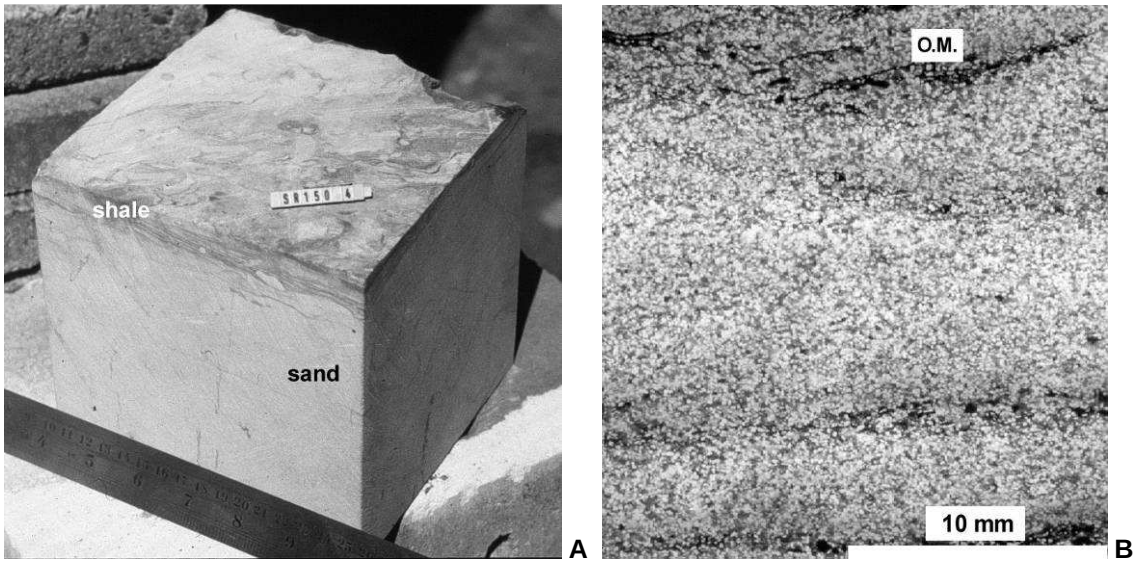

Figure 1: *SR150. A: Sandstone block (15 cm ribs) with a shale laminae rich top. Vertical carbonate filled fractures created during burial. B: Thin section, parallel nicols. Detail of cross laminae with organic matter (om) and clay/organic matter enrichment at the top. Cementation with secondary clay.*

Macroscopic structure: An alternating light grey to grayish-brown irregular or ripple laminated structure, with higher amounts of clay, dispersed organic matter and siderite aggregates in the darker grayish-brown parts (Figures 1.A, 2.A). The laminae have a vertical thickness of about two millimetres or less. Light brown siderite bands (mm to cm width) are frequently present. The laminae are sub-parallel to the bedding.

Microscopic description: In the grain rich laminae, the quartz and feldspar grains are usually in zones with a compacted grain framework. Rarely, smaller grains (< 120 μm) are also embedded in a matrix of clay minerals, organic matter and carbonate cement (Figure 2.B). In the grain rich parts, illite and kaolinite are present as weathering products of feldspars and muscovite. Leaching, pressure solution and fracturing of the quartz and feldspar grains is common. The grains are well sorted and usually < 400 μm for the sandstones and <60 μm for the siltstones. In the clay laminae, the principal minerals are illite, chlorite and kaolinite. In addition, small amounts (< 20 vol.%) of quartz silt and organic matter are present. Grain sizes are normally less than 30 μm, or silt- to clay-size. Siderite or Fe-calcite nodules and dispersed Fe-calcite are found in both quartz rich and clay/organic - matter rich zones. Calcite normally fills fractures and fissures. Some accessory isomorphous pyrite occurs near clay- and organic matter-rich zones. Sparse rutile is found in the silt-rich parts.

Mineralogy: Quartz (5-45 %), feldspar (1-10%), chlorite (3-15 %), illite (15-35 %), kaolinite (7-20 %), summed carbonates (2-35 %), organic matter (1-20 %), accessory minerals: pyrite, rutile.

Coal Laminated Shale or Carbonaceous Shale (V, VI)

Macroscopic structure: An alternating structure of dark brown, grey to black parallel laminations. The browner parts are siderite-rich bands. The dark grey to black zones contain dispersed organic matter. Locally silt bands (<0.5 mm) are the complementary element of the laminated structure.

Microscopic description: The principal minerals are illite, chlorite, kaolinite, quartz and organic matter. The grains have a very fine silt to clay size (< 6 μm). Minor amounts (< 10 vol.%) of larger, probably eolian, quartz grains (silt < 25 μm) are present. An indistinct lamina texture is visible due to the presence of gradually changing amounts of silt, organic matter and siderite. In the more or less laminated silt rich parts the grains are smaller than silt (Figure 3. A,B). The coal consists of thin bands of amorphous black-brown matter, sub-parallel to the layering; thickness usually less than 1 mm. Occasionally, maceral elements such as cell structures are recognised. Idiomorphous pyrite is present near organic matter rich zones. Sparse rutile is found in the silt-rich parts.

Mineralogy: Quartz (15-18 %), feldspar (3-5%), chlorite (3-5 %), illite (18-30 %), kaolinite (5-10 %), summed carbonates (15-17 %), organic matter (20-25 %), accessory minerals: pyrite, rutile.

Shale (VII)

Macroscopic structure: Medium grey to dark brown grey with a faint parallel lamination. The browner parts are siderite-rich bands. The darker parts contain higher amounts of dispersed organic matter. Sometimes silt or coal bands (<0.5 mm) are present.

Microscopic description: The principal minerals are illite, chlorite, kaolinite, quartz and organic matter. The grains have a very fine silt to clay size (< 6 μm). Minor amounts (< 10 vol.%) of larger, probably eolian, quartz grains (silt) are present. A weak lamina texture is recognised caused by varying amounts of silt, organic matter and siderite (Figure 4.A).

Mineralogy: Quartz (22 %), feldspar (3 %), chlorite (3 %), illite (55 %), kaolinite (5 %), summed

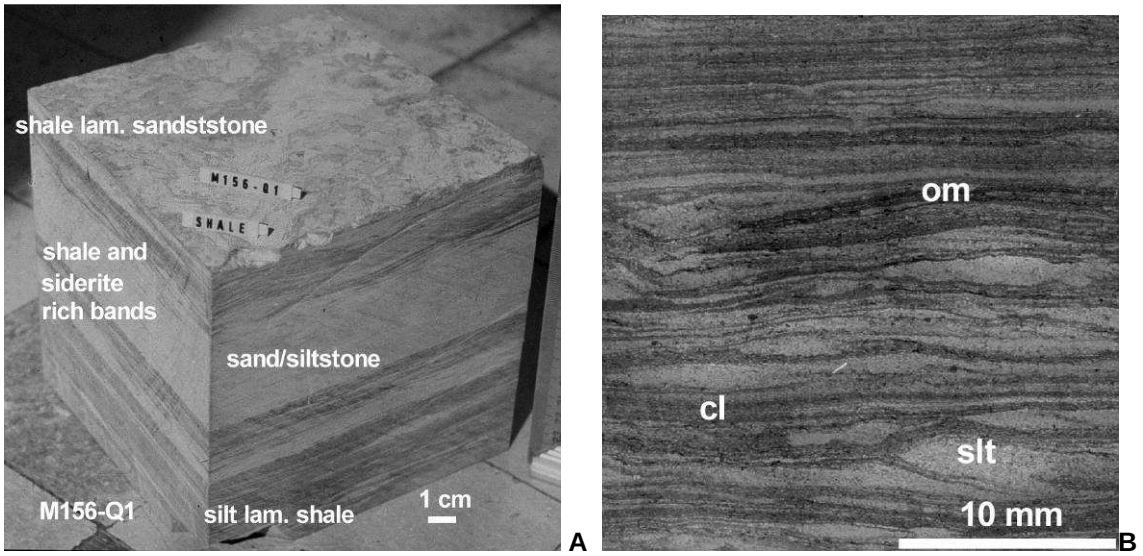

Figure 3: *M156. A: Fine sand/silt layer, silt laminated shale and shale in one block (15 cm ribs). Transitions between laminated silt- and shale dominated parts. B: Thin section, (parallel nicols), detail of organic matter (om) enriched shale. Rippled laminae of silt (slt) and clay (cl) rich zones.*

carbonates (7 %), organic matter (5 %).

Interpretation
Most of the samples show a gradual alteration in texture, which represents slowly changing depositional conditions. Depositional transitions from coal through organic shales to shales occur in back-swamp and lacustrine deposits. Laminated shales and sand/siltstones are also often the product of flood plains or overbank flood deposits. Our observations are in agreement with

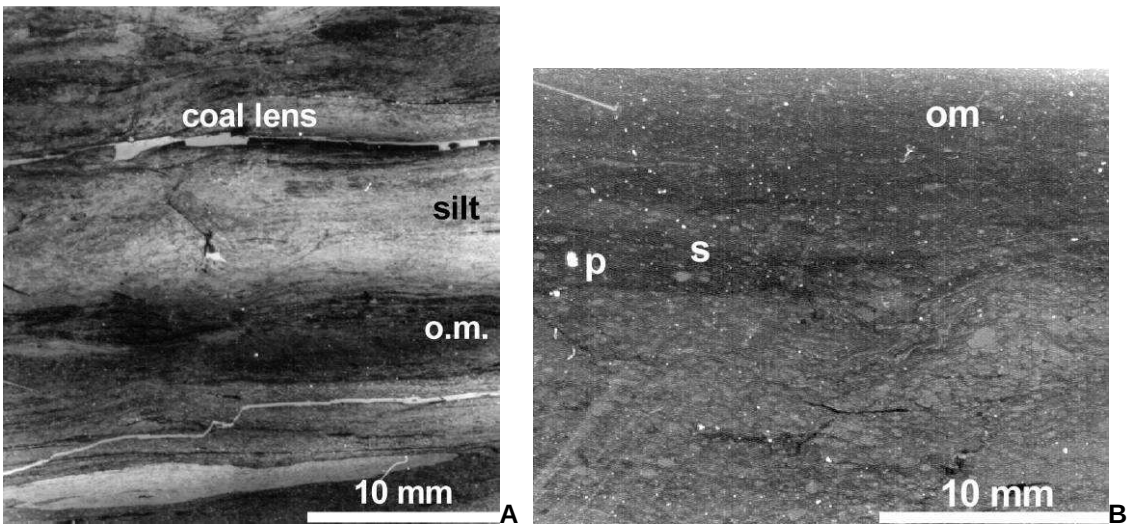

Figure 4. *A: F441-2: Thin section, (parallel nicols), Carbonaceous shale with organic matter (o.m.) and clay rich zones. Locally coal lamina and lenses. B: F441-1: Carbonaceous shale, thin section (parallel nicols), detail of faint bedding in the organic shale. Mostly organic matter, clay, siderite (s) and pyrite (p).*

extensive descriptions of such sediments by Diessel (1992), Guion (1984) and Merrit (1983). The organic constituents are coalified into ranks ranging from bituminous coals to semi-anthracites. The diagenetic process compacted the clay-related sedimentary textures to laminated shale textures and newly formed minerals. Textures without laminae occur in sandstones, siltstones and shales.

The Cretaceous Samples
The Cretaceous roof rocks originate from the Teruel province, Spain. The samples are all of Albian age and obtained at various sites:

- Outcrops; Mas de Venta Pitarra (claystones) and El Tremedal - Alcoriza (friable sandstones). To refer to the sample origin, they are coded with “Pit” and “ET”
- Open pit coal mines; Corta Barabassa - Andorra (claystones) and Daymsa - Foz Calanda (coal shales). The samples are coded by layer number (A3M,T) and “Day” respectively (Figure 5.A).
- Cores from the exploration well ET2 for the European demonstration test on in-situ coal conversion, El Tremedal - Alcoriza (sandstones and clayey sandstones).

The sample sites and rock types are explained in technical reports of the EC-programme by Novem (Wolf et al., 1996, 1997).

Sandstones

Macroscopic structure: A white homogeneous sand. Layering and some cross-bedding is observed on outcrops, in log readings of ET1,2 and drilling cores. The cores also show some dark grey to brown mm-scale laminated parts, which commonly consist of (carbonaceous) clay, coal streaks and Fe-oxide or pyrite.

Microscopic description: The quartz and feldspar (orthoclase) grains show a loose texture with a heterogeneous porosity distribution. The thin sections display an immature texture. The grains are moderately to well sorted, sub-angular and have a low sphericity. The grain size varies from 500 μm to 50 μm: medium to very fine sand. Fracturing of the quartz and feldspar grains is

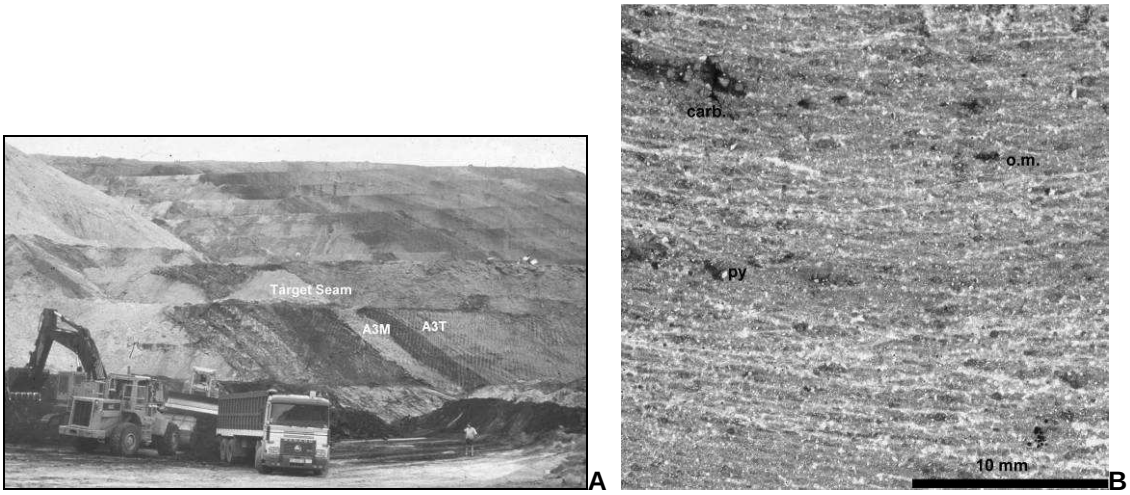

Figure 5: *A: Corta Barabassa open pit showing the roof rock claystones A3M and A3T. B: Thin section, (Parallel nicols), detail of the clay matrix containing idiomorphic siderite (carb), organic matter (om) and pyrite (py).*

locally noticed; leaching weathers the feldspars to clay minerals. In the matrix the principal minerals are primary kaolinite and montmorrilonite (recognised by XRD), some idiomorphic pyrite and organic matter.

Mineralogy based on microscopy, XRD and XRF: Quartz (54-72 %), feldspar (15-20 %), clay minerals (5.5-8.5 %), pyrite (0.5-5 %), organic matter (2-20 %), accessory anhydrite, rutile and Ca-phosphate.

Claystones

Macroscopic structure: Based on the samples from the Corta Barrabassa open pit mine (Figure 5.A), the claystones used in our experiments can macroscopically be divided in two types:

- The T-type, a brownish-grey to red flaser-like heterogeneous claystone, in layers with thicknesses up to a few meters.

- The M-type, a greyish-white band with a thickness ranging from 40 cm up to a few metres. No sedimentary structures were visible in the outcrop.

Cores of the coal overburden, from appraisal drillings near El Tremedal, show vertical alternations from (sandy) light grey to dark grey and brown laminated claystones. The colour is due to the presence of coal streaks, Fe-oxide and/or pyrite.

Microscopic description: The principal minerals are mainly illite and kaolinite. Minor amounts of chlorite and montmorillonite is also evident from XRD. Organic matter and goethite rich zones are randomly present in the matrix. In both types, grains are embedded in a matrix of clay minerals (Figure 5.B). The T-type contains disperse fine sand to silty quartz and orthoclase grains. In addition, dispersed medium sized idiomorphic siderite grains are recognized. The M-type grains consist of fine-grained quartz and siderite. The euhedral siderite grains range from 100 μm to 400 μm in size.

Mineralogy based on microscopy, XRD and XRF: Clay minerals (47-52 %), quartz (26-38 %), feldspar (15-20 %), carbonate (2-6 %), goethite (1-4 %), organic matter (8-15 %), accessory rutile and Ca-phosphate.

Geochemical Sample Classification

XRD and XRF Results

Many samples have been analysed with XRD and/or XRF. XRD-data is already used in chapter 3 for the description of the fine grain mineral-content, which is difficult to determine by polarization microscope. This qualitative approach gives an idea of the mineral content and mineral phases in relationship to specific sediment/mineral textures. The results can be used in a later stage of this study to explain thermo-mechanical behaviour. Ternary diagrams provide a good method to clarify the relationships of specific samples or sample groups to pre-defined end members. In addition, the XRD and XRF data are a good basis for the reconstruction of artificial bulk rock compositions. MINCOMP, a semi-normative program has been developed to calculate the pseudo-normative mineral compositions of the samples (Wolf, 2006).

The Chemical Bulk Composition Defined in Ternary Diagrams

Determination of the mineral components (XRD) and element oxides (XRF) forms the basis for the prediction of mechanical and thermal behaviour. Winkler (1979), Cox (1979) and Morse (1981) describe the use of ACF* and A'FK* ternary diagrams and multi-component systems to define XRF-bulk compositions of metamorphic mineral assemblages and associated P,T-conditions. The method was developed by Eskola (1939) for metamorphic rocks and meant exclusively for silica-mineral phases with an excess of quartz. In a limited way it is also applicable for sediments. Oxides, sulphides and retrograde - or weathered - mineral phases are neglected or compensated for in the three defined end members. In addition, SiO_2 is eliminated, so there is no relationship with the common component of a clastic sediment, quartz or sand. The XRF-results are obtained from standard glass melts, which in our case contain Fe_2O_3.

* ACF, A'KF: A = Al_2O_3+Fe_2O_3-Na_2O-K_2O, C = CaO-3.3(P_2O_5), F = MgO+MnO+FeO, A' = Al_2O_3+Fe_2O_3-(Na_2O+K_2O+CaO)[2], K = K_2O. A+C+F = 100, A'+K+F = 100

For sediments, the end members of the diagram have to be redefined. A classification into clastic and non-clastic sedimentary rocks explains the presence of a sand component, a clay component and carbonates. Mason (1952) proposed three end groups: (SiO_2), (Al_2O_3 + Fe_2O_3 + H_2O) and (MgO + CaO + CO_2). In this method soil/rock types such as sandstones, shales, laterites and limestones are clearly separated. However, the main oxides Na_2O and K_2O are neglected, so Fe-rich carbonates (e.g. siderite) and Fe- or Na, K-silicates (e.g. chlorite, albite) are not distinguished from each other.

The SAK/SAC Graphical Presentation

For sedimentary rocks, that have undergone diagenesis, a combination of the methods of Eskola (1939) and Mason (1952) avoid the above shortcomings. Two triangles with four groups of element oxides can provide a classification of the bulk sediments and main minerals present in sedimentary rocks, such as the Carboniferous and Cretaceous samples of our study. The following components should be distinguished:

1. Sandstones, sand/shale laminites and shales, according to the clastic sediment division by Diessel (1992).
    - In the sandstones, both quartz and feldspar are to be considered as part of the grain framework.
    - The clay/shale fraction includes the major clay minerals; illite, chlorite, kaolinite and montmorrilonite. They all contain all some water and/or hydroxyl.
2. The chemical and biogenic sediments.
    - Depositional carbonates (calcite and dolomite).
    - Diagenetic carbonates (calcite, dolomite, ankerite and siderite).

Hence, the presence of clay minerals is made evident by adding FeO, Na_2O and K_2O to the quartz and alumina groups. Therefore, using two triangles, the following end-members groups are proposed (Figure 6):
S : Si (derived from SiO_2)
A : Al (derived from Al_2O_3)
C: Ca + Fe + Mg + Mn (derived from CaO, FeO, Fe_2O_3, MgO and MnO)
K: K + Na (from K_2O and Na_2O)
The two triangles are formed by the end members SAC and SAK respectively (Figure 6). The SAK-triangle is sensitive to the distribution of the different clastic silica minerals. Conversely, the SAC-triangle exhibits the relationship between clastic silica components (sand, clay) and chemical sediments (carbonates and oxides). Some silicates, which can hold Na, K, Mg and Fe, such as chlorite and montmorillonite, are placed in both triangles. This double-triangle method shows differences with previously mentioned methods.

- The SiO_2-component is better emphasized.
- In several silica minerals, such as clay minerals and feldspars, the Si-atoms in the tetrahedron-octahedron molecule framework are substituted by Al-atoms (a compensation for the presence or absence of ions in the C- and K-group). The result is a slight shift towards A, which can be ignored in view of the dominating amount of Si.
- All measured accessory elements, including the element oxides TiO_2, MnO, P_2O_5, S and SO_2, are not added. They hold less than one weight percent of the bulk composition and are, at times present, in different amounts available. In addition, they are difficult to relate with the

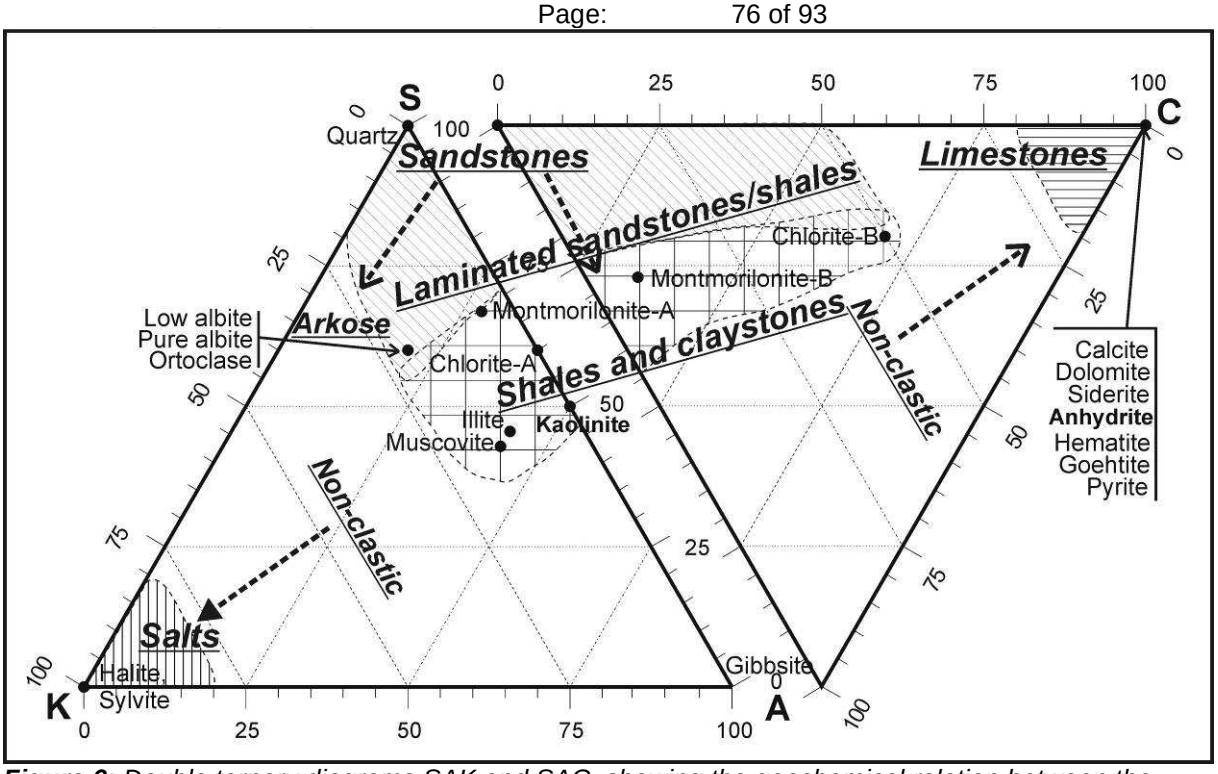

Figure 6: *Double ternary diagrams SAK and SAC, showing the geochemical relation between the detected minerals and sand(stone) and clay(stone)/shale as clastic components and carbonates/salts as non-clastic components. The upper half of the figure is used for lithology definition of the coal-related sediment rocks in this study.*

silicates and carbonates. When present in larger amounts, they represent atypical sediment types. Hence they are not inserted in this graphical representation of common sediments.

- Organic matter or coal is also ignored in the system, although mentioned by Diessel (1992) in his discussion on coal-bearing depositional systems. In his work, coal is considered as an autochthonous or migrated and deposited biogenic component in various sedimentary environments. Of interest are the coal/sediment contacts and the relationship of seams to the roof and floor strata. In other words, coal is a separate component, not recognized in XRD/XRF-measurements and derived from XRF weight loss information (chapter 3).
- Water and carbon(oxides) are also not included. However, all samples are characterised by both XRD and XRF. The weight lost in the XRF-measurements is a good indicator of the presence of water, the $(CO_3)^{2-}$-part in carbonates and organic matter.

This new representation gives a good illustration on the element shifts between primary clastic and chemical components, and diagenetic modifications. It improves the comparative quantification of the relative sedimentary nomenclature, such as "silt- laminated shale".

Chemical Sample Characterisation and Interpretation.

To characterise the rock overlying the coal on their geochemical heterogeneity, 52 samples have been analysed on their element composition (See Appendix). A major part of these samples is also analysed for the major mineral components with XRD. Figure 7 shows the results of the various coal associated overburden samples.

In both the SAK and SAC diagram the relationship between the sand/sandstone component and clay/shale component of the Carboniferous and Cretaceous series, is clearly visible as a band. Both sedimentary rocks, although of different age and origin, fall into the same geochemical zone. The clastic sediments are grouped mainly in the direction of the S-A line of the diagram. The sandstones or sands and shales/claystones lie at both ends of this band. Figure 8 also shows that the white Cretaceous beach barrier sands of the ET-series are contaminated with minor amounts of kaolinite and occasional pyrite. The laminated sediments are situated in between the sandstones (ET- and SR150-series) and shales (8670- and O268-series).

The relationship between Si, Al and K+Na, shows a very constant K+Na amount of about 3 to 8 mole% (Figure 7 left). This is the result of a homogenous sediment source combined with a high mineral maturity in coastal lowland environments. The XRD- and XRF-data show, in accordance with thin sections, no traces of metamorphic or igneous minerals and low accessory amounts of rutile, tourmaline, etc.. According to Wenselaer (1996), weathering of syn-sedimentary feldspar and transformation of the smectite type clays during burial, produce an additional amount of kaolinite and illite. Since the amount of K, Al and Si remains almost constant during this transformation, their place in the SAK graph is not changing.

The SAC triangle however, shows a less pronounced relationship between Ca+Fe+Mg+Mn, Si

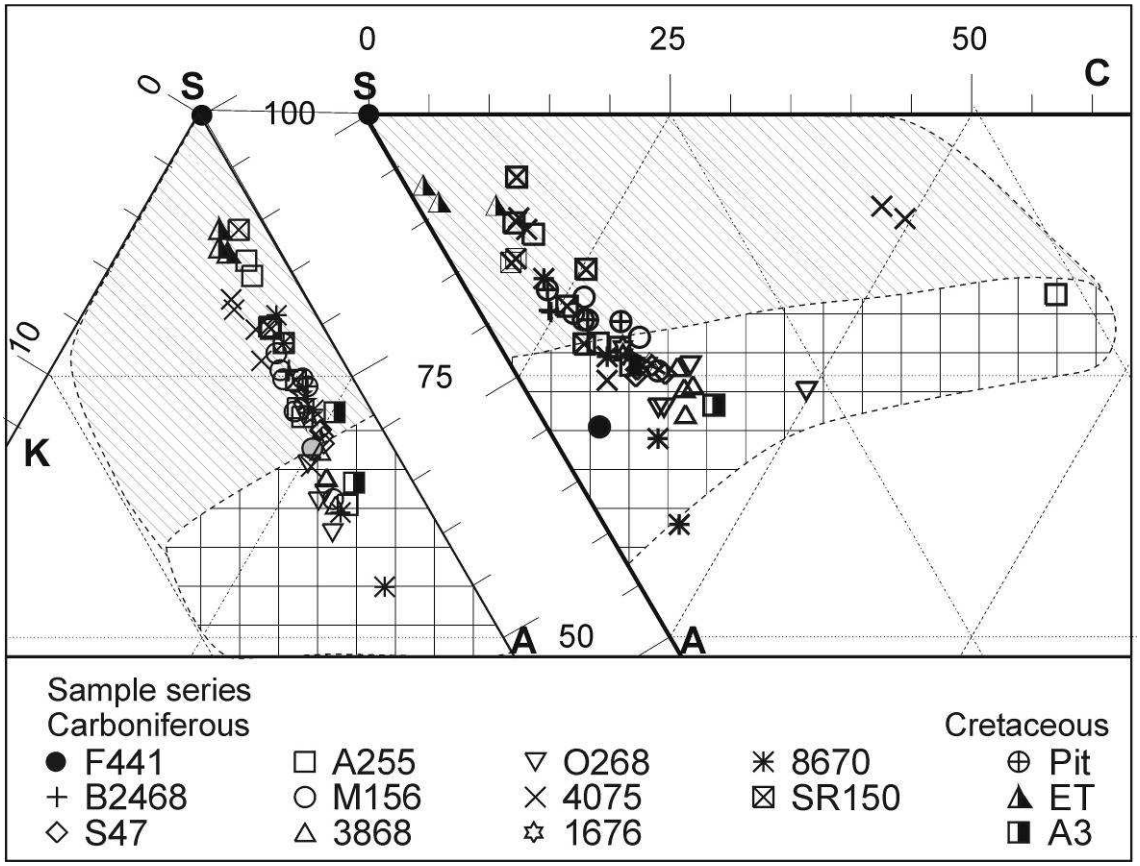

Figure 7: *The upper half of a SAK/SAC-diagram, showing the chemical and mineralogical relationships of Carboniferous and Cretaceous samples of the studied sand(stone), clay(stone)/shales and carbonates.*

and Al (Figure 7). In the direction of the shale component, a diversion in the S,A-trend toward the C-component is visible (4075- and A255-samples). Figure 6 shows that the Fe and Mg chlorite, Fe in the oxides and sulphides and Mg, Fe and Ca in the carbonates cause this phenomenon. Since siderite and chlorite are the major minerals in the analyzed samples, they increase with the amount of shale. This diversion toward C is caused by an increase of organic matter in the shale component of an originally organic mud named Gyttjae (Stach et al., 1982). This organic mud in swamp lakes has a relatively high pH and acts as an environment of precipitation for bicarbonate solutions ($FeHCO_3$), i.e. syngenetic siderite and ankerite. According to Diesel (1992) and Taylor et al. (1998) epigenetic siderite develops during the early burial phase as a result of Fe-transport in groundwater and mineralization with the CO_2 produced during coalification. Wenselaer et al. (1996, pp. 22) confirms this for the early diagenetic (pre-compaction) phase of the Campina Carboniferous samples. Some A255 and O2687 samples contain high amounts of siderite in diagenetic lenses supporting this hypothesis.

The apparent anomaly of some samples from batch 4075 in the SAC diagram, is due to the presence of secondary, vug-filling, calcite and dolomite. These calcites are very often present in the coal cleats as well as the coal overburden. The orientation of this cleat and fracture system often gives an indication of the burial and tectonical history.

Mineral Bulk Compositions Defined in Ternary Diagrams

Multi-component systems like ternary diagrams and tetrahedrons are also used to characterise mineral phases of igneous and metamorphic rocks (Morse 1981, Cox et al. 1979). For sediment classification based on grain components, the triangular diagrams for sandstones proposed by Pettijohn et al. (1973), give a reliable semi-quantitative impression of the maturity by distinguishing sandstones, graywackes and arkoses. However, when the samples include organic matter, carbonates, oxides and sulphates, all formed by either surface weathering, transport, chemical cementation, biological decay or diagenesis, multi-component diagrams are needed. Quantification of textures as discussed in the previous section, is impracticable with a ternary diagram. A four-component tetrahedron gives no satisfactory result when visualized in 2-D. However, unfolding a tetrahedron into four ternary diagrams shows the relationship of all combinations. Each time three out of four end-members are presented. In this way, Pettijohn (1957) visualized the relationship between clay and the non-clastic components coal/bitumen, carbonate and silica. The clay in this unfolded tetrahedron formed the end-members to present a rock nomenclature.

Diagrams with Organic Matter

Organic matter was not included in the ternary diagrams of the previous section. Moreover, the element oxides only provide mineral associated element information. The clastic and non-clastic components grain-, clay-, carbonate- and organic matter fractions are not considered as volume fractions. Using MINCOMP all present mineral phases are quantified in volume percentages (Wolf, 2006). With these results a comparable projection can be created, in order to recognize relationships between the end-members.

The four triangles of Pettijohn (1957) contain two clastic components; grains and clay/shales, and two non-clastic components; carbonates and organic matter (Figure 8):

- QF: The clastic grain component, which contains quartz and the feldspars albite, potassium feldspar and anorthite. The last two feldspars are not present in the studied samples.

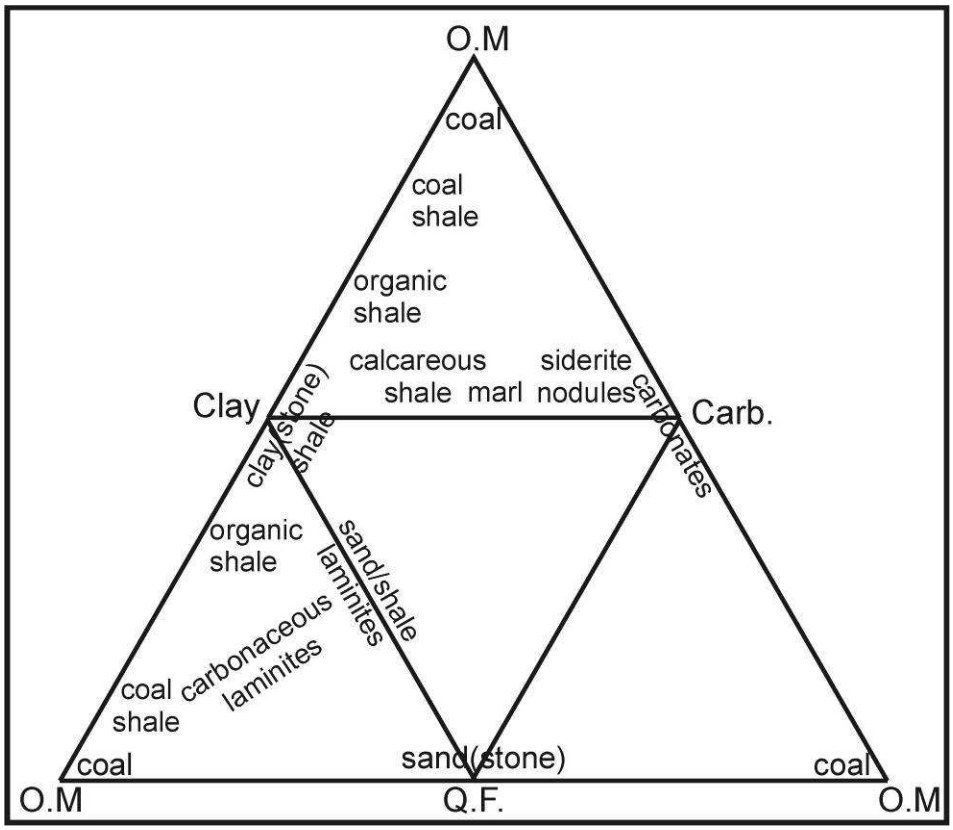

Figure 8: **Four ternary diagrams, showing the mineralogical relations between organic matter (O.M.) and the end members quartz/feldspar grains (Q.F.), clay minerals and carbonates (Carb.). Revised after Pettijohn (1957).**

- Clay: Represents the sheet silicates. In the samples of this study the clay minerals illite, kaolinite, smectites and the micas muscovite and chlorite are included. Chlorite is present in the Carboniferous samples, while smectites are present in the Cretaceous samples.
- Carb: The carbonates include siderite, calcite, magnesite and dolomite. In MINCOMP, ankerite is divided in the three end-members.
- O.M.: A combination of dispersed organic matter and thin coal laminae.

The central diagram compares the classical three components: the grain-, clay- and carbonate fraction. The other three diagrams contain organic matter and two components of the central diagram. In the diagrams of figure 8, the rock nomenclature used earlier is inserted at the appropriate places. Other components, like oxides, phosphates, halites and sulphides, are present as traces less than 1 vol.% in our samples and can be neglected as relevant components.

Mineralogical Characterisation and Interpretation.
Figure 9 shows the spread of 52 Carboniferous and Cretaceous samples, from 14 sample batches. Different symbols are used for the batches, which are designated by unique codes mentioned in layer numberings of the stratigraphical systems in the appendix.

The Clay-QF-Carb.-ternary diagram shows that the samples lie in a clear band following the Clay-QF line. Four samples show a higher carbonate content; two 4075-samples contain high amounts of ankerite and dolomite cement, while the A255-sample contains a siderite lens and carbonate filled cleats, and one O268-sample a relatively increased carbonate content due to a high content of organic matter.

The clay-QF-O.M. ternary diagram shows a wider band following the Clay-QF line. A minor increase of organic matter occurs when the shale components in the laminites increase. One sample of the O268-series tends towards a coaly shale. The cores of the clean sandstones (A3-series) contain dispersed organic matter and thin coal bands, which is clearly discernible.

The QF-Carb.-O.M. ternary diagram shows an explicit positive relationship between organic matter and carbonate. The earlier mentioned ability of organic mud, to precipitate bicarbonate solutions as syngenetic siderite/ankerite, is clearly recognizable in the thin sections. These carbonates are dispersed as amorphous aggregates in the zones rich in organic matter. Epigenetic carbonates are found in fissures and in clay mineral rich zones. The highest carbonate values are in siderite lenses and cements. Some samples free of carbonate, show highly variable amounts of organic matter.

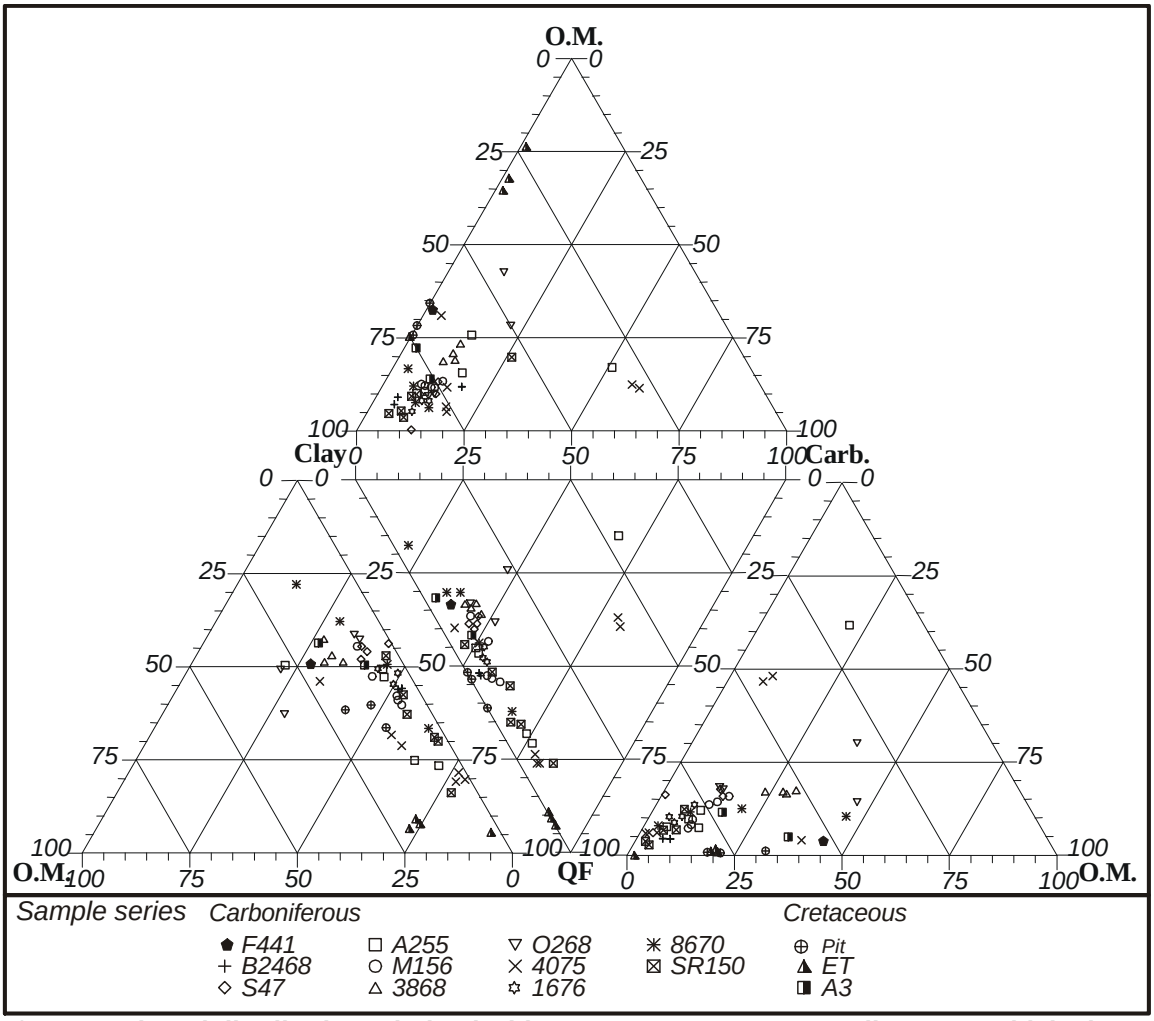

Figure 9: **Mineral distributions derived with MINCOMP. Four ternary diagrams, which show the grain, clay and carbonate relations to organic matter and coal of 14 batches with 52 Carboniferous and Cretaceous samples.**

The Clay-Carb.-O.M. ternary diagram shows a less explicit positive relationship between organic matter and carbonate. The highest carbonate values are in the earlier mentioned siderite lenses and cements. The clean A3 sandstones are richer in organic matter than the claystone samples.

Conclusive Remarks

The descriptions of most of the thin sections are possible with the laminite classification of Diessel (1992). Petrographical analysis with polarization microscopy proves to be a useful tool for the determination of mineral content, original sediment textures and diagenetical alterations of our samples. However, XRD/XRF-results on the same samples improve the determination of clay minerals.

Diagenetical alterations in the Carboniferous samples transformed a part of the original textures. Chemical changes and mineral transformations altered smectite and feldspars into chlorite and part of the kaolinite and illite. Fluid transport initiated dissolution and recrystallization of carbonates. In the presence of organic matter, the formation of amorphous Fe-rich ankerite and Fe-oxides is observed. Fissures are usually filled with calcite and dolomite. Microscopic texture characterization shows the presence and content of lamination, cementation and mechanical effects, such as pressure solution and mineral overgrowth.

The Cretaceous samples have a chemical composition comparable to the Carboniferous samples. However, their composition primarily consists of hardly mixed end-members of claystone and sandstone. Intermediate laminated sediments are not available in our sample series. Due to its shorter burial history at shallower depths, mechanical effects and mineral transformations are minimal. However, a coal-related chemical precipitation of ankerite is identified in the A3-samples.

The SAK/SAC classifications here proposed depict the chemical variation of the Carboniferous and Cretaceous samples. Gradual shifts between different sediment end-members, such as clay, shale, sand(stone)s, greywackes, carbonates and evaporites, are seen. The two sample groups with different ages and burial histories show in a chemical sense no significant differences. The Cretaceous sands are very clean when compared to the others. Both the Carboniferous and Cretaceous samples consist of mature sediments without volcano-clastic or other immature influences. The graphical representation can be used for both recent sediments and compacted sediments. A shortcoming is, that the method does not include organic matter as an end member.

This is corrected with a method of Pettijohn (1957) to plot the relationship between clay minerals, carbonates, silica and non-clastic organic matter, in four ternary diagrams. They show that the entire sample group consists of a continuous band ranging from an almost clean sandstone, through laminites, to a shale. The amount of organic matter increases slightly with increasing amounts of clays. A strong positive correlation is present between organic matter and carbonates. The carbonates are usually dispersed amorphous aggregates in coal and clay rich zones. As an exception carbonate cementation is found in some sandstones.

The entire sample set is representative for coal overburden rocks, deposited in coastal lowlands and flood plains. All samples can be used for cap rock testing. During the experiments, the sample choice is based on composition, consistency and availability. For this reason sandstones and laminated sandstones/shales can be obtained from the Carboniferous group, while shales and claystones can be taken from both the Carboniferous and Cretaceous sample series.

Literature

Cox, K.G., Bell, J.D., Pankhurst, R.J., 1979, The interpretation of igneous rocks, Ed. George Allen & Unwin. ISBN 0-04-552015-1 (B)

Diessel, C.F.K., 1992. *Coal bearing depositional systems.* Springer Verlag Berlin Heidelberg, ISBN 3-540-52516-5, 720 pages. (B)

Eskola, P., 1939: *In* Barth, Correns und Eskola, "Die Entstehung der Gesteine", Springer Verlag, Berlin.

Guion, P.D., 1984. Crevasse splay deposits and roof-rock quality in the Threequarters Seam (Carboniferous) in the East Midland Coalfield, U.K., *In: Sedimentology of Coal and Coal-bearing Sequences*, ed. R.A. Rahmani, R.M. Flores, Blackwell Scientific Publications, ISBN 0-632-012186-2.

Mason, B., Principles of Geochemistry, Wiley, New York. Triangle diagram referred to in: Sedimentary rocks, 2nd.ed., Pettijohn, F.J., 1957, pp.106. Harpers Geoscience Series, Harper & Row, New York.

Merrit, R.D., 1983. Coal Overburden: geological characterization and premine planning. Noyes Data Corporation, Park Ridge, N.J.,U.S.A., ISBN 0-8155-0964-2

Morse, S.A., 1981, Basalta and phase diagrams, Springer Verlag.

Pagnier, H.J.M., Van Tongeren. P.C.H., 1996. Upper Carboniferous of Borehole 'de Lutte-6' and evolution of the Tubbergen Formation in Eastern and Southeastern Parts of the Netherlands. Meded. Rijks Geolog. Dienst, vol.55, p. 3 – 30.

Pettijohn, F.J., 1957, *Sedimentary rocks*, publ. Harper & Row, 2nd ed., pp. 361. (B)

Pettijohn, F.J., P.E. Potter, R. Siever, 1973. Sand and sandstone, Springer Verlag, Berlin. Referred in: J.T. Greensmith, 1978, Petrology of sedimentary rocks, 6th.ed.. pp.66-123, George Allen & Unwin Ltd, ISBN: 0-04-55e011-9

Stach,E., Mackowsky, M.T., Teichmüller,M., Taylor,G.H., Chandra,A.D., Teichmüller,R., 1982, *Stach's Textbook of Coal Petrology*, 3rd ed., Borntraeger, Berlin. 535 pp.

Winkler, H.G.F., 1979: Petrogenesis of sedimentary rock, 5th ed., pp. chapter 4,5. Springer Verlag, NY inc., ISBN 0-387-90413-1. (B)

Wenselaers, P.J.J., Dusar, M., and Tongeren, P.C.H. van, 1996. Steenkoollaag methaan-gaswinning in het Kempisch kolenbekken, proefproject te Peer. Project report for the Ministerie van de Vlaamse Gemeenschap, afdeling Natuurlijke Rijkdommen en Energie, Brussels, Belgium, in Dutch.

Wolf, K-H.A.A., Kühnel, R.A., de Pater, C.J., 1987. *Thermal behaviour of country rock in laboratory experiments; mineralogical and textural aspects.* Proc. of the 13th Annual Underground Coal Gasification Symposium, Laram, Wyoming, DOE/METC-88/6029, 163-173. (A)

Wolf, K-H.A.A., Kühnel, R.A. & Pater, C.J. de, 1987. Laboratory experiments on thermal behaviour of roof and floor rocks of carboniferous coal seams. *In:* J.A. Moulijn et al. (eds.) *1987 International conference on coal science*, Elsevier science publishers B.V., Amsterdam, 911-914.

Wolf K-H.A.A., de Pater, C.J., 1989, *Laboratory tests on Carboniferous overburden rock, textural and mineralogical properties at elevated pressure and temperature*., proc, 15th Annual UCG-symposium, Delft, the Netherlands. pp. 322-334. ISBN 90-6275-566-6. (A)

Wolf, K-H.A.A., de Pater, C.J., 1990. *Chemical and Petrophysical Characterization of Coal and Overburden Rock*. Final Report, TU-Delft-Novem, Contract: 20.11-015, 105 pages. (R)

Wolf, K-H.A.A., Hettema, M.H.H.., 1995. *Petrophysical and Mineralogical Properties of Overburden Rock and Coal*. NOVEM- Delft University, technical report, 22.1.40/13.11, april 1995. Part 1 (R)

Wolf, K-H.A.A., Hettema, M.H.H., 1995. *Petrophysical and mineralogical properties of overburden rock and coal*. Novem technical report nr 22.1.40/13.11. 121 pages. Part 2 (R)

Wolf, K-H.A.A., Hettema, M.H.H., November 1996. *Thermo-mechanical behaviour and stability of wall rock during underground coal gasification; El Tremedal Field Test, Phase 1.* Final Report, TU-Delft-Novem, Contract nr: 94/E0767/230110/04/03, 90 pages. (R)

Wolf, K-H.A.A., Hettema, M.H.H., July 1997. *Thermo-mechanical behaviour and stability of wall rock during underground coal gasification; El Tremedal Field Test, Phase 2. Final Report.* TU-Delft-Novem, Contract nr: 94/E0767/230110/04/03, 74 pages.

Wolf, K-H. Underground Coal fires, Geological and Geotechnical Aspects. PhD Thesis, Delft University of Technology, to be published in 2006.

Appendices

Comparison of the Basin Stratigraphy of the Collieries of Beringen and Zolder for Westphalian A and B.

		Beringen	KS Layer No.	Zolder	Extract of the original compilation by J.Tricot and R. Claus. (Geol. Survey of the Kempense Steenkool Maatschappij, 06.1981)
		Marine Horizon of Eisden			
Middle Westphalian (B)	Mining Zone of Asch	Ei	37		
			38		
		A	39		
		A/2	40		
		Lohest	***41***	J	F441-series, 780 m
		Habets	42	I	
		Sauvestre	43	H	
		SA/9	44	G	
		Jadot bl	45 a	F	
		Jadot ol	45 b	E	
		Ja/3	46	E/2	
		Cavallier	***47***	E/3	S147-series, 740 m
		Sous Cav.	48	C.B	
		sC/1	49	A	
		47 - 48	***50***	A/4-A/8	SR150-series, 738 m
		Marine Horizon of Quaregnon			
Lower Westphalian (A)	Mining Zone of Genk	51	51	1+1	
		55	***55***	3	A255-series, 750 m
		56	***56a/b***	4/5	M156-series, 660 m
		57	57/56c	6/7	
		57/2	57/2	8/1	
		58	58	9	
		59	59	10/11	
		60	60	13	
		61	61a	14	
		62	61b		
		63	63	15	
		64	64	16	
		(66)67	67	19	
		68	***68***		O268-series, 790 m
		70 bl	***70a***	***20***	3868-series, 745 m
		70 ol	***70b***		8670-series, 745 m
		71	***71a/b***	***23/24***	
		72	72	25	
		75	***75***	27	4075-series, 740 m
		76	***76***	31	4076-series, 740 m
		76/3	76/3	31/1	1676-series, 710 m
		77	77	32	
		78	78	--	
		80	80	33/a	
		81	81	33/b	
		Marine Horizon of Wasserfall			

Figure A.1: *Campine basin stratigraphy of the Lower and Middle Westphalian. The samples for experiments are named with code and depth of excavation.*

Table A.1: *XRF- Oxide percentages of Carboniferous and Cretaceous samples from Belgium, the Netherlands and Spain.*

Sample code	Report number	SiO2	Al2O3	Fe2O3	TiO2	CaO	MgO	MnO	K2O	Na2O	P2O5	SO3	S	Cl	Melt loss	Total, excl. sulphur	H2O+CO2+ OM+SO2
Belgium – Beringen and Zolder																	
F441-4	8512	52	20.6	2.8	0.83	0.09	1.41	0	4.09	0.4	0	0	0	0	16.6	98.82	17.78
B2468.A	8531	69.2	15.92	2.99	0.95	0.06	0.96	0	2.79	0.02	0	0	0	0	4	96.89	7.11
B2468.B	8531	69.5	16.05	3.02	0.95	0.05	0.96	0	2.79	0.09	0	0	0	0	4	97.41	6.59
S47-1	8862	56.9	18.6	7.2	0.97	0.34	1.83	0	3.94	0.34	0	0	0	0	8.3	98.42	9.88
S47-4	9011	61.8	19.6	8.1	1.1	0.45	2.03	0.26	3.98	0.46	0.15	0	0	0	1.1	99.03	2.07
S47-5	8862	55.1	17.5	8.4	0.99	0.5	2.06	0	3.67	0.4	0	0	0	0	10	98.62	11.38
S47-10.1	8862	54	18.1	9.2	0.96	0.48	2.09	0	3.93	0.35	0	0	0	0	9.8	98.91	10.89
A255-1	8862	60.1	17	6.8	0.95	0.36	1.63	0	3.44	0.25	0	0	0	0	8.2	98.73	9.47
A255-3 *	8862	22.7	9.8	31.4	0.38	1.41	3.93	0	1.77	0	0	0	0	0	27	98.39	28.61
A255-5	8862	62.6	16.9	5.4	0.97	0.26	1.51	0	3.41	0.33	0	0	0	0	7.2	98.58	8.62
A255-C	9019	71.5	9	5.3	0.51	0.64	1.17	0.21	1.56	0.34	0.08	0	0	0	8.8	99.11	9.69
A255-I	9019	76.2	8.5	4.2	0.46	0.98	0.99	0.18	1.46	0.36	0.08	0	0	0	6	99.41	6.59
M156-D	9019& X94048	64.6	15.3	5.3	0.88	0.36	1.41	0.15	2.92	0.48	0.1	0	0	0	8	99.5	8.5
M156-F	9019& X94048	57.7	16	8.2	0.92	0.5	1.9	0.27	3.28	0.33	0.11	0	0	0	10	99.21	10.79
M156-I	240392NN	55.2	18.4	8	0.91	0.43	2.02	0	3.75	0.17	0	0	0	0	10.2	99.08	11.12
M156-M	9019& X94048	65.9	14.9	4.9	0.88	0.33	1.37	0.14	2.83	0.47	0.09	0	0	0	7.4	99.21	8.19
M156-Q	240392NN	65.7	13.7	6.15	0.86	0.51	1.58	0	2.64	0.33	0	0	0	0	7.6	99.07	8.53
3868-7	8862	49.6	19.9	8.6	0.92	0.3	1.5	0	4.02	0.2	0	0	0	0	14.3	99.34	14.96
3868-9	8862	49.2	17.6	9.1	0.87	0.92	1.76	0	3.59	0.15	0	0	0	0	15.1	98.29	16.81

3868-11	8862	52.4	16.9	9.8	0.87	0.39	1.76	0	3.34	0.05	0	0	0	0	13.3	98.81	14.49
3868-BULK	8862	50.5	18.1	9.2	0.9	0.5	1.66	0	3.65	0.13	0	0	0	0	14	98.64	15.36
O268-0	8512	53	20.3	8.3	0.84	0.41	1.66	0	3.76	0.5	0	0	0	0	11	99.77	11.23
O268-3	8512	52.3	20.2	8.7	0.84	0.4	1.7	0	3.76	0.9	0	0	0	0	11.1	99.9	11.2
O268-4 *	8512	43.5	14.4	10.4	0.74	0.62	1.63	0	2.5	0.7	0	0	0	0	24.2	98.69	25.51
O268-7 *	8512	35.8	15.9	18	0.54	0.89	1.61	0	3.1	0.5	0	0	0	0	23.7	100.04	23.66
4075-2/1	8512	41.8	6.7	6.4	0.42	13.65	6.12	0	0.86	0.6	0	0	0	0	22.4	98.95	23.45
4075-2/2	8512	39.3	7.4	6.5	0.46	13.7	6.45	0	1.08	0.7	0	0	0	0	23	98.59	24.41
4075-3/1	8512	77.4	9.2	4.2	0.62	0.51	1	0	1.16	1.6	0	0	0	0	4.5	100.19	4.31
4075-3/2	8512	75.8	9.7	4.7	0.63	0.4	1.12	0	1.31	1.6	0	0	0	0	5	100.26	4.74
4075-3/3	8512	55.3	18.5	3	0.89	0.11	1.42	0	3.62	0.3	0	0	0	0	17	100.14	16.86
4075-3/verz.	8512	76.6	8.8	4.3	0.59	0.68	1.04	0	1.11	1.5	0	0	0	0	4.3	98.92	5.38
1676-4	8862	62.7	17	6.1	0.98	0.26	1.76	0	3.32	0.72	0	0	0	0	6.2	99.04	7.16
1676-5	8862	58.9	17.1	7.6	1	0.34	1.91	0	3.36	0.65	0	0	0	0	7.7	98.56	9.14
1676-7A	8862	62.3	16.2	6.4	0.97	0.29	1.75	0	3.16	0.77	0	0	0	0	6.9	98.74	8.16
8670-I	240392nn	61.7	17.3	6.23	0.93	0.29	1.52	0	3.25	0.24	0	0	0	0	7.8	99.26	8.54
8670-R	240392nn	45.8	27.4	3.74	1.24	0.21	1.35	0	4.94	0.2	0	0	0	0	13.9	98.78	15.12
8670-X	240392nn	71.7	12	5.29	0.78	0.33	1.18	0	1.88	0.53	0	0	0	0	5.7	99.39	6.31
8670W	951103	52.5	22.4	5.9	0.95	0.27	1.7	0.1	4.7	0.45	0.11	0.1	0	0	10.46	99.54	10.92
SR150-C-dark	240392nn	66.8	15.5	4.4	0.91	0.28	1.3	0	2.92	0.38	0	0	0	0	6.1	98.59	7.51
SR150-C-light	240392nn	75	12.4	3.2	0.82	0.22	0.84	0	2.11	0.87	0	0	0	0	4.1	99.56	4.54
SR150-E	240392nn	66	12.6	6.5	0.79	0.98	1.68	0	2.35	0.29	0	0	0	0	7.9	99.09	8.81
SR150-H	240392nn	77.1	6.1	3.09	0.38	2.91	1.34	0	0.67	0.68	0	0	0	0	7	99.27	7.73
SR150-I-dark	240392nn	75.3	12.7	2.44	0.82	0.3	0.8	0	2.12	0.86	0	0	0	0	4	99.34	4.66
SR150-K	240392nn	64.7	18.5	3.82	1.1	0.063	1.57	0	3.1	0	0	0	0	0	6.6	99.453	7.147
Spain – Pitara Outcrop																	

Pit 013	X96007	70	13	5.3	1.04	0.2	0.4	0.03	2.46	0.07	0.09	0	0.11	0	6.8	99.386	7.414
Pit 014A	X96007	65.3	15.1	7.2	1.03	0.22	0.53	0.07	2.45	0.07	0.11	0	0.13	0	7.12	99.146	7.974
Pit 014B	X96007	60.6	14.7	10	0.95	0.23	0.51	0.02	2.27	0.07	0.115	0	0.13	0	9.8	99.264	10.536
Spain – El Tremedal SST																	
ET2-01	X94015	87.3	5.7	1.24	0.09	0.04	0.012	0	3.06	0.17	0	0	1.8	0	2.4	100	2.396
ET2-02	X94015	70.3	6.2	6.8	0.29	0.18	0.13	0.02	2.42	0.10	0.06	0	5.8	0	13.5	100	13.502
ET2-03	X94015	78.3	6.6	0.88	0.21	0.03	0.06	0	2.81	0.14	0.02	0	0.69	0	11.0	100	10.955
ET2-04	X94015	76.7	6.1	1.46	0.23	0	0.02	0	2.93	0.15	0	0	1.2	0	12.41	100	12.408
Spain – Corta Barabassa																	
A3m	9028	59.7	17.8	5.5	1.26	0.78	0.95	0.04	2.02	0	0.04	0	0	0	10.1	100	11.91
A3T	9028	50.0	19.8	9.9	1.28	0.72	1.4	0.1	2.94	0	0.04	0	0	0	11.6	100	13.78

Table.A.2: *Mincomp-calculations* ***in vol.%,*** *XRD-results at 20℃*
Bold: mineral detected with XRD and reconstructed with Mincomp; +; XRD- values but no XRF-values. Note: all minerals add to 100 vol.%

Sample code	Report number	Muscovite/illite	Kaolinite	Chlorite	Montmorillonite	Calcite	Magnesite	Dolomite	Siderite	Quartz	Anorthite	Na-albite	Orthoclase	Hematrite	Goethite	Pyrite	Angydrite	Rutile	Ca-Phosphate	Halite	Organic matter
North-West Europe - Belgium - 'Beringen/Zolder																					
F441-4	8512	31.16	13.39	4.34		0.14			1.84	23.23		3.09						0.47			22.35
B2468.A	8531	23.36	15.91	3.25		0.10			2.42	49.72		0.17						0.59			4.47
B2468.B	8531	23.49	16.03	3.26	0.00	0.09			2.47	49.86		0.77						0.59			3.45
S47-1	8862	33.46	10.55	6.28		0.60			6.16	33.28		2.92						0.61			6.15

S47-4	9011	33.20	11.75	6.84		0.44			7.07	35.84		3.89						0.68	0.29		0.00
S47-5	8862	31.04	9.29	7.04		0.88			7.19	32.31		3.43						0.62			8.22
S47-10.1	8862	33.65	8.93	7.23		0.85			8.06	31.06		3.04						0.61			6.58
A255-1	8862	29.18	11.32	5.58		0.63			5.86	38.78		2.15						0.60			5.90
A255-3 *	8862	16.46	11.52	0.00		2.72	8.01		33.68	12.33								0.26			15.02
A255-5	8862	28.76	11.11	5.14		0.45			4.52	40.91		2.82						0.61			5.69
A255-C	9019	12.88	6.63	3.90		0.91			4.69	57.96		2.84						0.31	0.16		9.72
A255-I	9019	12.31	6.53	3.37		1.53			3.78	64.46		3.07						0.29	0.16		4.52
M156-D	9019 & X94048	24.59	10.61	4.80		0.40			4.61	44.19		4.09						0.55	0.20		5.97
M156-F	9019 & X94048	27.84	9.29	6.51		0.62			7.36	37.15		2.84						0.58	0.22		7.59
M156-I	240392N N	31.76	12.02	6.91		0.75			6.83	32.30		1.46						0.57			7.41
M156-M	9019 & X94048	23.80	10.42	4.65		0.37			4.22	45.94		4.00						0.55	0.18		5.87
M156-Q	240392N N	22.36	9.24	5.40		0.89			5.24	47.95		2.83						0.54			5.55
3868-7	8862	33.06	13.94	4.98		0.51			7.45	24.25		1.67						0.56			13.58
3868-9	8862	29.17	11.33	5.77		1.55			7.70	26.28		1.23						0.52			16.45
3868-11	8862	27.79	12.31	5.91		0.67			8.56	31.26		0.42						0.54			12.55
3868BULK	8862	30.03	12.48	5.51		0.85			7.94	27.41		1.08						0.55			14.14

O268-0	8512	32.00	16.13	5.70		0.72			7.33	26.82		4.31						0.53			6.45
O268-3	8512	32.04	14.10	5.85		0.71			7.72	24.69		7.77						0.53			6.60
O268-4 *	8512	18.84	9.41	4.96		0.97			8.33	20.78		5.34						0.41			30.96
O268-7 *	8512	25.42	9.96	5.33		1.51			16.26	14.16		4.15						0.33			22.87
4075-2/1	8512	7.36	4.97	5.53		12.98		19.53	5.53	31.48		5.20						0.27			7.16
4075-2/2	8512	9.22	4.48	5.51		12.21		20.89	5.61	27.63		6.05						0.29			8.11
4075-3/1	8512	9.92	5.65	3.45		0.90			3.65	60.90		13.86						0.39			1.27
4075-3/2	8512	11.21	5.48	3.87		0.71			4.08	58.65		13.86						0.40			1.74
4075-3/3	8512	27.78	12.52	4.40		0.17			2.03	29.00		2.33						0.51			21.26
4075-3verz.	8512	9.41	5.35	3.56		1.19			3.70	60.43		12.88						0.37			3.11
1676-4	8862	28.54	10.25	6.11		0.46			5.18	40.05		6.27						0.62			2.52
1676-5	8862	28.76	10.18	6.60		0.60			6.56	36.12		5.64						0.63			4.91
1676-7A	8862	26.94	9.23	6.02		0.51			5.43	40.06		6.65						0.61			4.54
8670-I	240392nn	27.71	14.01	5.23		0.51			5.38	40.32		2.07						0.59			4.18
8670-R	240392nn	39.52	24.85	4.36		0.35			2.83	11.66		1.62						0.73			14.08
8670-X	240392nn	16.08	11.16	4.08		0.58			4.64	55.91		4.59						0.49			2.47
8670W	951103	39.29	13.53	5.74		0.22			4.92	23.58		3.81						0.59			8.08
SR150C dark	240392nn	24.62	11.74	4.43		0.49			3.65	46.63		3.24						0.57			4.63

SR150C light	240392nn	17.96	9.31	2.89		0.39			2.73	57.30		7.50						0.52			1.41
SR150-E	240392nn	19.95	8.86	5.76		1.72			5.54	49.80		2.49						0.50			5.37
SR150-H	240392nn	5.58	4.97	4.51		5.02			2.33	66.04		5.74						0.23			5.57
SR150Idrk	240392nn	17.93	10.05	2.73		0.53			1.99	56.92		7.36						0.51			1.98
SR150-K	240392nn	26.32	19.29	5.38		0.11			2.97	42.66		0.00						0.69			2.58
Netherlands - Kemperkoul																					
KK1		+	+	+						+								+			
KK2		+	+	+					+	+								+			
KK3		+	+	+					+	+								+			
Spain – La Pitara Outcrop																					
Pit 013	X96007	19.53	11.18	1.26	0.18	0.00				51.11		0.52			3.31		0.16	0.61	0.17		11.97
Pit 014A	X96007 X95002	17.54	16.36	1.39	2.67					42.99		0.00	1.35		4.46	0.05	0.01	0.60	0.20		12.39
Pit 014B	X96007	15.59	16.30	1.28	2.58					37.75		0.00	1.31		6.06	0.05	0.01	0.54	0.22		18.34
Spain – Daymsa mine: Foz Calanda																					
Day 01	X95002		+											+		+	+				+
Spain – El Tremedal SST																					
SST-core nr.4	X95002		+	+	+	+				+		+				+					

ET2-01	X94015		5.50				0.02			71.69		1.21	18.56			0.98	0.09	0.06		0.06	1.84
ET2-02	X94015		8.54				0.23			54.19		0.63	14.18			5.18	0.21	0.17	0.11	0.05	16.49
ET2-03	X94015		7.88				0.10			57.28		0.97	15.65		0.01	0.62		0.12	0.04	0.03	17.30
ET2-04	X94015		6.27				0.03			55.40		1.06	16.13			1.04		0.13	0.21	0.03	19.70
Spain – Corta Barabassa																					
A3m	9028	16.73	26.97	3.18	0.00	1.25			4.80	37.74								0.77	0.08		8.49
A3T	9028	24.06	23.44	4.63		1.13			0.76	25.81			0.00		4.08			0.77	0.08		15.24